

**DESIGN AND EVALUATION OF METAL OXIDE SURGE
ARRESTER PARAMETERS FOR LIGHTNING
OVERVOLTAGES**

SYAHIRAH BINTI ABD HALIM

**FACULTY OF ENGINEERING
UNIVERSITY OF MALAYA
KUALA LUMPUR**

2016

**DESIGN AND EVALUATION OF METAL OXIDE
SURGE ARRESTER PARAMETERS FOR LIGHTNING
OVERVOLTAGES**

SYAHIRAH BINTI ABD HALIM

**THESIS SUBMITTED IN FULFILMENT OF THE
REQUIREMENTS FOR THE DEGREE OF
DOCTOR OF PHILOSOPHY**

**FACULTY OF ENGINEERING
UNIVERSITY OF MALAYA
KUALA LUMPUR**

2016

UNIVERSITY OF MALAYA
ORIGINAL LITERARY WORK DECLARATION

Name of Candidate: **SYAHIRAH BINTI ABD HALIM**

Registration/Matric No: **KHA110088**

Name of Degree: **DOCTOR OF PHILOSOPHY**

Title of Thesis: **DESIGN AND EVALUATION OF METAL OXIDE SURGE
ARRESTER PARAMETERS FOR LIGHTNING OVERVOLTAGES**

Field of Study: **POWER SYSTEM TRANSIENT**

I do solemnly and sincerely declare that:

- (1) I am the sole author/writer of this Work;
- (2) This Work is original;
- (3) Any use of any work in which copyright exists was done by way of fair dealing and for permitted purposes and any excerpt or extract from, or reference to or reproduction of any copyright work has been disclosed expressly and sufficiently and the title of the Work and its authorship have been acknowledged in this Work;
- (4) I do not have any actual knowledge nor do I ought reasonably to know that the making of this work constitutes an infringement of any copyright work;
- (5) I hereby assign all and every rights in the copyright to this Work to the University of Malaya ("UM"), who henceforth shall be owner of the copyright in this Work and that any reproduction or use in any form or by any means whatsoever is prohibited without the written consent of UM having been first had and obtained;
- (6) I am fully aware that if in the course of making this Work I have infringed any copyright whether intentionally or otherwise, I may be subject to legal action or any other action as may be determined by UM.

Candidate's Signature

Date:

Subscribed and solemnly declared before,

Witness's Signature

Date:

Name:

Designation:

ABSTRACT

Surge arrester is widely used as a protective device to reduce possibility of flashover during transient overvoltage. It is important to understand the characteristics of surge arrester as over-specification of its rating will result in a reduction of the protective characteristics. Researches on reliability and stability of surge arrester normally involve detailed experimental works, which are usually not feasible due to high cost in conducting test using actual prototype. The usage of computer tools in carrying out virtual testing is important to verify the performance of the arresters in early stages before proceeding with actual prototype built-up.

In this work, transmission line surge arresters with different dimensions and ratings were modeled to investigate their discharge energy during lightning discharge using the finite element analysis (FEA) method. The main advantage of FEA models in this work is real dimensions of the actual surge arrester can be modeled, which may increase the accuracy of the results obtained. To validate the accuracy of the method, the arrester models were also simulated by the use of PSCAD/EMTDC and EMTP-RV software and compared with the specifications provided by the manufacturer. In spite of distinctive representations of the arrester models in COMSOL Multiphysics, EMTP-RV and PSCAD/EMTDC, the comparison made between the results indicates a satisfactory agreement. Parametric analyses were also conducted using finite element method to study the effects of varying the design geometry of the arresters, which cannot be evaluated using PSCAD and EMTP-RV software.

The surge arrester models that have been developed were then used in designing protection scheme for a 275/132 kV quadruple circuit transmission line in Malaysia. The best arrester configuration was selected by considering the effects of tower footing resistance, lightning current and power frequency angle on the line lightning

performance. Improvement on the lightning performance could be achieved by installing surge arresters on all phases of a 132 kV circuit, where the double circuit outages were successfully eliminated. The results are useful for the utility company in determining the most effective installation position with the minimum number of installed surge arresters.

University of Malaya

ABSTRAK

Penangkap kilat digunakan secara meluas sebagai alat pelindung untuk mengurangkan kemungkinan 'flashover' semasa voltan fana. Adalah penting untuk memahami ciri-ciri lonjakan penangkap kerana penarafan melebihi spesifikasi akan mengurangkan ciri-ciri perlindungannya. Kajian mengenai reka bentuk penangkap lonjakan yang dijalankan melibatkan kajian eksperimen terperinci mengenai kebolehpercayaan dan kestabilan penangkap kilat, yang biasanya tidak boleh dilaksanakan kerana kos yang tinggi dalam menjalankan penyelidikan dan ujian menggunakan prototaip yang sebenar. Penggunaan alat komputer dalam menjalankan ujian maya adalah penting untuk mengesahkan prestasi penangkap kilat dalam peringkat awal sebelum prototaip sebenar dibina.

Dalam kajian ini, penangkap kilat talian penghantaran dengan dimensi dan penarafan yang berbeza telah dimodelkan untuk mengkaji keupayaan tenaga pelepasan semasa kejadian kilat dengan menggunakan analisis kaedah unsur terhingga (FEA). Kelebihan utama model FEA dalam kerja-kerja ini adalah dimensi sebenar penangkap kilat sebenar dapat dimodelkan, yang boleh meningkatkan ketepatan keputusan yang diperolehi. Model tersebut juga disimulasi dengan menggunakan perisian PSCAD/EMTDC dan EMTP-RV dan dibandingkan dengan spesifikasi yang disediakan oleh pengeluar. Walaupun kaedah berbeza digunakan dalam COMSOL Multiphysics, EMTP-RV dan perisian PSCAD/EMTDC, perbandingan yang dibuat antara ketiga-ketiga keputusan menunjukkan ketepatan. Keputusan dari model juga sama dengan data ujian yang diperolehi dari pengeluar dan menepati kadar keupayaan tenaga, sekaligus menunjukkan bahawa semua kes yang dikaji telah dimodelkan secukupnya. Analisis berparameter juga dijalankan dengan menggunakan kaedah unsur terhingga untuk mengkaji kesan

geometri reka bentuk berbeza, yang tidak boleh dinilai dengan menggunakan perisian PSCAD dan perisian EMTP-RV.

Model-model penangkap kilat tersebut kemudiannya digunakan dalam mereka bentuk skim perlindungan litar talian penghantaran 275/132 kV di Malaysia. Konfigurasi penangkap kilat terbaik telah dipilih berdasarkan kesan footing resistance, lightning magnitude dan power voltage frequency angle. Peningkatan prestasi dapat dicapai dengan memasang penangkap kilat pada semua fasa litar 132 kV, di mana gangguan litar berkembar telah berjaya dihapuskan. Keputusan yang diperoleh berguna untuk syarikat utiliti dalam menentukan kedudukan pemasangan yang paling berkesan dengan bilangan minimum penangkap kilat yang digunakan dalam servis.

ACKNOWLEDGEMENTS

First and foremost, I am expressing my appreciation and praise to God for His Guidance and blessings throughout my entire study in University of Malaya. I would also like to sincerely thank my supervisors, Dr. Ab Halim bin Abu Bakar and Dr Hazlee Azil bin Illias, who have contributed a lot towards the accomplishment of my research work. Thank you for guiding, monitoring and teaching me throughout the whole duration of course.

Special thanks to my parents, Abd Halim bin Said and Noraini binti Ismail, my husband, Mohd Zarulsyafiq bin Mustafa and all my siblings, who have always provided me with their love, support and inspiration to accomplish this work.

I wish to thank Dr Hazlie bin Mokhlis of the UM Power System Research Group, who has been very supportive of me throughout my study for the PhD.

My appreciation is extended to the academic and non-academic members of the Faculty of Engineering who have been providing assistance to me in completing this work. I would also like to express my gratitude to my friends and colleagues from the faculty for their helps and ideas. You always had words of encouragement when things got tough.

TABLE OF CONTENTS

Abstract	iii
Abstrak	v
Acknowledgements	vii
Table of Contents	viii
List of Figures	xii
List of Tables.....	xv
List of Symbols and Abbreviations.....	xvii
CHAPTER 1: INTRODUCTION.....	1
1.1 Background of Study	1
1.2 Problem Statement.....	2
1.3 Objectives	4
1.4 Scope of Study.....	5
1.5 Contributions of Thesis	6
1.6 Outline of Thesis.....	7
CHAPTER 2: LITERATURE REVIEW.....	9
2.1 Lightning Flash.....	9
2.1.1 Lightning Stroke Mechanism	9
2.1.2 Breakdown Process	10
2.1.3 Lightning Flash Parameters.....	11
2.2 Overvoltages in Transmission Line System	11
2.2.1 Direct Lightning Strike.....	12
2.2.1.1 Back flashover.....	12
2.2.1.2 Shielding failure	14

2.2.2	Indirect Lightning Strike	15
2.2.3	Other Types of Overvoltages	16
2.3	Insulation Coordination of Power Systems	17
2.4	Lightning Protection by ZnO Surge Arrester	19
2.4.1	Introduction	19
2.4.2	ZnO Varistor Structure	20
2.4.3	Electrical Characteristics of ZnO Varistor	21
2.4.4	Principle of Operations of ZnO Surge Arrester.....	22
2.5	Discharge Current and Voltage Characteristics.....	24
2.6	Electric Field Distribution	27
2.7	Energy Absorption Capability	30
2.7.1	Introduction	30
2.7.2	Modeling of Discharge Energy Capability.....	31
2.7.3	Degradation of ZnO Surge Arrester	35
2.8	Lightning Current Impulse	36
2.8.1	Engineering Return-Stroke Current Models.....	36
2.8.2	Analytical Representation of Current Wave Shape.....	39
2.9	Chapter Summary	43
 CHAPTER 3: MODELING OF SURGE ARRESTER FOR DISCHARGE ENERGY DETERMINATION		45
3.1	Design Parameters	45
3.1.1	Surge Arrester Parameters.....	45
3.1.2	Analytical Representation of Lightning Impulse Current	46
3.2	Modeling of Surge Arrester	47
3.2.1	Finite Element Method.....	48
3.2.2	PSCAD/EMTDC and EMTP-RV.....	55

3.3	Chapter Summary	61
CHAPTER 4: MODELING OF 275/132 KV QUADRUPLE CIRCUIT OVERHEAD TRANSMISSION LINE.....		62
4.1	Introduction.....	62
4.2	Tower Configuration	62
4.3	Phase Conductor and Shield Wire	66
4.4	Power Frequency Voltage.....	68
4.5	Line Insulation Flashover	69
4.6	Tower Footing Resistance	71
4.7	Lightning Surge Current	72
4.8	Chapter Summary	74
CHAPTER 5: RESULTS AND DISCUSSION		75
5.1	Introduction.....	75
5.2	Energy Discharge of Surge Arrester Due to Impulse Current.....	75
5.3	Parametric Analysis Using FEA Model	84
5.3.1	Effect of the Diameter of the ZnO Blocks.....	84
5.3.2	Effect of the Height of the ZnO Blocks	86
5.3.3	Effect of the Dielectric Constant of the Insulation Layer.....	87
5.3.4	Effect of the Thickness of the Insulation Layer	89
5.3.5	Effect of the Length of the Housing Sheds	91
5.4	Flashover Performance Analysis	92
5.4.1	Effect of Power Frequency Voltage	92
5.4.2	Effect of Coupling Coefficient	98
5.4.3	Effect of Lightning Surge Current Magnitude	101
5.4.4	Effect of Tower Footing Resistance	103

5.4.5	Effect of Current Wave Front Time	105
5.5	Installation of Surge Arrester.....	109
5.5.1	Lightning Current Magnitude.....	111
5.5.2	Tower Footing Resistance	115
5.5.3	Power Frequency Voltage	119
CHAPTER 6: CONCLUSIONS AND RECOMMENDATIONS.....		124
6.1	Conclusions	124
6.2	Recommendations.....	125
References		127
List of Publications and Papers Presented		136

LIST OF FIGURES

Figure 2.1: Charge distribution on transmission line and cloud (Lucas, 2001)	10
Figure 2.2: Type of overvoltages (IEC Standard TR, 2004).....	12
Figure 2.3: Back flashover phenomenon (Ab Kadir & Cotton, 2010).....	13
Figure 2.4: The electrogeometric (EGM) model.....	15
Figure 2.5: Withstand voltages of insulation systems for various types of overvoltages (Hinrichsen, 2001).....	18
Figure 2.6: Microstructure of ZnO element	20
Figure 2.7: Simplified equivalent model of ZnO material.....	21
Figure 2.8: Metal oxide varistor conduction mechanism.....	23
Figure 3.1: Lightning impulse test waveform of 8/20 μ s.....	47
Figure 3.2: Complete geometry of surge arrester in COMSOL Multiphysics	49
Figure 3.3: Material domain.....	50
Figure 3.4: Voltage-current characteristics of the surge arrester models.....	51
Figure 3.5: Surge arrester model geometry with boundaries	53
Figure 3.6: Mesh elements in the model geometry	54
Figure 3.7: Equivalent circuit based on IEEE WG 3.4.11 (Jones, et al., 1992).....	56
Figure 3.8: Procedures for determining surge arrester parameters	57
Figure 3.9: Adjusted A_0 and A_1 characteristics of the 120 kV rated arrester	59
Figure 3.10: 8/20 μ s impulse current model in PSCAD	59
Figure 3.11: 120 kV arrester circuit simulated in PSCAD	60
Figure 3.12: Overall surge arrester equivalent circuit in PSCAD.....	60
Figure 4.1: Tower representations of 275/132 kV quadruple circuit monopole tower structure.....	65
Figure 4.2: Modified M. Ishii's tower model for a quadruple tower modeling	66

Figure 4.3: The simulated 275/132 kV line configuration.....	67
Figure 4.4: 275/132 kV transmission line modeled in EMTP-RV	68
Figure 4.5: AC power frequency voltage source in EMTP-RV.....	69
Figure 4.6: Tower footing resistance model in EMTP-RV.....	72
Figure 4.7: CIGRE lightning concave waveform (CIGRE W.G. 01, 1991)	73
Figure 4.8: Simulated lightning current waveform in EMTP-RV	73
Figure 5.1: Electric potential distribution (V) of surge arrester at different time instants from the FEA model.....	77
Figure 5.2: Simulated discharge current from FEA, PSCAD and EMTP.....	79
Figure 5.3: Simulated discharge voltage from FEA, PSCAD and EMTP	79
Figure 5.4: Simulated discharge energies from the FEA model, EMTP and PSCAD software	80
Figure 5.5: Comparison of residual voltages for different arresters' rating.....	82
Figure 5.6: Comparison of discharge energies for different arresters' rating.....	83
Figure 5.7: Discharge energy as a variation in diameter of ZnO blocks.....	85
Figure 5.8: Discharge energy as a variation in height of ZnO block.....	86
Figure 5.9: Discharge energy as a variation in dielectric constant of insulation layer ...	88
Figure 5.10: Electric field intensity as a variation in dielectric constant of insulation layer.....	88
Figure 5.11: Discharge energy as a variation in thickness of insulation layer.....	90
Figure 5.12: Electric field intensity as a variation in thickness of insulation layer	90
Figure 5.13: Discharge energy as a variation in length of housing sheds.....	91
Figure 5.14: Power frequency voltages for (a) lower voltage circuits and (b) higher voltage circuits	96
Figure 5.15: Coupling coefficient determination based on phase conductor's position	100
Figure 5.16: Effect of coupling coefficient on the flashover pattern	100

Figure 5.17: Lightning overvoltage at phase R1 for a variation in tower footing resistance 104

Figure 5.18: Lightning overvoltage at phase R1 for a variation in current front time.. 106

University of Malaya

LIST OF TABLES

Table 3.1: Physical and electrical properties of the simulated surge arresters.....	46
Table 3.2: Material properties	50
Table 3.3: Non-linear conductivity of ZnO used in FEA modeling	51
Table 3.4: Boundary conditions of surge arrester model	53
Table 3.5: Initial values of A_0 and A_I characteristics	58
Table 3.6: Linear element parameters of different types of surge arresters.....	58
Table 4.1: RL circuit parameters of quadruple 275/132kV tower model	64
Table 4.2: Geometrical and electrical data for conductors	68
Table 4.3: Geometrical and electrical data for insulator strings	70
Table 5.1: Relative error of residual voltage for a 8/20 μ s injected impulse current.....	83
Table 5.2: Flashover patterns for a variation in power frequency voltage angle ($R_f = 10$)	94
Table 5.3: Flashover patterns for a variation in power frequency voltage angle ($R_f = 50$)	97
Table 5.4: Flashover patterns for a variation in lightning stroke current (100°).....	101
Table 5.5: Flashover patterns for a variation in lightning stroke current (350°).....	102
Table 5.6: Critical lightning current (I_C) for a variation in tower footing resistance....	105
Table 5.7: Critical lightning current (I_C) for a variation in current front time (t_f)	107
Table 5.8: Flashover patterns for a variation in current front time (t_f).....	107
Table 5.9: Configuration of surge arrester	110
Table 5.10: Flashover pattern for a 122 kA lightning current.....	113
Table 5.11: Flashover pattern for a 150 kA lightning current.....	113
Table 5.12: Flashover pattern for a 170 kA lightning current.....	114
Table 5.13: Flashover pattern for a 200 kA lightning current.....	114

Table 5.14: Insulator flashovers for different lightning current magnitudes	115
Table 5.15: Flashover pattern for tower footing resistance of 10 Ω	117
Table 5.16: Flashover pattern for tower footing resistance of 20 Ω	117
Table 5.17: Flashover pattern for tower footing resistance of 30 Ω	118
Table 5.18: Flashover pattern for tower footing resistance of 50 Ω	118
Table 5.19: Insulator flashovers for different tower footing resistances	119
Table 5.20: Flashover pattern for power frequency voltage of 0°	121
Table 5.21: Flashover pattern for power frequency voltage of 70°	121
Table 5.22: Flashover pattern for power frequency voltage of 180°	122
Table 5.23: Flashover pattern for power frequency voltage of 300°	122
Table 5.24: Insulator flashovers for different power frequency voltage angles	123

LIST OF SYMBOLS AND ABBREVIATIONS

FEA	:	Finite element analysis
ZnO	:	Zinc oxide
LDS	:	Lightning detection system
V-I	:	Voltage-current
EGM	:	Electrogeometric
SW	:	Shield wire
PC	:	Phase conductor
TOV	:	Temporary overvoltage
MCOV	:	Maximum continuous operating voltage
RMS	:	Root mean square
ANNs	:	Artificial neural networks
UHV	:	Ultra high voltage
FEM	:	Finite element method
MO	:	Metal oxide
DCS	:	Distributed current source
CIGRE	:	International Council on Large Electric Systems
BIL	:	Basic insulation level
LIWV	:	Lightning impulse withstand voltage
2D	:	Two-dimensional
PDE	:	Partial differential equation
RL	:	Resistance and inductance
NT	:	No tripping
ST	:	Single tripping
DT	:	Double tripping

CHAPTER 1: INTRODUCTION

1.1 Background of Study

Lightning interference has been a major source of disturbance that causes numerous tripping on overhead transmission lines (132/275kV system) in Malaysia due to severe lightning environment (Caulker et al., 2011; Rawi & Hudil, 2010). The Malaysian Meteorological Services Department has reported that the country has a relatively high isokeraunic level up to more than 200 thunder days per year. The event, which is unpredictable and cannot be prevented, causes severe impact to the utility companies and the consumers. Lightning overvoltages may result in power outages due to failure in system equipment (Caulker et al., 2010). Meanwhile, power outages do greatly affect industrial customers in Malaysia, whereby the production is interrupted resulting in high amount of loss. Majority of the customers are demanding for a better and reliable power supply due to a more complicated production process and reliance on computer devices.

It is fundamental for the utility to analyse lightning performance of the operated lines before implementing any protection solution available nowadays. Analysis of lightning performance normally depends on how frequent an overhead transmission line is likely to be struck by lightning. The analysis is essential especially when designing new transmission line configuration and performing voltage uprating of existing line. Various studies involving lightning protection solutions have been conducted to evaluate and improve overhead transmission line lightning performance (Rawi & Hudil, 2010; Sardi, 2008). Several lightning protection solutions have been implemented to improve efficiency and reliability of the transmission line, which include earthing design enhancement, reduction of tower footing resistance and installation of shield wires (Caulker et al., 2010). However, these methods have been found to be not very

effective in minimizing the effect of overvoltage surge associated with lightning events. Installation of lightning arrester has been proven to be the optimum solution for improving transmission line reliability (Caulker et al., 2011; Wahab et al., 2003). The arrester is widely used nowadays as a protective device that maintains voltage across an insulator below insulation withstand level to reduce the possibility of flashover during transient overvoltage events.

1.2 Problem Statement

Zinc oxide (ZnO) surge arresters have been widely used nowadays in overvoltage protection of transmission line systems, particularly in the event of lightning and switching surge (Lee et al., 2010). Majority of the ZnO surge arresters have some similar basic components, but each arrester configuration varies and should be designed for each specific application. The most recently developed ZnO surge arresters are gapless due to their highly nonlinear properties which react against overvoltage in a very short period of time (Christodoulou et al., 2009). Nevertheless, previous analyses have shown that the removal of the serial gap causes the arresters being stressed by both power frequency voltage and transient overvoltage (Lee et al., 2010). Excessive voltage stressing the arresters might result in degradation of their thermal and electrical stabilities, and consequently reducing the energy absorption capability (He et al., 2007). As performance of the ZnO arresters is primarily determined by the energy absorption capability, it is necessary to further evaluate the combined effects of AC voltage stress and surge operations on their electrical, thermal and mechanical properties.

Numerous publications on degradation due to power frequency voltage stress have been found (He et al., 2009; Lee et al., 2010; Zhong et al., 2005). However, only few researches were conducted for overvoltage degradation due to lightning surges. (He & Hu, 2007; Lee & Kang, 2006). According to previous analysis, the effect of lightning

surge on the arrester life performance is more important than the effect of continuous AC voltage (Lee & Kang, 2006). During conduction mode, repeated lightning discharge duties may cause higher degradation rate of the arrester characteristics as the device needs to withstand energy discharged by the overvoltages. Severe high magnitude of discharge current will possibly result in non-uniform overheating and thermal instability of the disks, which will then cause total breakdown of the arrester.

Furthermore, recent developments related to the technology of ZnO varistors have resulted in massive design improvements of the surge arresters. However, there are still some misunderstandings on different aspects of their energy handling capabilities, which include thermal energy absorption capability and impulse energy absorption capability (Tuczek & Hinrichsen, 2014). It is crucial to evaluate the energy capabilities as most of the existing surge arresters nowadays are having higher energy rating which exceed their requirements. Over-specification of energy absorption capabilities will only result in reduction of the arresters' protective characteristics due to high residual voltage during surge events.

However, detailed experimental studies on the reliability and stability of surge arresters are usually not feasible due to high cost involved in conducting research and test using actual prototype (Seyyedbarzegar & Mirzaie, 2015). The usage of computer tools in carrying out virtual testing is important to verify the operability and performance of the arresters in early stage before proceeding with actual prototype built-up. For instance, recent development in numerical-based method such as finite element analysis has enabled the researchers to develop a replacement model in order to assess various stability problems affecting the electrical and thermal properties of the arresters (Fritz et al., 2011).

Therefore, in this work, simulation model of real dimensions of the actual surge arresters is developed to evaluate the residual voltage and discharge energy during high current conduction mode using finite element analysis method. The proposed FEA method is capable in determining electrical and physical properties of the designed lightning arrester during lightning discharge phenomena. Thus, the FEA model will enable the researchers and designers to evaluate various stability problems which affect the surge arrester operation before the actual models are fabricated.

Furthermore, it is important to determine the performance of the designed arresters on actual transmission line as cost of installing and maintaining this type of protective equipment is quite high compared to other conventional method. Hence, this study also aims to investigate design requirements and characteristics of the designed arresters in order to obtain adequate lightning protection for a specific transmission line as well as to reduce probability of failure.

1.3 Objectives

The objectives of this work are:

- i. To design a model of lightning arrester using FEA method to calculate the discharge current and residual voltage across the lightning arrester due to lightning impulse.
- ii. To evaluate variation of lightning arrester dimensions on the electric field distribution and discharge energy in the arrester using the model that was developed.
- iii. To compare the simulation results obtained from the FEA method with other computational methods and actual practical data.

- iv. To determine appropriate lightning overvoltage protection method of a 275/132 kV quadruple circuit transmission line by installing the developed surge arrester models.

1.4 Scope of Study

A series of simulations were performed to determine the energy capability of surge arresters during a single discharge operation. Different types of medium line surge arresters were simulated against a typical impulse current of wave form 8/20 μ s using FEA, EMTP-RV and PSCAD/EMTDC software. Each arrester response was then compared with measured data from the manufacturer to validate their design accuracy. The thermal energy capability is not considered in the study as the characteristics of the ZnO varistors are mainly determined by their single impulse energy handling capability, regardless of the rest of the arresters' design (Tuczek & Hinrichsen, 2014). Furthermore, the most important factor affecting the stability of the surge arresters is related to high surge energy absorptions during impulse current discharge event rather than the power frequency voltage stress (Lee & Kang, 2006).

The developed surge arrester models were then used in the next part of the work to determine lightning overvoltage performance of a 275/132 kV overhead transmission lines in the country. The quadruple circuit line, which consists of double circuits of 275 kV and 132 kV are located within an area of a town centre in Malaysia. Based on data recorded by the Lightning Detection System (LDS) from 2004 to 2011, it was found that the town centre has the highest ground flash density ranging from 35 to 40 flashes per km² per year compared to other areas in the Klang Valley.

Furthermore, the line also consists of monopole towers, which are highly susceptible to lightning strikes due to the significant height of almost 80 m. Hence, flashover performance of the dual voltage 275/132 kV transmission line needs to be determined

and analysed as it consists of quadruple circuits, which are very critical to the National Grid System. Sensitivity analyses were also conducted to investigate the influence of several parameters namely power frequency voltage, tower footing resistance and lightning surge current on the flashover pattern. The conducted study was then used in designing appropriate protection scheme to further improve the transmission line lightning performance, mainly in terms of reducing the double circuit line outages.

1.5 Contributions of Thesis

The contributions of this work are:

- i. This work provides modeling techniques of surge arresters by using finite element analysis method to evaluate the discharge current, residual voltage and discharge energy during lightning impulse current injection. The FEA method has since several years been one of the mostly preferable methods in the industry to evaluate stability problems which involve coupled simulations of electric and thermal properties. However, thorough studies which involve both experiment and simulation are conducted by the manufacturers and designers mainly on reliability and stability of an arrester due to continuous power frequency voltage stress. As the impact of lightning overvoltage is more severe on the arrester's performance, this work is useful in carrying out virtual testing to verify the discharge characteristics due to high current impulse before proceeding with new arrester fabrication. We can also determine how its physical characteristics such as the discharge energy and electric field intensity are influenced by the actual design parameters, which cannot be evaluated using electrical circuit analysis in PSCAD/EMTDC and EMTP-RV software.

- ii. This work also provides guidance in modeling of electric components of a quadruple circuit transmission line by considering propagation of lightning overvoltages. Furthermore, the conducted tripping pattern analysis of the back flashover phenomena in the quadruple circuit transmission line system is also useful for designing the line protection system which consists of shielding wires and surge arresters. The work also provides an efficient technique to mitigate double circuit line outages of the specific transmission line due to back flashover by installation of surge arrester, which could be useful for future transmission line planning.

1.6 Outline of Thesis

Chapter 1 describes the influences of lightning overvoltages on transmission line systems in Malaysia. A brief explanation is given on the insulation coordination of the systems, which emphasizes on the application of line surge arrester in lightning protection design. The chapter also presents the motivation of implementing finite element in the analysis of transient effects on surge arrester properties. The objectives of the study and the thesis's outline are provided at the end of the chapter.

Chapter 2 presents characterization of transient overvoltages stress on insulation system of transmission line. Several lightning protection approaches to mitigate lightning overvoltage impacts on the transmission line system are explained further in this chapter. Furthermore, this chapter includes literature review on previous publications which are related to the characteristics and design requirements of line surge arrester. Different analytical models of lightning surge current are described at the end of the chapter.

Chapter 3 details the modeling of ZnO surge arresters that have been developed by means of PSCAD/EMTDC, EMTP-RV and FEA method. The voltage-current

characteristics as specified by the manufacturer are used for comparative analyses of residual voltage and discharge energy of the modelled surge arresters.

Chapter 4 describes the components of insulation coordination models of the quadruple circuit transmission line system. The components which include phase conductors, shield wires, line towers, grounding system, line insulation and lightning surge current are represented based on mathematical modeling. The complete insulation coordination models were then used to simulate the line lightning performance due to back flashover in PSCAD/EMTDC and EMTP-RV software.

Chapter 5 provides explanations on the simulated surge arrester characteristics due to single impulse discharge test, which were determined from different methods. Analyses were also carried out to investigate influence of the model parameters selection on the arresters' energy discharge duties and electric field distributions. In addition, this chapter includes investigation on the application of the developed surge arresters in mitigating back flashover occurrences on the quadruple circuit transmission lines.

Chapter 6 elaborates the main conclusions drawn throughout the study. Finally, future work recommendations to further improve the study are proposed in the chapter.

CHAPTER 2: LITERATURE REVIEW

2.1 Lightning Flash

In this section, a brief explanation on the lightning mechanism and basic principle of the phenomenon are presented.

2.1.1 Lightning Stroke Mechanism

Extensive researches on the lightning phenomenon have been published in previous literature (Kasemir, 1960; Ogawa & Brook, 1964; Golde, 1977; Greenwood, 1991; Romero et al., 2014; Caicedo et al., 2016). Lightning phenomenon happens when charges accumulated in the clouds discharge into the vicinity cloud or to the ground.

Lightning is basically an electrical discharge in the form of a spark or a flash originating from a charged cloud comprises of positive charge centre and negative charge centre. Charge separation as shown in Figure 2.1 occurs when the lower part of the cloud is negatively charged with temperature of about -5°C while the positive charge is located in the upper portion with temperature of typically below -20°C . Positive charges may also be created on the ground beneath the cloud. A localized positively charged region near the base of the cloud with temperature of 0°C exists in majority of the storm clouds (Lucas, 2001). A large number of charges up to kilo-Coulombs in a volume of about 50km^3 would be generated during an average lightning event while the average current discharged by the lightning is usually in the order of kilo-Amperes.

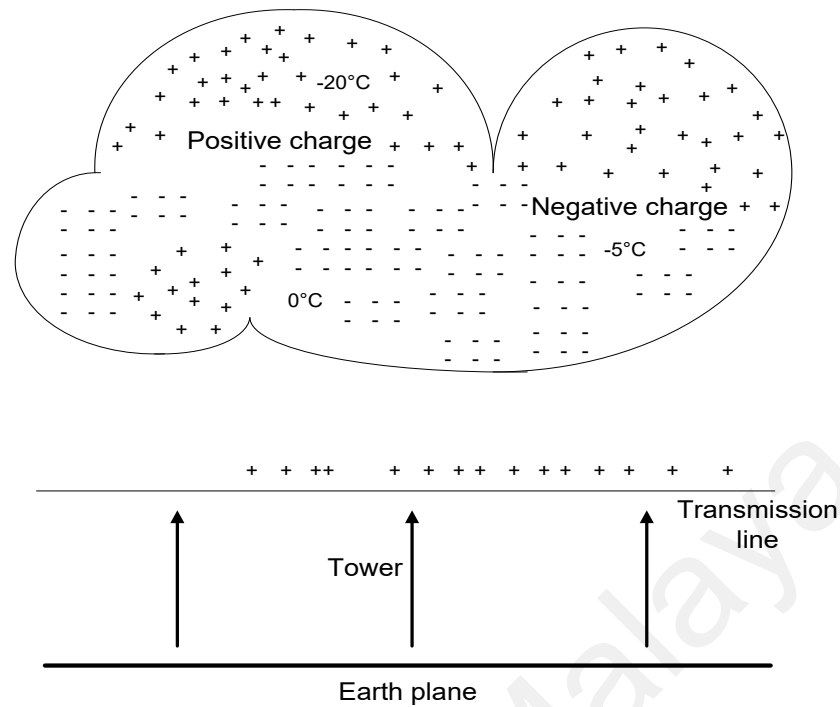


Figure 2.1: Charge distribution on transmission line and cloud (Lucas, 2001)

2.1.2 Breakdown Process

Air breakdown occurs when the potential between the positive and negative charge centres increases due to high charge separation occurrence. The breakdown occurs initially between negatively charged region and lower positively charged region. Propagation of ionised channel or also known as streamer happens for only a short distance from cloud to earth. The stepped leader stroke event, which is caused by sequence propagation of multiple streamers travels toward ground surface. An upward streamer is then induced as the field intensity is sufficiently high, resulting in large current flows along the ionised path in order to neutralize the charge. The current flow is named the return stroke, which may consist of crest current magnitude value of more than 200 kA. After the first stroke terminates, second leader stroke propagates to ground surface in a continuous and rapid manner, resulting in a return stroke. The second and following leader strokes are called dart leader strokes. A breakdown or lightning flash

event discharges a large amount of current that may cause transmission line tripping and outage (Lucas, 2001).

2.1.3 Lightning Flash Parameters

Lightning parameters are considered as the major concern in the design of lightning protection equipment to minimise transient overvoltage effects on transmission line.

The parameters are inclusive of:

- i. the crest current of the first and subsequent strokes
- ii. the wave shape of the stroke current
- iii. correlation between the parameters
- iv. number of lightning strokes per flash
- v. ground flash density

The return stroke magnitude and the stroke charge volume are the most significant parameters in investigating the severity of lightning strike terminating on the overhead transmission line system (Chowdhuri et al., 2005).

2.2 Overvoltages in Transmission Line System

Insulation systems of an AC transmission line system are normally subjected to various types of electrical stresses, which include system voltage under normal operating conditions, lightning overvoltages, temporary overvoltages and switching overvoltages, as illustrated in Figure 2.2 (IEC 60071-1, 2006).

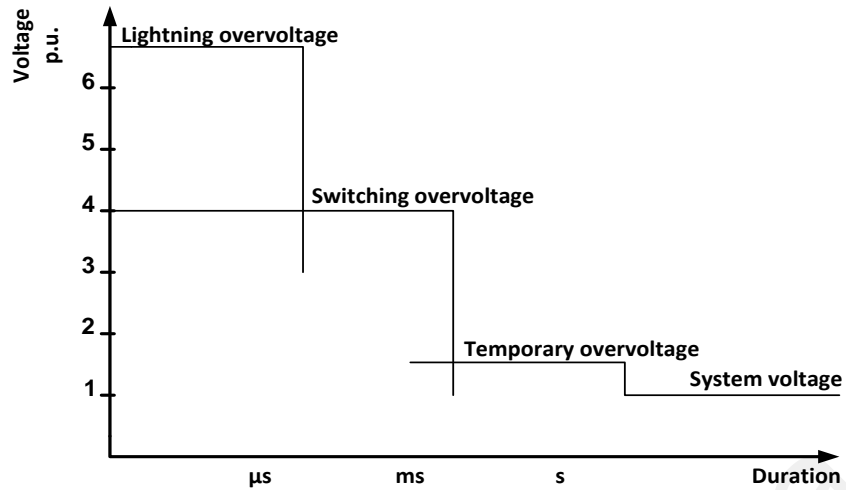


Figure 2.2: Type of overvoltages (IEC Standard TR, 2004)

2.2.1 Direct Lightning Strike

Direct lightning strike terminating on the transmission line may result in the event that interrupts the power system, such as over voltage. The lightning over voltage is regarded as the major cause of the line insulation flashover, which can be divided into three types namely back flashover, shielding failure and induced overvoltage.

2.2.1.1 Back flashover

Previous researches have shown that the back flashover phenomenon is more prominent in insulation system of overhead transmission line rather than shielding failure (Okabe et al., 2011; Bakar et al., 2011; Han et al., 2012; Sarajcev, 2015). In order to reduce the impact of lightning strokes termination on the phase conductors, overhead shield wires are normally installed at top of the tower. Hence, shielding failure occurrences are less likely to occur when the strokes terminate on the shield wire.

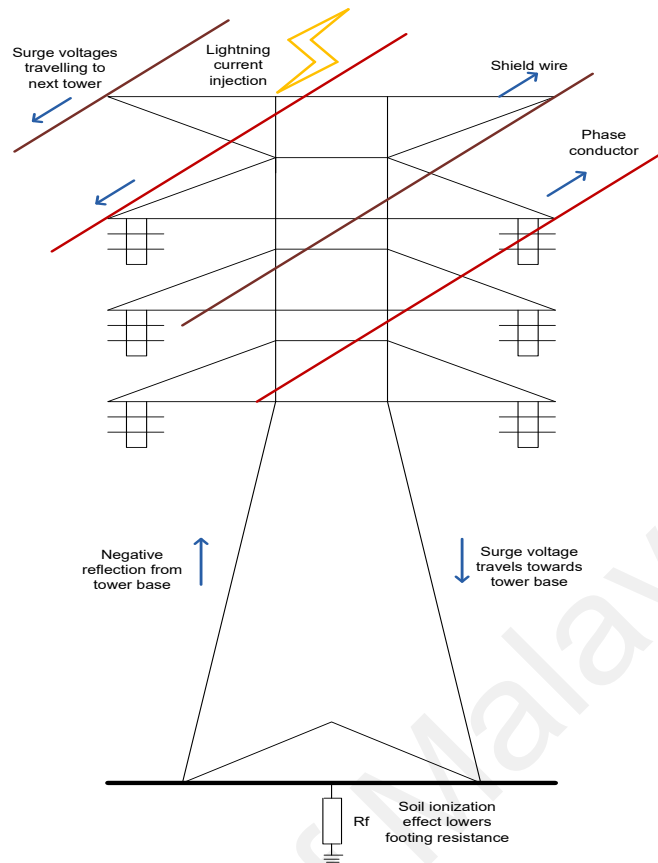


Figure 2.3: Back flashover phenomenon (Ab Kadir & Cotton, 2010)

Back flashover occurs when lightning strikes a shield wire or tower top as depicted in Figure 2.3. Part of the surge current will flow to the adjacent towers via the shield wires, while another part of the resulting travelling wave will propagate down the struck tower to the ground. The effective surge impedance of the tower will cause the travelling wave to be reflected to the tower top and the phase conductors. Consequently, this will increase the potential of the tower top while decreasing the potential across the line insulation. The voltage difference between the phase conductor and the cross arm must exceed the line critical flashover (CFO) voltage in order to cause flashover from the tower back to the conductor. The surge current, which creates transient voltage on the phase conductors, will also travel to the end of line substation. Hence, improper insulation coordination design will definitely cause damage to the connected equipment.

2.2.1.2 Shielding failure

Shield wires are normally used as one of the conventional methods in protecting the overhead transmission line against direct lightning strikes. The wires are installed directly at the top of the towers in order to prevent the phase conductors from direct lightning termination. If the shield wires fail to intercept the stroke from terminating on the conductors, a short circuit to ground fault might occur which will possibly result in severe line outage (Datsios et al., 2014).

To further analyse the transmission line protection design by means of shield wire, a simplified concept of the electrogeometric (EGM) model is employed. The EGM model was constructed based on the striking distance concept. In the case of equal striking distances to all shield wires, phase conductors and ground plane, the stroke current will probably terminate on the closest object. However, the striking distances are normally treated as unequal and hence some calculations are needed to determine the accurate striking point. The striking distance is formulated by Equation (2.1).

$$r = Ai^b \quad (2.1)$$

where A and b are the constant, which depends on the strike object, i.e. the phase conductor, shield wire, or the earth plane and i is the stroke current in kA.

Figure 2.4 depicts the general model of phase conductors and shield wires of overhead transmission line for a specific value of stroke current. The arcs of the circles with radius of r_c are drawn at the center of both the phase conductors and the shield wire. The radius, r_c is known as a striking distance. A horizontal line is also constructed in parallel to the earth plane at height of r_g . In insulation coordination design, the shield wire location is normally specified by the shielding angle, δ . A horizontally disposed shield wire beyond the phase conductors will result in a negative value of shielding angle. Downward leaders approaching the transmission line with a potential stroke

current will develop the arcs. The developed arcs, which reach the arc between B and C will then terminate on the shield wire (SW). Meanwhile, the arcs which reach the arc between A and B will terminate on the phase conductor (PC). The rest of the arcs which are beyond A will terminate on the earth plane (CIGRE W.G. 01, 1991).

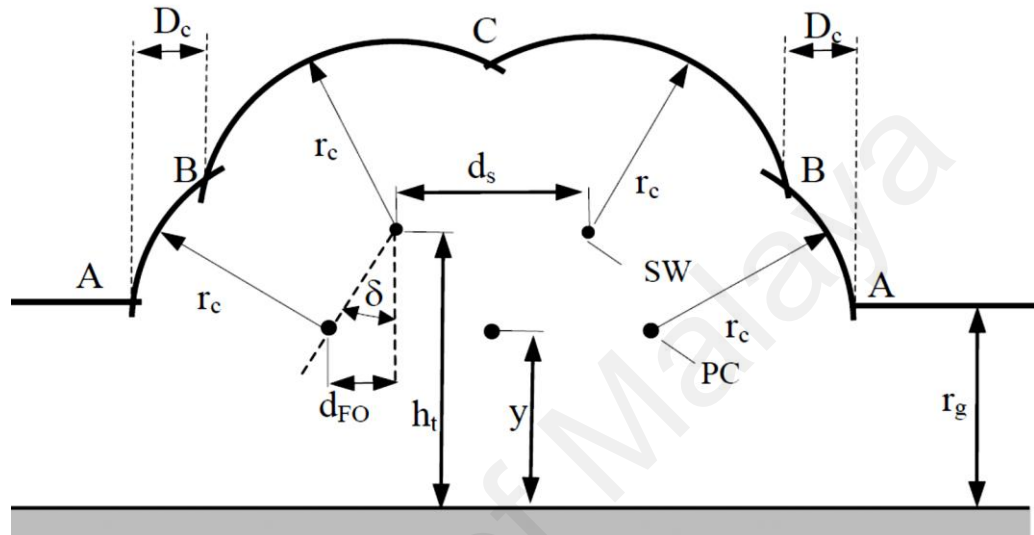


Figure 2.4: The electrogeometric (EGM) model

2.2.2 Indirect Lightning Strike

Induced overvoltage event occurs when a cloud-to-ground lightning flash generates a transient electromagnetic field, which consequently induces a significant surge voltage on overhead lines in the vicinity. The lightning-induced overvoltage is responsible of the majority of faults occurring in distribution overhead lines (Borghetti et al., 2007). However, these induced voltages have negligible effect on high-voltage transmission lines. The voltage induced on a transmission line affected by an indirect lightning stroke normally consists of four main aspects which are (Chowdhuri et al., 2001):

- i. Bound charges are induced on the line due to the presence of the charge cloud above the line. Meanwhile, the neutrals of connected transformers

and the insulators' leakage cause the line to be held electrostatically at ground potential. The bound charges are released when the cloud is either partially or fully discharged. The charges will then travel in both directions on the line and consequently results in increasing magnitude of the travelling voltage and the current waves.

- ii. The charges lowered by the stepped leader results in further charges induction on the line. The bound charges on the line will be released due to the neutralization of the stepped leader by the return stroke. Therefore, travelling waves will be produced which exhibit similar properties to that caused by the cloud discharge.
- iii. The residual charges on the upper component of the return stroke current generate an electrostatic field surrounding the overhead line and consequently inducing voltage on it.
- iv. A magnetically induced voltage is produced due to the rate of change of the current in the return stroke. In the case of a lightning which consists of subsequent strokes, the subsequent parts of the induced voltage will be comparable to the four components previously described.

2.2.3 Other Types of Overvoltages

Temporary overvoltages are normally different from switching overvoltages in term of longer time durations, typically from a few cycles to a few seconds. The temporary overvoltages behave like undamped or slightly damped oscillations at a frequency close to the normal power frequency. There are three main causes of this type of overvoltage, which include earth faults, load rejection as well as ferroresonance and resonance. Characterization of the temporary overvoltages severity is mainly done based on their maximum values and durations. It is important to analyse the temporary overvoltages in insulation coordination as this type of stress is crucial for determining appropriate surge

arrester selection and placement. Furthermore, the repetition of successive temporary overvoltages with opposite polarity can be used to determine appropriate design of internal and external insulation of particular equipment.

Meanwhile, a rapid surge voltage in the form of travelling waves is generated when a sudden change occurs in the configuration of the electrical transmission network due to the operation of a circuit breaker or sudden appearance of a fault (Samitz et al., 2002). This type of overvoltage known as switching surge overvoltage is normally caused by specific switching operations due to:

- i. line energisation
- ii. energisation of a line with trapped charges (reclosing)
- iii. low voltage side energisation of a line
- iv. energisation of a line terminated by an unloaded transformer
- v. load rejection at the receiving end of a line followed by line dropping at the sending end

2.3 Insulation Coordination of Power Systems

The selection of dielectric strength of equipment in power systems related to the voltage which can appear on the system is known as insulation coordination. A good insulation coordination study considers the necessary insulation characteristics of the equipment in order to obtain uniform normal operating voltage and to provide sufficient protection level against overvoltage stresses. Furthermore, proper insulation design is needed to ensure reliable and optimum distribution of electrical power by reducing the insulation failures and preventing over specifying of the equipment. The optimized insulation design is determined based on the best possible economic balance which depends on the following aspects:

- i. cost of insulation
- ii. cost of protective device
- iii. cost of equipment failures

The initial step in minimizing the harmful effects of overvoltage stresses is by determining the origins of the phenomena. The next step is to locate the point at which the current generated from the overvoltage will possibly flow, before installing protective device with high dielectric withstand at all the other network equipment.

In general, the lightning overvoltages withstand capability of all insulation systems is normally greater than that of switching and temporary overvoltages, as depicted in Figure 2.5. Therefore, this type of overvoltage is regarded as the major risk affecting the power system reliability due to the severity of the generated surge current. In order to accurately analyse the impact, it is crucial to determine the voltage-time characteristics of the lightning overvoltages as they exhibit great influence on the insulation coordination (Ancajima et al., 2010; Chowdhuri et al., 1997).

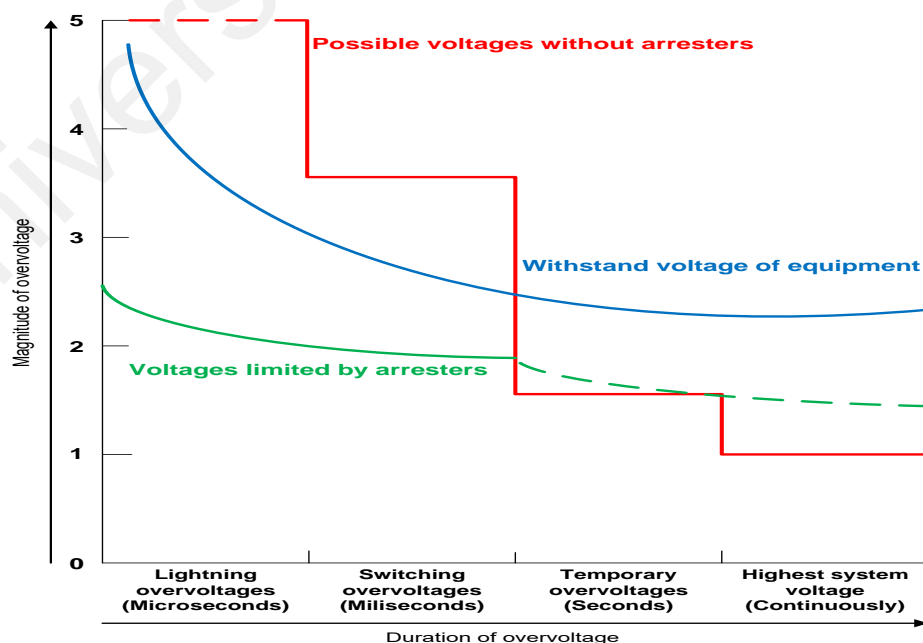


Figure 2.5: Withstand voltages of insulation systems for various types of overvoltages (Hinrichsen, 2001)

On the other hand, switching overvoltages with positive polarity exhibit the lowest withstand voltage of air insulation systems. The distance between electrodes and time to crest of the switching surge waveform normally determines the minimum value of the flashover voltage. Great consideration should be given on the critical withstand voltage particularly in coordination of high voltage insulation systems. The insulation withstand voltage of electrical power network is basically determined by a certain value of critical voltage. If the generated surge voltage across the insulation system exceeds the critical withstand voltage, a flashover might occur which will then result in breakdown of the power network.

2.4 Lightning Protection by ZnO Surge Arrester

2.4.1 Introduction

Lightning and switching overvoltage are regarded as the main factors contributing to insulation system failure in electric power systems. Any equipment failure must be avoided to ensure the overall system reliability. Hence, a protective measure by installation of ZnO surge arrester has been widely practiced nowadays to minimize the overvoltage impact. The protective device, which is usually installed between phase and earth acts as an insulator during normal operating conditions. It reacts to overvoltage by diverting surge current to the ground and limit surge voltage on the system. The arrester develops a residual voltage across its terminal, which is a function of the magnitude and wave shape of the discharge current wave, arrester design and voltage rating. After discharging the high magnitude of surge current, the correctly installed surge arrester must return to its steady state condition with its initial V-I characteristics restored.

It is important to further understand behavior of any ZnO surge arrester when it is stressed by overvoltages with different wave shapes and amplitudes. Although most of the surge arresters consist of the same basic component, it is crucial to design them according to their specific configuration and application. Proper selection of a line surge

arrester is beneficial in providing the optimum solution to major lightning problems and resulting in economical installation cost.

2.4.2 ZnO Varistor Structure

Zinc oxide varistor is the main component in a surge arrester, which represents the protective characteristics. The ZnO varistor is normally in the form of a densely sintered block, pressed to a cylindrical body. The block primarily comprises of a high nonlinear resistance material, namely zinc oxide and mixed with other material additives. Conductive ZnO grains are separated by boundaries forming semiconductor junctions, which is comparable to principle operation of a back-to-back Zener diode (Levinson & Philipp, 1977).

The ZnO varistor microstructure (microvaristor) is correspondent to combinations of a group of semiconducting diodes connected in series and parallel, resulting in the electrical characteristics. Figure 2.6 depicts the microstructure of zinc oxide element. To ensure high energy and surge current absorption capability, each microvaristor is provided with energy absorbers in the form of grains with good thermal contact. A simplified equivalent model, which represents the ZnO material in the form of electrical components, is illustrated in Figure 2.7.

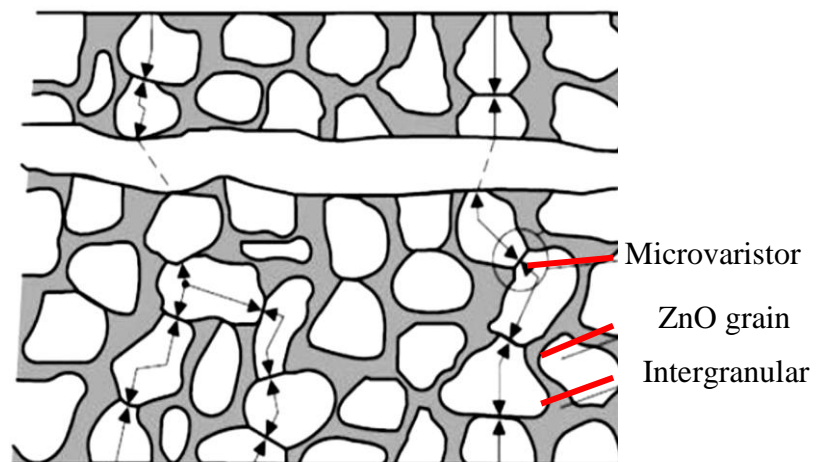


Figure 2.6: Microstructure of ZnO element

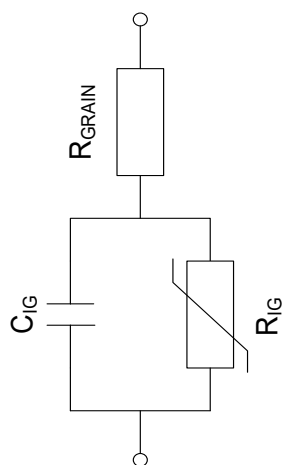


Figure 2.7: Simplified equivalent model of ZnO material

The circuit consists of $R_{\text{IG}}-C_{\text{IG}}$ parallel circuit which is connected in series with another resistor, R_{GRAIN} . R_{IG} represents a highly nonlinear resistor with increasing voltage while C_{IG} is a capacitance representing the nonlinear behavior of intergranular layers of ZnO element. The resistance of the conducting ZnO grains is represented by R_{GRAIN} . However, the small value of the ZnO grains capacitance is assumed to be insignificant and can be omitted from the simplified circuit. Furthermore, the series inductance, which represents the arrester body inductance, is only considered in the case of steep response currents.

2.4.3 Electrical Characteristics of ZnO Varistor

The most important parts of surge arresters are the cylindrical zinc oxide varistor blocks, which exhibit ideal non-linear V-I characteristics. The varistor blocks, which mainly comprise of ZnO material exhibit high energy absorption capability due to the polycrystalline nature and large amount of intergranular barriers. A reliable ZnO varistor must be capable of sustaining its original V-I characteristics during normal operating condition and after discharging high energies due to transient surges. The discharge current and voltage dependency of the ZnO varistor can be approximated by the power law equation:

$$I = k \times V^\alpha \quad (2.2)$$

where I is the discharge current through varistor blocks, k is the ceramic constant depending on the varistor element, V is the residual voltage through varistor blocks and α is the nonlinear exponent of the V-I characteristics curve; variable between $\alpha \leq 50$ and $\alpha \approx 50$.

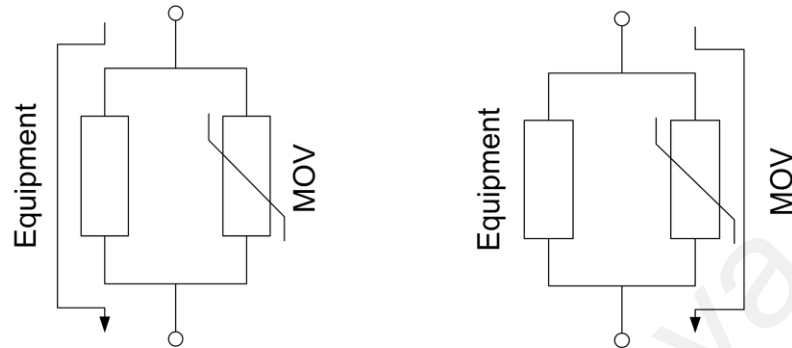
A typical varistor normally has a linear V-I characteristic with the value of α equals to one. Generally, increasing the value of α will cause the V-I characteristics to approaching the ideal value. The exponent α normally reaches a maximum value of about 50 in the temporary overvoltage (TOV) region and decreases to about 7 to 10 in the lightning overvoltage region (Hileman, 1999).

2.4.4 Principle of Operations of ZnO Surge Arrester

Zinc oxide surge arresters are normally installed closely to the equipment being protected from rapid and high magnitude of surge current. The principle of operations during both normal operating voltage and under surge overvoltage are illustrated in Figure 2.8(a) and Figure 2.8(b). During normal operating condition, the ZnO surge arrester is considered to be open circuited due to very high impedance of up to several mega Ohms. Consequently, the current will flow through the protected equipment circuit path (i.e. insulator string) instead of through the surge arrester.

During the occurrence of surge overvoltage, the impedance of the ZnO surge arrester will decrease to a small value of few Ohms to prevent high current passing through the protected equipment. After completely discharging the surge energy, the arrester will then return to its normal high impedance with its original characteristics restored. The main advantage of the ZnO varistor is that the nonlinearity of its V-I characteristics would eliminate the power follow current flowing through the arrester after completion

of the discharging event. Hence, the residual voltages developed across the surge arrester due to high surge currents can be reduced.



a) under normal operating voltage b) under surge overvoltage

Figure 2.8: Metal oxide varistor conduction mechanism

In addition, initial selection of zinc oxide surge arrester needs to take into account on the type of equipment to be protected, the location and environment of the equipment and the expected function for the arrester. Selection procedure of a ZnO surge arrester is done based on various rating parameters of the varistor. The voltage rating is selected by first determining the nominal steady state voltage of the system. This nominal line to ground voltage takes into consideration any overvoltage factor that may occur on a continuous basis.

The voltage level in which the arrester will expose over most of its life is about 5% above the nominal line to ground voltage. It is necessary to ensure that the maximum continuous operating voltage (MCOV) must be equal or greater than the specified voltage. The MCOV is defined as the maximum permissible root mean square (RMS) value of the normal power frequency voltage that may be continuously applied between the high voltage and grounded terminals of the surge arrester. Furthermore, the selection

criteria must also consider temporary overvoltages that can occur on other unfaulted phases of a system when a fault occurs on different phases.

2.5 Discharge Current and Voltage Characteristics

A proper design of surge arrester model is important before evaluating their effectiveness in minimising the impact of overvoltage on transmission line. For instance, the surge arrester's failure probability due to lightning surge is normally determined by theoretical computation. Hence, accurate representation of the surge arrester is needed, as the arrester possesses dynamic properties which are significantly dependent on the impulse current. According to previous literatures, great emphasis has been given on the arrester's electrical parameters design by using circuit simulation software such as PSCAD/EMTDC and EMTP-RV.

Christodoulou et al. conducted a study on different types of frequency-dependent surge arrester modeling by using electrical circuit representation in PSCAD software (Christodoulou et al., 2010). Analyses were carried out on the residual voltage and the absorbed energy due to impulse current injection for each model. The simulation results obtained were then compared with measured data. Dynamic models were also proposed in this study, which successfully represent actual properties of the surge arrester. The developed models were then used to determine the installed arresters' failure probability of a 150 kV transmission line. The simulated dynamic models have successfully reproduced the nonlinear behavior of the surge arrester, which can be used to estimate the line lightning performance.

Nafar et al. proposed a novel method based on the combination of PSO and ACO algorithms to determine the parameters of surge arrester models (Nafar et al., 2011). The proposed optimisation algorithm was computed in MATLAB and EMTP software. The parameters used in the computation were estimated based on actual residual voltage

measurement obtained from datasheet. The results indicated that the proposed algorithm was capable in estimating parameters of different type of arresters, in which the simulated peak residual voltages were in good agreement with the actual measurements. The proposed method novelty lies in its ability to estimate the parameters without involving any mathematical formulation or actual arrester's dimensions.

Evaluation of surge arrester's circuit parameters was also conducted by Christodoulou et al., by utilizing Powell's optimisation method (Christodoulou et al., 2010). The main contribution of the study lies in its ability to compute the residual voltage obtained from the equivalent circuit models, which produces small deviation from the actual manufacturer measurement. Reduction in the difference between the simulated and experimental values proved that the proposed optimisation method has successfully reproduced the frequency dependent behaviour of the modeled surge arresters. It was found that the IEEE model results in the lowest relative error as compared to other arrester's equivalent circuit due to complexity in determining the parameters. However, the method requires longer iteration time in order to obtain the final optimised parameters.

Christodoulou et al. also proposed a method to determine accurate arrester equivalent circuit models parameter, which uses artificial intelligence techniques as basis (Christodoulou et al., 2011). Genetic algorithm was developed in order to optimise the defined objective function, mainly to reduce the error between the calculated value and the manufacturer's data in term of discharge voltage due to lightning and switching impulse current. The main contribution of the proposed algorithm lies in its capability in adjusting the parameter values of each circuit model simultaneously for different peak discharge values and waveform. By considering a wide range of the parameter values, this method produces more accurate results as compared to other proposed optimisation

methods such as Powell and Downhill methods. Furthermore, the developed algorithm extracts the best solution that minimise the objective function by examining the local minima and analysing the possible combinations of the parameter values for each model. The proposed algorithm is also less complex as compared to other optimisation methods as the user is allowed to define the desired accuracy and the speed of the simulation.

Genetic algorithm method was also proposed by Dobrić et al. to evaluate surge arrester equivalent circuit parameters (Dobrić et al., 2015). By estimating the parameters based on the manufacturer's datasheet, voltage-current characteristics were derived purposely to assess the surge arrester's performance. The proposed algorithm in this study uses actual practical measurements of the normal operating voltage and the leakage current. The IEEE model was not considered in this study as the proposed genetic algorithm was developed mainly for the analysis of surge arrester during continuous power frequency voltage condition. The simulated results indicated that the proposed algorithm has insignificant effect on the operating voltage harmonics and possesses a very low sensitivity of algorithm dynamics. The accuracy of the proposed method was also validated by performing tests on actual surge arrester in laboratory conditions. The main contribution of the proposed method lies in its capability in separating the resistive and the capacitive component of the leakage current, which is useful for arrester diagnostic methods.

However, the previously proposed methods which normally utilised PSCAD/EMTP and EMTP-RV as basis of simulation are not capable in evaluating electrical and physical properties of the surge arrester such as electric potential distribution and electric field intensity. Furthermore, the modeling in the PSCAD/EMTDC and EMTP-RV only involves electrical circuit representation of the arrester, in which the

difficulties arise when determining the lumped parameters and non-linear resistance characteristics of A_0 and A_1 . Hence, a more accurate modeling using FEA method is proposed in this work, which is capable in representing real dimension and actual material properties of the surge arrester rather than the electrical circuit representation.

2.6 Electric Field Distribution

The most recently developed ZnO surge arresters do not require serial gaps owing to their excellent nonlinear properties, which react against overvoltage in a very short period of time (Christodoulou et al., 2009). Nevertheless, the removal of the serial gap causes ZnO disks being continuously stressed by AC power frequency voltage (Lee et al., 2010). According to previous analysis, the AC voltage stress may cause degradation in thermal and electrical stability of a ZnO surge arrester. Stray capacitance to earth is the main factor of the unequal potential distribution during non-conduction mode, where capacitive current flows more on the upper part of the arrester than the lower part. Hence, uniform potential distribution of ZnO disks must be given a priority in design consideration of a lightning arrester to reduce probability of failure. To increase the uniformity of the electric potential distribution, optimization of the electric field intensity around the surge arrester is needed. The optimized distribution of the electric field will reduce the voltage stress on the insulation housing which will then increase service life span of the surge arrester.

Numerous researches related to surge arrester electric field magnitude calculation have been published. Han et al. describe the formulation of semi-analytic finite element method to determine potential distribution of high voltage metal oxide arrester (Han et al., 2005). Formulated based on the standard finite element approach with slight improvements, the method is capable of solving unbounded axisymmetric electric field problem. The method is also capable of eliminating high-order harmonics instability,

which is due to utilization of a point match technique. In order to reduce the complexity of computations, the radius of the artificial boundary is also excluded in the functional expression. Verification of the proposed method was made by calculating the electric potential distribution along a 330 kV ZnO arrester. Comparison made between the computed results and the measured results indicates that the maximum deviation errors are only about 3%.

Meanwhile, Haddad & Naylor computed electric potential and field distribution of a typical polymer zinc oxide surge arrester by means of finite element method (Haddad & Naylor, 1998). The calculated electric field magnitudes were then used to determine equivalent capacitance network of various electrode configurations. The reduced equivalent capacitance network was then simulated using circuit simulation software (SPICE) to determine the electric potential distribution across the arrester during normal power frequency voltage. The results indicate that the electric potential distribution calculated from the capacitance network is in good agreement with the electric potential distribution obtained from numerical computation.

Ekonomou et al. have formulated an artificial neural networks (ANNs) based method, which could be useful in determining electric field distribution of medium voltage surge arresters for design processes and diagnostic tests (Ekonomou et al., 2014). Laboratory experiments were conducted on a medium voltage metal oxide surge arrester to measure the actual electric field distribution. The measured electric field was then used to validate the accuracy of the proposed ANNs method. The ANN models with the best generalising abilities are selected based on the tests carried out on transfer functions, learning algorithms and several structures of the ANN multi-layer perceptron network.

He et al. have proposed a combination of electric circuit and electric field method in order to analyze electric potential distribution of suspended-type metal oxide surge arresters (He et al., 2003). A charge simulation method, matrix transformation and electromagnetic field theory were used to obtain the equivalent electric circuit. The complexity of the electromagnetic field problem of the potential distribution was reduced by converting it to an equivalent electrical circuit. Finally, the electric potential distribution was calculated based on the equivalent circuit analysis by the use of Kirchoff's first law. The analytical results are comparable with the conducted experimental results. To further validate the proposed method, the potential distributions of the surge arresters in various installation conditions were also examined.

Several studies had presented methods to minimize the electric field intensity of surge arresters during normal operating conditions. He et al. discussed their findings on the electric potential distribution of an AC 1000 kV ultra high voltage (UHV) metal oxide surge arrester (He et al., 2003). The study had focused on analysing and improving the electric potential distribution of the UHV surge arrester by the application of three different approaches; field-circuit combination, three-dimensional (3D) finite element method (FEM) and circuit analysis. The 3D method which involves numerical computation of the quasi-static field was employed to determine the stray capacitances and potential distribution of the UHV surge arrester. Both calculated values were then used to obtain the equivalent circuit of the UHV surge arrester. In order to improve the electric potential distribution coefficient within 5%, parallel capacitors are then added to the UHV surge arrester. Furthermore, the dependencies of electric field intensity and potential distribution on the mounting height and grading ring of the surge arresters were also investigated.

Meanwhile, Kumar & Mogaveera had attempted to improve the voltage distribution uniformity of a 220 kV and a 400 kV surge arresters under clean and polluted environment by means of numerical field computation (Kumar & Mogaveera, 2002). In their study, design optimization of the surge arresters' geometries, which include grading ring and spacers was conducted in order to investigate their influence on the voltage distribution under normal operating conditions. The maximum voltage gradient for all cases was observed at the top of the surge arrester under clean environment. Increasing the cross sectional diameter of the grading ring significantly reduces the maximum voltage gradient. Furthermore, significant decrement on the voltage gradient was observed when the spacers were placed at the bottom of the ZnO cylindrical column. It was found that varying the base height and the diameter of the ZnO cylindrical column does not significantly affect the voltage gradient for a range of variation. Meanwhile, the voltage gradient was not uniformly distributed under both uniformly polluted and dry environments.

2.7 Energy Absorption Capability

2.7.1 Introduction

A line surge arrester is normally dimensioned based on two main aspects, which are protection against overvoltages and reliability of service. It must be designed in such a way that it can withstand the energy without failing and causing problems to the transmission line system, while uneventfully diverting the surge current to the ground at abnormal conditions, such as back flashover. In addition, the arrester must be able to cool down quickly after the energy absorption as the prolonged heating will damage the element of the arrester (He & Hu, 2007).

Energy absorption capability of a line surge arrester is defined as the amount of energy that a varistor can absorb without failure (Bartkowiak et al., 1999; Bartkowiak et al., 2001; Stockum, 1994). It can be classified into two common groups, which are

thermal energy absorption capability and single impulse energy absorption capability. The thermal energy absorption capability is defined by the maximum amount of energy that can be absorbed by an arrester in the form of several subsequent discharges within a short time interval, without leading to thermal instability. The thermal energy capability is usually greater than the single impulse energy handling capability.

Meanwhile, the single impulse energy capability is defined as the maximum absorbable energy of an arrester during a single discharge operation. Besides some other influencing factors, it is mainly limited by the maximum allowable thermo-mechanical stress on the ceramic of the ZnO varistors. If this energy value is exceeded thermo-mechanical breaking or flashover of the ZnO varistor may occur. The single impulse energy handling capability is usually smaller than the thermal energy handling capability.

2.7.2 Modeling of Discharge Energy Capability

Several researches concerned with measurements and discussions on the energy absorption capability of ZnO varistors have been published. Ringler et al. have successfully demonstrated the energy absorption capability as a function of current magnitude by carrying out destructive tests on various varistors used in station class surge arrester (Ringler et al., 1997). In all cases, it was found that the energy absorption capability increases significantly with the increase in the current magnitude of kilo-Ampere range. The study also presented a significant data on the failure modes of the tested varistors with respect to the applied current. It was shown that the logarithm of the mean time-to-failure shows a linear dependency with the logarithm of the mean varistor current over a range of five orders of magnitude.

The dependencies of the applied impulse current, nonuniformity of microstructure, and nonuniformities of electrical and thermophysical properties on the energy

absorption capability of ZnO varistors have been investigated based on experiments and numerical simulations (He & Hu, 2007). The experimental results show that the measured energy absorption capabilities scatter extremely according to the time duration and the current density of the applied impulse current. It was also found that the absorbed impulse destruction energy is not linearly increasing with the increment of the varistor surface area due to the nonuniformity in the microstructure of varistor and the nonuniformity of absorbed energies in different segments inside the varistor. Furthermore, the numerical simulations indicate that the microstructural nonuniformity of ZnO varistors leads to current and energy concentration, which in turn decreases the overall energy absorption capabilities.

Petit et al. has described an experimental approach to determine a coupled electro-thermal model of metal oxide varistor elements (Petit et al., 1991). Firstly, electrical heat production from the varistor elements was determined by computing watt-losses from voltage-current-temperature characteristic of the studied arrester. Next, single high-energy discharge based on linear system analysis and least-squares minimization curve fitting was then used to determine the thermal parameters. The precision of the complete electro-thermal model was then quantified by a sensitivity analysis. According to the individual parameter study, the most critical value that must be measured with high precision in the laboratory is the voltage parameter, which sensitivity is mainly affected by extreme non-linearity of the metal oxide varistor elements.

Different aspects concerning impulse energy handling capability of metal oxide (MO) varistors for use in high voltage surge arresters have been extensively discussed in (Bartkowiak et al., 1999). Various kinds of stresses which include single impulse stress, double impulse stresses and repetitive impulse stresses were tested to determine up to which extent the energy level that can be withstand without pre-damaging the MO

varistors. According to the findings, the single impulse energy handling capability per unit volume decreases with the increase in the diameter of the MO varistors. This phenomenon was assumed to be originated from higher inhomogeneity of the metal oxide element at larger diameters. In the case of multiple long duration current impulse stresses, the study has proven that the energy contained in the two impulses must be summed up and considered as one single-energy injection event. Finally, it was found that the injected energy varies for different current densities in the case of repetitive impulse stresses. For equivalent amount of energy injections, higher current density of the impulse current results in lower energy that can be injected without pre-damaging the MO varistor. It was also proven that the energy withstand capability of the MO varistor due to repeated energy injections under ac stresses is close to the single-impulse energy handling capability.

Boggs et al. described the formulation of a transient nonlinear finite element model for investigating the electro-thermal phenomena, which cause deterioration at the electrode edge of the surge arrester (Boggs et al., 2000). In this case, the effect of the electro-thermal phenomena was reduced to obtain maximum energy absorption in the tested ZnO elements by controlling the electrode topology. The electrode was designed in such a way that the ZnO elements will heat uniformly to its maximum stable operating temperature in the range of 550°C. By controlling the electrode edge margin and improving the material uniformity, the hot regions within the ZnO arrester will be minimized, which will result in more uniform power dissipation throughout the material. It was found that the energy absorption capability of the tested ZnO elements has been improved by 50%, to the point that high gradient elements can be utilized in producing single-column, metal-enclosed high voltage arresters for application in gas-insulated substations. The arresters comprise only about 40% of the weight and volume

of a standard metal-enclosed arrester, and thus resulting in significant reduction of cost and materials usage reduction as well as structural complexity.

Significant findings on failure mechanisms of ZnO varistors and their influences on the energy absorption capability have been presented by Bartkowiak et al. (Bartkowiak et al., 1996; 1999; 2001). Investigations on thermal and mechanical properties of high voltage ZnO surge arresters have been performed by simulating various magnitude and duration of current impulses. The time dependence of the temperature profile and the distribution of thermal stresses were then determined based on numerical computation of heat transfer equations. The results show dependencies of the energy handling capability of varistor elements on the applied current intensity and duration. Failure mechanisms of the varistor elements such as puncture, thermal runaway, cracking under tension, and cracking under compression were also identified from the simulations. Furthermore, the effects of electrical nonuniformities of metal oxide varistor disks on the energy handling capability have been investigated thoroughly in the study. The electrical nonuniformities are caused by the localization of the current in the breakdown mode, which in turn causes local heating that may lead to nonuniform thermal expansion and thermal stresses.

It was found that failure due to cracking becomes more likely as the hot spots are larger, and thus increasing the degree of nonuniformities of the disks. Meanwhile, failure due to puncture happens for only disks with a slight nonuniformity. In order to minimize the possibility of metal oxide varistor disks' failure, improvement on the energy handling capability at high current has also been made by adjusting the resistivity of the element in the upturn region (Hileman, 1999).

2.7.3 Degradation of ZnO Surge Arrester

A ZnO surge arrester must possess excellent nonlinear V-I characteristics, which is capable of withstanding high electrical stresses due to surge overvoltages before returning to its normal operating condition. However, the V-I characteristics may experience degradation resulting from the effects of various electrical and thermal stresses and environmental pollution. Degradation due to the thermal stresses is normally caused by the effect of high energy surge discharge, which results in increased temperature of the ZnO varistors. Furthermore, the effect of solar radiation and environmental pollution on the surge arrester housing may also contribute to the thermally effected degradation. Meanwhile, degradation due to the electrical stresses is normally caused by the effects of lightning discharge, switching operation and temporary overvoltages (Vipin et al., 1991).

Previous researches have shown that the degradation greatly influences the pre-breakdown region of the nonlinear V-I characteristics, which in turn produces higher leakage current through the surge arrester. Since the pre-breakdown region is grain boundary controlled, the degradation is regarded as a grain boundary related phenomenon. The microstructure of a stressed ZnO element will be changed when it is preheated to certain temperatures. The change which is dependent on its previous degree of degradation mainly affects its capacitive and resistive characteristics (Sargent et al., 1991).

Further degradation may damage the ZnO varistors, which can be determined from cracks on the ZnO surface or defect surfaces due to high stresses. Failure modes of the ZnO varistors can be classified into thermal runaway, physical cracking and electrical puncture (Bartkowiak et al., 1999). Failure mode due to thermal runaway can be investigated through the relationship between heat generation and heat dissipation of the

ZnO element. During surge energy absorption event, the temperature of the ZnO varistors may exceed the maximum permissible temperature limit. Subsequently, continuous stress from the normal operating voltage (AC voltage) increases with the leakage current, thus causing more heat to be generated. An elevated temperature of the ZnO varistors will cause the surge arrester assembly to be thermally unbalanced, and thus resulting in thermal runaway.

Both cracking and puncture failures happen due to a localization of the current, resulting in local heating that leads to non-uniform thermal expansion and stresses (Bartkowiak et al., 2001). The puncture failure mode is originated from the current localization and its associated joule heating (Vojta & Clarke, 1997). The phenomenon consequently produces a melted hole through the ZnO varistor, resulting in a short circuit between the electrodes. Puncture is more probable to occur for intermediate values of the current density as well as in varistor disks with low aspect ratio. Meanwhile, the cracking failure mode is originated from non-uniform heating, which in turn produces higher thermal stresses than that of the failure stress of the ZnO element (Andoh et al., 2000). Cracking is very probable at higher current densities as well as in varistor disks with high aspect ratio.

2.8 Lightning Current Impulse

2.8.1 Engineering Return-Stroke Current Models

An accurate assessment of lightning effects on electrical power systems is highly dependent on appropriate representation of a lightning current wave shape. The current wave shape is normally represented by a return-stroke current model based on mathematical formulation. The model is capable of defining the observed properties of the return stroke which include the temporal and spatial distribution of the current along

the discharge path, the variation of the wavefront velocity and the electromagnetic fields at distant points (Uman & McLain, 1969; Gomes & Cooray, 2000).

In term of engineering design, the return stroke parameters of particular interest are the current magnitude and the electromagnetic fields. The engineering models are defined based on the physics of transmission lines, in which the leader channel is regarded as a transmission line while the return stroke as a consequential current pulse in this line due to the grounded end. Generally, there are two different ways to represent the engineering return stroke model as a current pulse in transmission line.

The first method known as Lumped Current Source Models considers the return stroke as a current pulse originating at ground level and propagating from ground to cloud along the transmission line generated by the leader. This concept has been developed based on the measurements of the return stroke channel luminosity as a function of time and space. The return stroke engineering models employing the concept were proposed by Bruce and Golde, Uman and McLain, Nucci et al., Rakov and Dulzon and Cooray and Orville (Bruce & Golde, 1941; Uman & McLain, 1969; Nucci et al., 1988; Rakov & Dulzon, 1991; Cooray & Orville, 1990). The difference between each model exists in the way how they define the return stroke current variation while propagating along the leader channel. For instance, the transmission line model proposed by Uman and McLain assumes that the stroke current propagates along the leader channel without constant velocity and attenuation. The proposed model by Rakov and Dulzon assumes that the stroke current amplitude decreases linearly while Nucci et al. assume that the current amplitude decreases exponentially. Another model proposed by Cooray and Orville consider both current attenuation and dispersion effects while allowing the variation of return stroke velocity along the leader channel.

The second method considers the leader channel as a charged transmission line while treating the return stroke current as a potential wave travelling along it from ground to cloud. Upon arrival of the return stroke wavefront at a given point on the leader channel, the cloud potential is changed to ground potential which causes the bound charge to be released on the corona sheath. Consequently, this produces higher current magnitude in the channel. This method, known as Distributed Current Source (DCS) models proposed that the return stroke which propagates upward at certain speed, v , causes the stored charge on the leader channel to collapse into the highly conducting return stroke channel. Therefore, an assumption can be made by treating each point on the leader channel as a current source which is turned on upon the arrival of the wave front for that particular point.

The return stroke engineering model employing the DCS concept was first proposed by Wagner and Hileman (Wagner & Hileman, 1960). Further assumptions on the basic DCS principles were introduced by Heidler, which treat the channel base current and the return stroke velocity as input parameters. The model presents the concept of instant neutralization of the corona sheath (Heidler, 1985). A Dirac Delta function was then used to represent the corona current generated by a specific channel section. However, the model is said to be physically unreasonable due to a current discontinuity at the current wave front.

Based on consideration of the leader charge distribution and corona current as the input parameters, a model which is capable of predicting the channel base current and return stroke velocity was proposed by Cooray (Cooray, 1993). In addition, the neutralization process of the corona sheath is considered as a finite time in reality which results in the representation of the corona current as a finite duration exponential function. The model is also capable of deriving the return stroke velocity by considering

the dart leader as an arc and assuming the equality of the electric field at the return stroke wave front with the electric field along the arc channel.

Meanwhile, Diendorfer and Uman proposed a model which considers the channel base current, the corona current and the return stroke velocity as input parameters (Diendorfer & Uman, 1990). The corona current was also divided into two parts which comprises the faster part and the slower part. Thottappillil et al. proposed further modifications on the model by considering the variable return stroke velocity and variable corona discharge time constants (Thottappillil et al., 1991).

2.8.2 Analytical Representation of Current Wave Shape

Lightning interference is regarded as the major source of disturbance in medium voltage overhead transmission lines. As a substantial stroke current and charges are injected into the phase conductor or shield wire, a significant overvoltage will be experienced by the line insulations which may lead to flashovers. If the first contact of the return stroke current is with the overhead line, the lightning current is normally represented as a transient current generator. The current generator is then connected to a system consisting of transient surge impedances which represents the phase conductors and the tower. The overvoltages magnitude will then be calculated numerically using travelling wave techniques.

An accurate representation of lightning current waveshape parameters is essential to analyse the risk of lightning overvoltage on electrical power systems. The waveshape parameters include the peak current amplitude (crest value), time to crest, time to half, steepness, duration, polarity and time interval. Three important features that are essential to simulate the concave front for the lightning current representation are:

- i. the peak current magnitude of the current.

- ii. the highest steepness which is closer to the peak current.
- iii. in the case of first current stroke, the average steepness must be accurately expressed by the front time passing through the 30% and the 90% of the current magnitude.

The first return stroke current reaches its peak in a few microseconds and decays slowly approaching zero magnitude after reaching the peak. The time to peak is well defined as the front time t_f . Meanwhile, the time duration from $t = 0$ to the instant when the current subsequently decays to the 50% value of the peak is called the time to half value t_h . The time to half value which is normally much longer than the front time has insignificant influence in the severity of the lightning overvoltage. However, the peak magnitude of the current, I_{max} and the front time t_f exhibit greatly influence the overvoltage occurrence. To accurately obtain the concave current wave shape, the front time must be ensured to have larger value than the current maximum value divided by the maximum steepness.

Extensive discussions on the representation of lightning current waveform have been performed by previous researches (Bruce & Golde, 1941; Cooray & Orville, 1990; Heidler, 1985; Cooray, 1993). These models greatly influence the time courses and severity of the lightning overvoltages, which are generated in overhead lines. The most commonly used expression to represent lightning current waveform consists of double exponential functions (Golde, 1977). However, the model is incapable of determining the maximum steepness near the peak current amplitude, which is one of the main aspects in the first stroke current. Furthermore, double exponential functions have been proven as inadequate due to its discontinuity of its first time derivative at $t = 0$.

Recent finding proposed by Heidler has proven its capability of representing accurate lightning current waveform in computational analysis (Heidler et al., 1999). The

function can accurately produce impulsive waveforms with continuous time derivatives and a maximum steepness which is approximately closer to the lightning peak current. In addition, a coupled Heidler function is normally used to represent subsequent stroke currents (Nucci et al., 1993). However, these two functions exhibit drawback due to their incapability of reproducing the prominent concavity which exists at the wave front of the first stroke current. In order to overcome the drawback, the usage of two independent functions in representing the current waveform has been recommended by the International Council on Large Electric Systems (CIGRE). The first function mainly describes the current front which leads to a gradually increasing steepness up to 90% of the peak amplitude while the second function describes the current tail of the respective waveform (CIGRE W.G. 01, 1991). A set of parameters as described as follows is usually adopted to characterize the lightning current waveform proposed by CIGRE. The current front of the first return stroke can be estimated by:

$$I = At + Bt^n \quad (2.3)$$

The current shape is assumed to reach the point of maximum steepness at a time t_n which depends on the exponent n . An iterative solution of the following generalized equations is used to determine the variables,

$$(1 - 3x/2S_N)(1 - x)^n = x(n - 1)/2S_N + (1 - 3X_N/2S_N)(1 - x) \quad (2.4)$$

$$S_N = S_m t_f / I \quad (2.5)$$

$$X_N = 0.6 t_f / t_n \quad (2.6)$$

where I is the current amplitude; S_m is the maximum steepness and t_f is the front time. A sufficient accurate solution can be obtained by solving Equation (2.7) to Equation (2.10).

$$n = 1 + 2(S_N - 1)(2 + 1/S_N) \quad (2.7)$$

$$t_n = 0.6t_f \left[3S_N^2 / (1 + S_N^2) \right] \quad (2.8)$$

The constants, A and B can be predicted from:

$$A = \frac{1}{n-1} \left[0.9 \frac{I}{t_n} \cdot n - S_m \right] \quad (2.9)$$

$$B = \frac{1}{t_n^n (n-1)} [S_m \cdot t_n - 0.9I] \quad (2.10)$$

To accurately describe the current tail, the maximum steepness is needed at its beginning in order to provide a steady transition from one part to the other. Furthermore, it is necessary to reach the correct amplitude value. Equation (2.11) to Equation (2.15) were used describe the current tail.

$$I = I_1 e^{-(t-t_n)/t_1} - I_2 e^{-(t-t_n)/t_2} \quad (2.11)$$

$$t_1 = (t_h - t_n) \ln 2 \quad (2.12)$$

$$t_2 = 0.1I/S_m \quad (2.13)$$

$$I_1 = \frac{t_1 t_2}{t_1 - t_2} \left[S_m + 0.9 \frac{I}{t_2} \right] \quad (2.14)$$

$$I_2 = \frac{t_1 t_2}{t_1 - t_2} \left[S_m + 0.9 \frac{I}{t_1} \right] \quad (2.15)$$

where t_1 and t_2 are the time constants, I_1 and I_2 are the current constants and t_h is the time to half value.

2.9 Chapter Summary

This chapter presents fundamentals theory of lightning discharge events. The breakdown process which initiates the lightning discharge is briefly discussed to give an overview about basic principle of the phenomena. Furthermore, the lightning parameters involved in the design of overvoltage protection scheme of transmission line are also discussed. Different characterization of transient overvoltages in transmission line insulation system and methods to mitigate the overvoltages impact are also explained further in this chapter. In addition, this chapter presents detailed discussions on the structure, electrical properties and principle of operations of a ZnO surge arrester. The selection criteria and design requirements of the ZnO surge arrester in order to ensure optimum protection to the equipment are also discussed. Moreover, various literature reviews on previous publications which are related to electric field distribution of the ZnO surge arrester are presented in this chapter. Justifications on the need of ensuring uniform potential distribution of the ZnO surge arrester are given. It was found that the non-uniform electric potential distribution due to stray capacitance to earth may results in thermal and electrical degradation of the ZnO surge arrester.

Furthermore, several researches related to measurements and discussions on the energy absorption capability of the ZnO surge arresters are reviewed in details. Different aspects concerning energy stresses on the ZnO surge arresters which include thermal energy absorption capability and single impulse energy absorption capability are also elaborated in this chapter. As the performance of the ZnO surge arrester is primarily determined by its nonlinear V-I characteristics, discussions on the impact of thermal stresses and electrical stresses on its degradation rate are also presented in this chapter. Finally, various analytical models of lightning current wave shape representation at the end of the chapter. As an accurate modeling of the lightning surge current is essential in overvoltage performance analysis, the main design parameters of

the wave shape which include the peak current amplitude (crest value), time to crest, time to half, steepness, duration, polarity and time interval are discussed thoroughly based on previously published researches.

University of Malaya

CHAPTER 3: MODELING OF SURGE ARRESTER FOR DISCHARGE ENERGY DETERMINATION

3.1 Design Parameters

This section further elaborates on parameter selection criteria for the surge arrester models which include the dimensions, material properties and electrical properties. Brief explanation on the double exponential lightning current test waveform model was also included in this chapter. Moreover, detailed modeling approaches of the surge arresters by means of finite element method, PSCAD/EMTDC and EMTP-RV software are also discussed in this section. The simulated surge arrester in PSCAD/EMTDC and EMTP-RV was modeled based on the frequency dependent model recommended by IEEE WG 3.4.11.

3.1.1 Surge Arrester Parameters

In this work, transmission line arresters having MCOV between 31 kV and 206 kV were chosen. Table 3.1 specifies the characteristics of the simulated surge arresters in this work. It tabulates the physical dimension, rated voltage, maximum continuous operating voltage, residual voltage due to current impulse, rated discharge energy, as specified in the manufacturer's datasheet.

In insulation coordination study, the system voltage is the primary criterion for the voltage rating of surge arresters. For instance, a solidly earthed 132 kV line experiences maximum system voltage of 145 kV with an assumption of 10% tolerance. The arrester voltage rating is 80% of the maximum system voltage, which equals to 116 kV. However, the selected voltage rating is usually higher by a margin of about 5%. Hence, arresters with rated voltage of 120 kV should be selected. The required line discharge

class for the surge arrester is class 2. The protective characteristic of the arrester is then assessed based on its lightning impulse protective level, as shown by Equation (3.1). Basic insulation level (BIL) of 550 kV line is assumed as the lightning impulse withstand voltage of the line (LIWV). The calculated protective value of 1.76, as shown in Equation (3.1) is higher than the safety factor, K_s specified by the IEC 60071-2, which indicates that the selected surge arrester is sufficient for the line protection (IEC 60071-2, 1996).

$$LIWV|_{i_{10kA}, 8/20\mu s} = 550kV/312kV = 1.76 \quad (3.1)$$

Table 3.1: Physical and electrical properties of the simulated surge arresters

Height (mm)	Creepage distance (mm)	Continuous operating voltage, U_c (kV _{crest})	Rated voltage, U_r (kV _{rms})	Maximum residual voltage at impulse current of 8/20 μ s (kV _{crest})			Rated discharge energy (kJ/kV)
				V_{5kA}	V_{10kA}	V_{20kA}	
750	1640	31.6	39	97.7	107	123	5.1
1100	2990	68.1	84	214	230	264	5.1
1500	4340	97.2	120	294	312	350	5.1
2872	9520	206	258	576	607	667	7.8

3.1.2 Analytical Representation of Lightning Impulse Current

Lightning current waveform used in this study was simulated based on the double exponential current model proposed by Bruce and Golde, as derived from Equation (3.2) (Bruce & Golde, 1941):

$$i_0(t) = kI_0(e^{-\alpha t} - e^{-\beta t}) \quad (3.2)$$

$$i_0(t) = 4I_0(e^{-86600t} - e^{-173200t}) \quad (3.3)$$

where I_0 is the peak magnitude of the current, $i_0(t)$ is the instantaneous lightning current, α is the wave-front attenuation quotient of the lightning current, β is the wave-tail attenuation quotient of the lightning current and k is the current waveform correction index.

In this study, the coefficient values of α , β and k were set as 8.66×10^4 , 1.732×10^5 and 4 respectively, as shown in Equation (3.3). Figure 3.1 depicts the current-time dependences of the 10 kA lightning impulse waveform, represented by a front time and time to half of 8 μ s and 20 μ s respectively. The waveform was chosen as it is normally used in carrying out tests to determine the capability of low-impedance device such as surge arresters to withstand the currents associated with lightning discharges (Jones, et al., 1992).

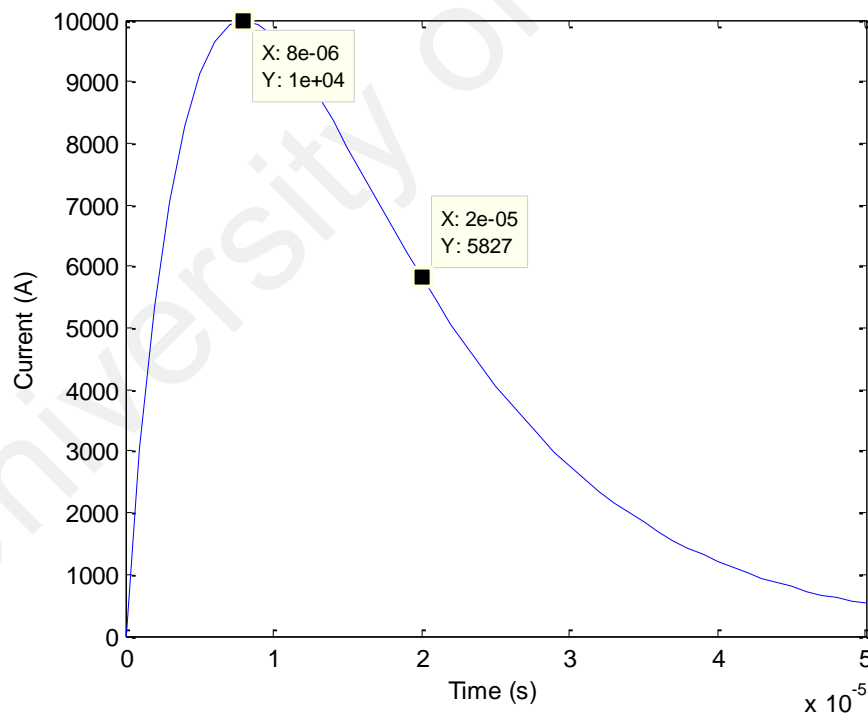


Figure 3.1: Lightning impulse test waveform of 8/20 μ s

3.2 Modeling of Surge Arrester

A set of transmission line surge arresters with different dimensions and ratings was simulated to investigate their discharge energy capabilities during fast-front surge

events using finite element analysis method. In order to validate the accuracy of the method, the arrester models were also simulated by the use of PSCAD/EMTDC and EMTP-RV software and compared with the specifications provided by the manufacturer.

The advantages of the simulation using FEA model are real dimensions of the actual surge arrester can be modeled, which will increase more confidence of surge arrester designers on evaluating the discharge current, residual voltage and discharge energy. Meanwhile, PSCAD/EMTDC and EMTP-RV software is not capable of simulating the actual dimension of the surge arrester, in which the model can only be represented in the form of electrical circuit. Moreover, feasibility of the software is also limited to simulating the electrical properties of the surge arrester, rather than other physical properties such as thermal properties.

3.2.1 Finite Element Method

The designed surge arrester was assumed as geometrically symmetric, hence, it was developed using two-dimensional (2D) axial-symmetry representation. Figure 3.2 shows complete model geometry of the surge arrester that has been modeled in the FEA software. Various main components including the ZnO varistor blocks, electrodes, and silicone rubber casing were defined in the model. The 'Electric Current' interface of the 'AC/DC' module available in the software was used to solve the developed model. A layer of air surrounding the designed arrester was also drawn to observe the electric field distribution on the surface of the insulation layers.

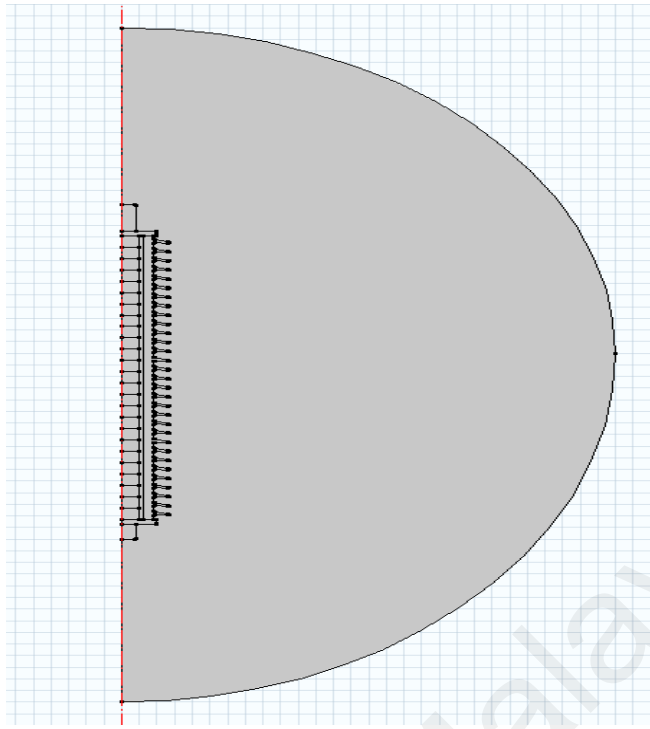


Figure 3.2: Complete geometry of surge arrester in COMSOL Multiphysics

After assembling the full geometry, material properties which include relative permittivity and electrical conductivity were assigned to each domain. Materials' assignment is one of the most important steps involved in the FEA modeling, as the solver will not be able to solve the governing equations of physics without adequate information from the material properties. In COMSOL Multiphysics software, some materials are available by default in the library; otherwise users are allowed to define the material properties such as electrical conductivity (σ), relative permittivity (ϵ_r), relative permeability (μ_r) and so on. The material domains of the simulated arrester and their corresponding values are displayed in Figure 3.3 and Table 3.2.

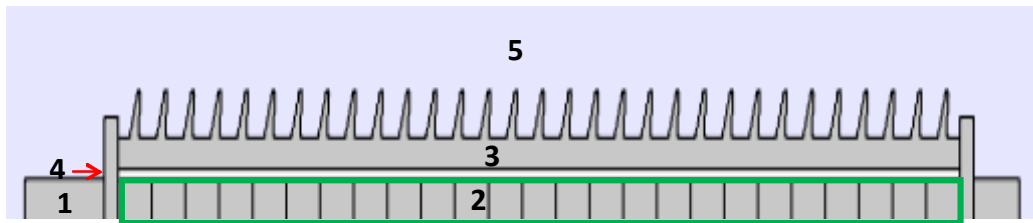


Figure 3.3: Material domain

Table 3.2: Material properties

Domain	Material	Relative permittivity, ϵ_r	Conductivity, σ (S/m)
1	Aluminium	1	3.774×10^4
2	Zinc oxide	800	Non-linear
3	Silicone rubber	3.6	1×10^{-18}
4	Fiberglass	4.2	1×10^{-18}
5	Air	1	0

In order to assess performance of the proposed FEA model, the voltage-current characteristics of the surge arrester need to be estimated based on the discharge voltage values obtained from the manufacturer's datasheet. The estimation of the V-I characteristics is a complex task since accurate limits can either be determined based on the engineering experience and expert knowledge or be defined by the arrester's manufacturer. The non-linear conductivity, σ of the ZnO varistor blocks representing the high current region was then estimated based on the residual voltage and discharge current, as shown in Figure 3.4.

Given the radius of zinc oxide disc and length of stack of zinc oxide disc of equal to 0.05 m and 1.219 m respectively, the conductivity, σ is calculated using Equation (3.4) and Equation (3.5). The current-dependent conductivity setting used in COMSOL Multiphysics software is shown in Table 3.3.

Table 3.3: Non-linear conductivity of ZnO used in FEA modeling

Current (A)	Voltage (V)	Conductivity (S/m)
1000	250977.4	0.618414
1500	257962	0.902505
3000	273128.9	1.704778
5000	287592.9	2.698398
10000	313076.3	4.957515
20000	347432.2	8.934579
40000	393749.7	15.76718
100000	480602.9	32.29444

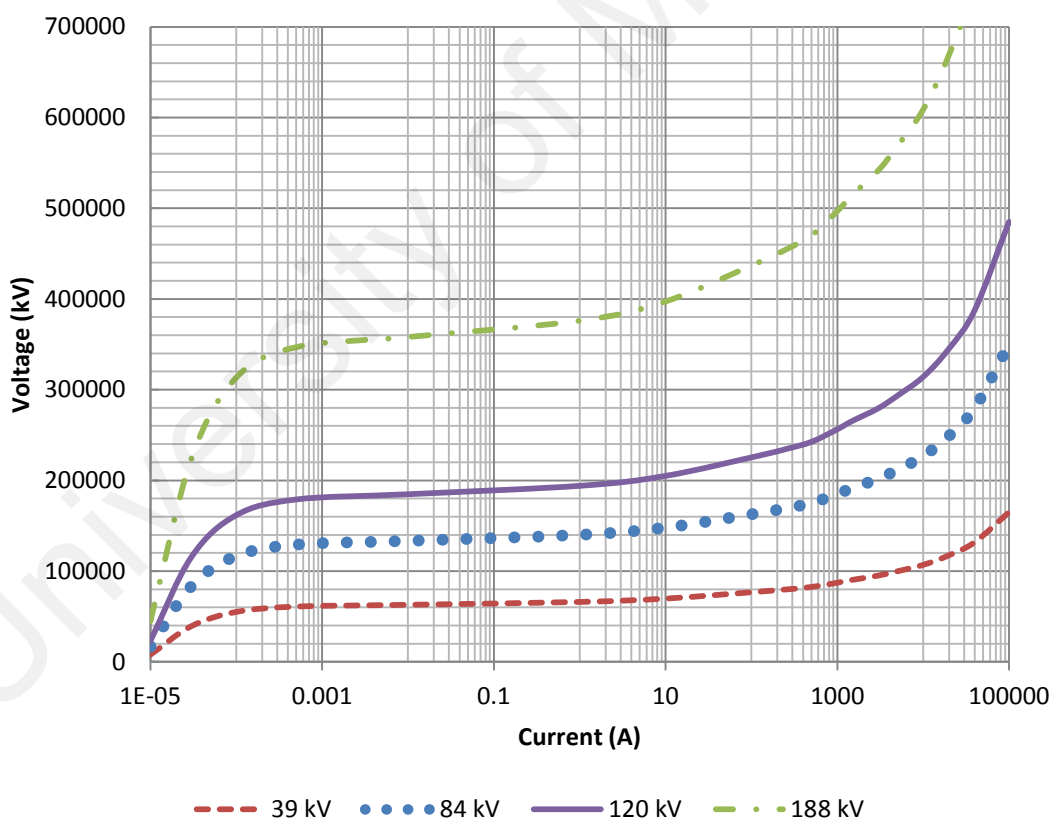


Figure 3.4: Voltage-current characteristics of the surge arrester models

$$\sigma = \frac{1}{R} \cdot \frac{1}{A} \quad (3.4)$$

$$R = \frac{V}{I} \quad (3.5)$$

where R is resistance in Ω , A is cross-sectional area of ZnO block in m^2 , and l is length of stack of ZnO discs in m.

During transient overvoltages, the arrester will exhibit a relatively low resistance to allow surge current flow through the ZnO blocks while limiting the voltage across the protected equipment below than the basic insulation level. Higher impulse current will increase the voltage stress impressed across the device, and consequently will cause reduction in the resistance value of the ZnO blocks, so that more current will be conducted to the ground. As the resistance is primarily determined by the voltage stress, the conductivity of the ZnO blocks will also be affected in which it varies in inverse proportion to the resistance value.

After assigning the material domains, relevant interface conditions were applied at each boundary in the geometry. Figure 3.5 illustrates the boundaries assigned in the surge arrester model while Table 3.4 describes the boundaries' conditions. The COMSOL Multiphysics software should obtain the electric field and the displacement from the gradient of V as per Equation (3.6). Meanwhile, the electric displacement boundary condition of the geometry is governed by Equation (3.7).

$$E = -\nabla V \quad (3.6)$$

$$D = \varepsilon_0 \varepsilon_r E \quad (3.7)$$

The ground boundary condition was applied at the bottom part of the arrester, which specifies zero electric potential. The upper part of the arrester was specified as a terminal source of time-dependent surge current as per Equation 3.8.

$$I(t) = 4 \times I_{peak} \times (e^{-86600t} - e^{-173200t}) \quad (3.8)$$

Since the arrester was enclosed in a spherical air domain, its outermost boundary condition was assigned to:

$$n \cdot J = 0 \quad (3.9)$$

The interface condition of the remaining geometry boundaries was set to continuity, given by:

$$n_2 \cdot (J_1 - J_2) = 0 \quad (3.10)$$

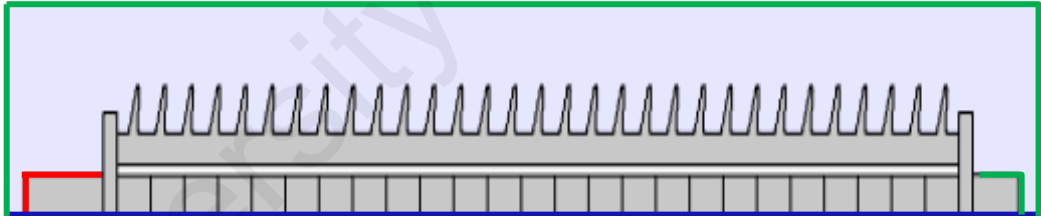


Figure 3.5: Surge arrester model geometry with boundaries

Table 3.4: Boundary conditions of surge arrester model

Boundary line	Boundary condition	Description
Blue	Axial symmetry	Boundaries along $r=0$ line
Red	Terminal	High-voltage terminal boundaries
Green	Ground	Ground terminal and air boundaries
Black	Continuity	Internal and external boundaries

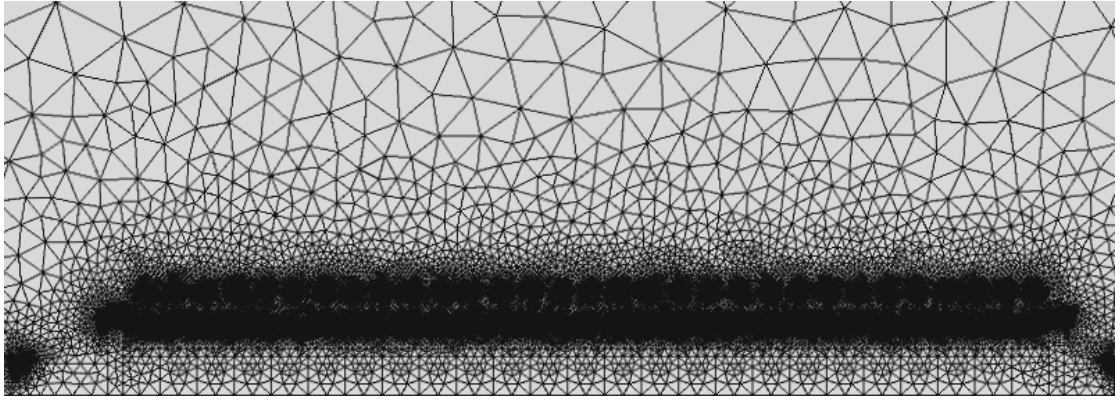


Figure 3.6: Mesh elements in the model geometry

The next step was meshing the geometry into smaller elements for effective computation. The mesh is programmed to contain the material properties, which define how the structure will react to certain loading conditions. In this model, extremely fine mesh elements were applied on the area surrounding the ZnO column, as depicted in Figure 3.6. This was done to increase the precision of the electric field distribution as the ZnO column is the most important part which determines the arrester's behaviour during impulse current injection. Meanwhile, coarser mesh was applied on the air domain since the area is of less importance in determining the electrical properties of the surge arrester. Effective handling of mesh size is needed in order to save the memory usage during FEA computation. Finally, the electric potential distributions in the geometry were solved by the FEA software using partial differential equation (PDE).

$$-\nabla \cdot (\sigma \nabla V) - \nabla \cdot \frac{\partial}{\partial t} (\epsilon \nabla V) = 0 \quad (3.11)$$

where ϵ is the permittivity, V is the electric potential and σ is the conductivity.

3.2.2 PSCAD/EMTDC and EMTP-RV

The frequency dependent model recommended by IEEE WG 3.4.11 model was used to design the arrester in PSCAD/EMTDC and EMTP-RV software, as depicted in Figure 3.7 (Jones, et al., 1992). By considering the electrical and physical parameters of the arrester, the resistor and inductor initial values were calculated based on the following expressions:

$$L_1 = \frac{15d}{n} \mu H \quad (3.12)$$

$$R_1 = \frac{56d}{n} \Omega \quad (3.13)$$

$$L_0 = \frac{0.2d}{n} \mu H \quad (3.14)$$

$$R_0 = \frac{100d}{n} \Omega \quad (3.15)$$

$$C = \frac{100n}{d} pF \quad (3.16)$$

where d is the height of the arrester in meter and n is the number of parallel columns of metal oxide disks in the arrester.

Before proceeding with energy evaluation, two basic tests were conducted to ensure the accuracy and precision of the designed arrester which include switching surge test and V_{10} surge test. Procedures for determining the surge arrester parameters are briefly described in Figure 3.8. Firstly, a switching surge impulse current was injected into the arrester model with the initial lumped parameters. The initial relative V-I characteristics for both A_0 and A_1 elements as tabulated in Table 3.5 were adjusted until a good

agreement with the manufacturer's data of residual voltage due to switching surge, V_{SS} was achieved.

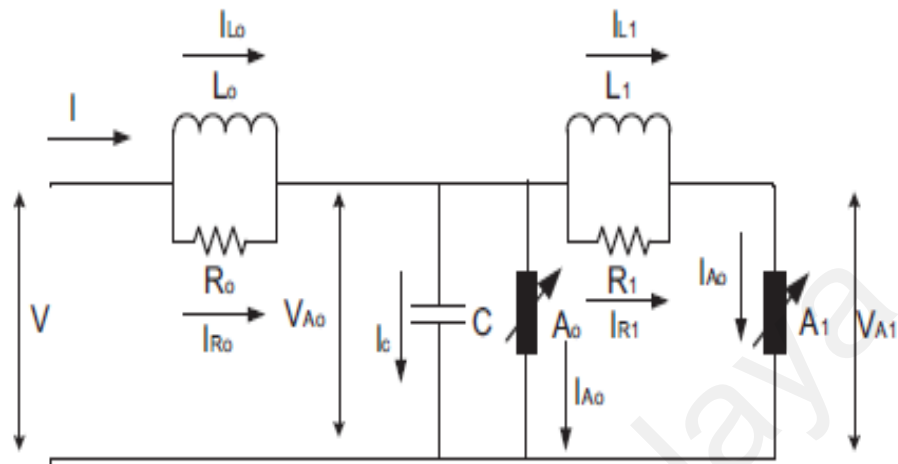


Figure 3.7: Equivalent circuit based on IEEE WG 3.4.11 (Jones, et al., 1992)

The final adjusted values of A_0 and A_1 characteristics setting in PSCAD are shown in Figure 3.9(a) and Figure 3.9(b). Next, the revised arrester model with the correct value of nonlinear resistances of A_0 and A_1 was tested to obtain a close match with the manufacturer's residual voltage for an 8/20 μ s impulse current. Figure 3.10 shows the circuit model built in PSCAD to represent the 8/20 μ s impulse current. This model can be constructed based on the double exponential expression (Equation 3.3), by having a Ae^{Bx} block subtracted by another Ae^{Bx} block in which the constants A and B were assigned to values as described previously in Section 3.1.2. A slider is also introduced so that the value of current can be varied if necessary.

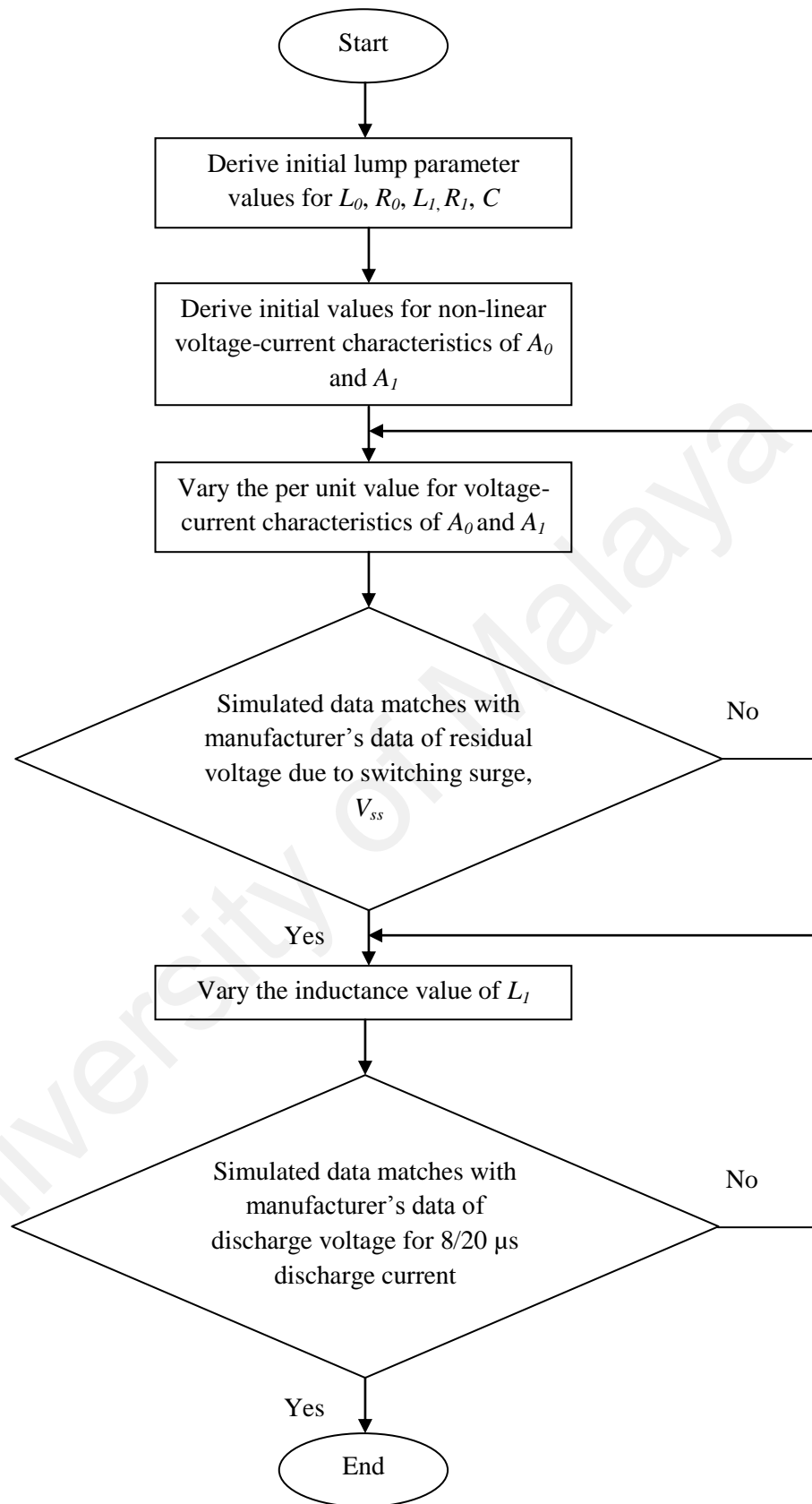


Figure 3.8: Procedures for determining surge arrester parameters

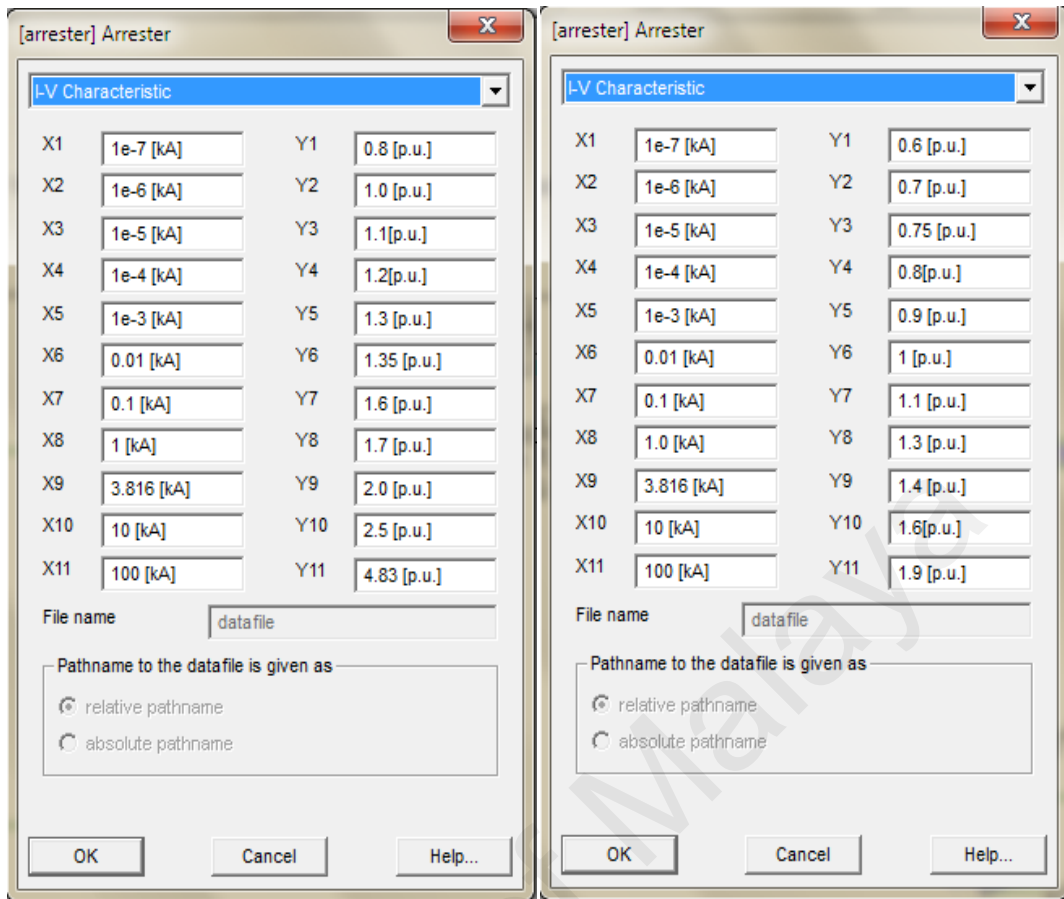
A trial and error approach was performed to adjust the value of L_I until a good match with the desired V_{I0} residual voltage was obtained. Figure 3.11 shows the finalized arrester circuit configuration for the 120 kV rated circuit. Meanwhile, the finalized lumped parameter values of L_0 , R_0 , L_I , R_I and C for different surge arresters' rating are tabulated in Table 3.6. The overall simulation circuit representing the surge arrester equivalent circuit in PSCAD is given in Figure 3.12.

Table 3.5: Initial values of A_0 and A_I characteristics

Current (kA)	A_0 (per unit, V)	A_I (per unit, V)
1.0e-7	1.1	0.72
1.0e-6	1.28	1.0
1.0e-5	1.33	1.08
1.0e-4	1.37	1.11
0.001	1.39	1.15
0.01	1.42	1.18
0.1	1.52	1.22
1.0	1.65	1.32
3.816	1.75	1.40
10.0	1.9	1.55
100.0	3.8	1.95

Table 3.6: Linear element parameters of different types of surge arresters

U_r (kV _{rms})	Linear element parameters				
	L_0 (μ H)	R_0 (Ω)	L_I (μ H)	R_I (Ω)	C (pF)
39	0.15	75	11.25	42	133.33
84	0.22	110	16.5	61.6	90.91
120	0.3	150	22.5	84	66.67
258	0.52	262	39.3	146.7	38.17



a) A_0 characteristics

b) A_1 characteristics

Figure 3.9: Adjusted A_0 and A_1 characteristics of the 120 kV rated arrester

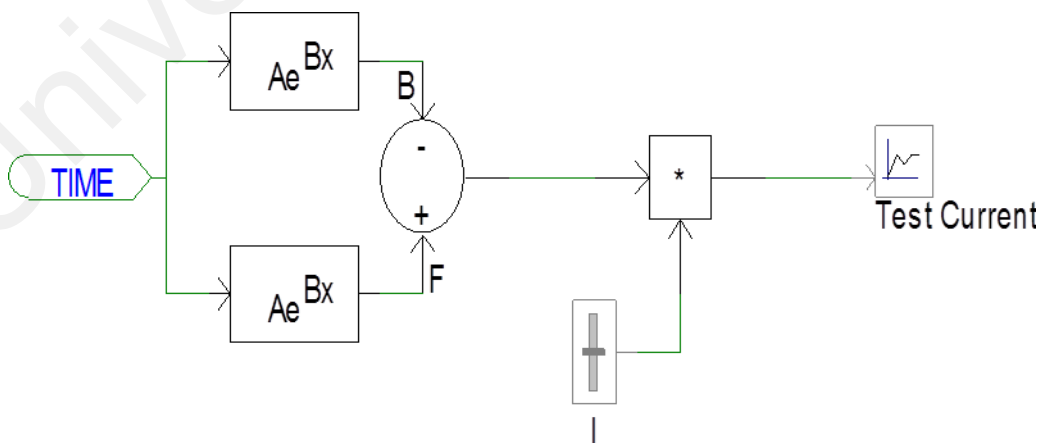


Figure 3.10: 8/20 μ s impulse current model in PSCAD

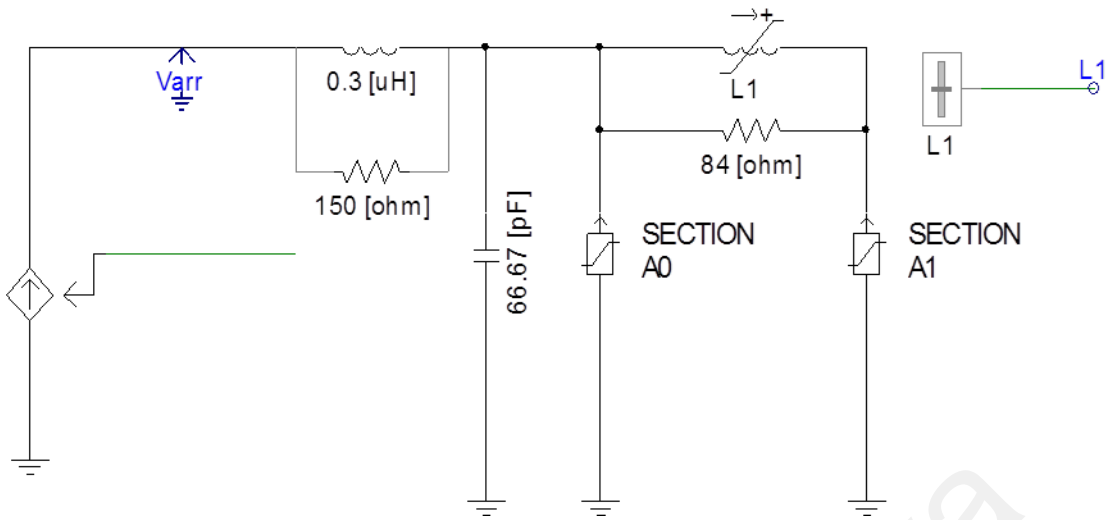


Figure 3.11: 120 kV arrester circuit simulated in PSCAD

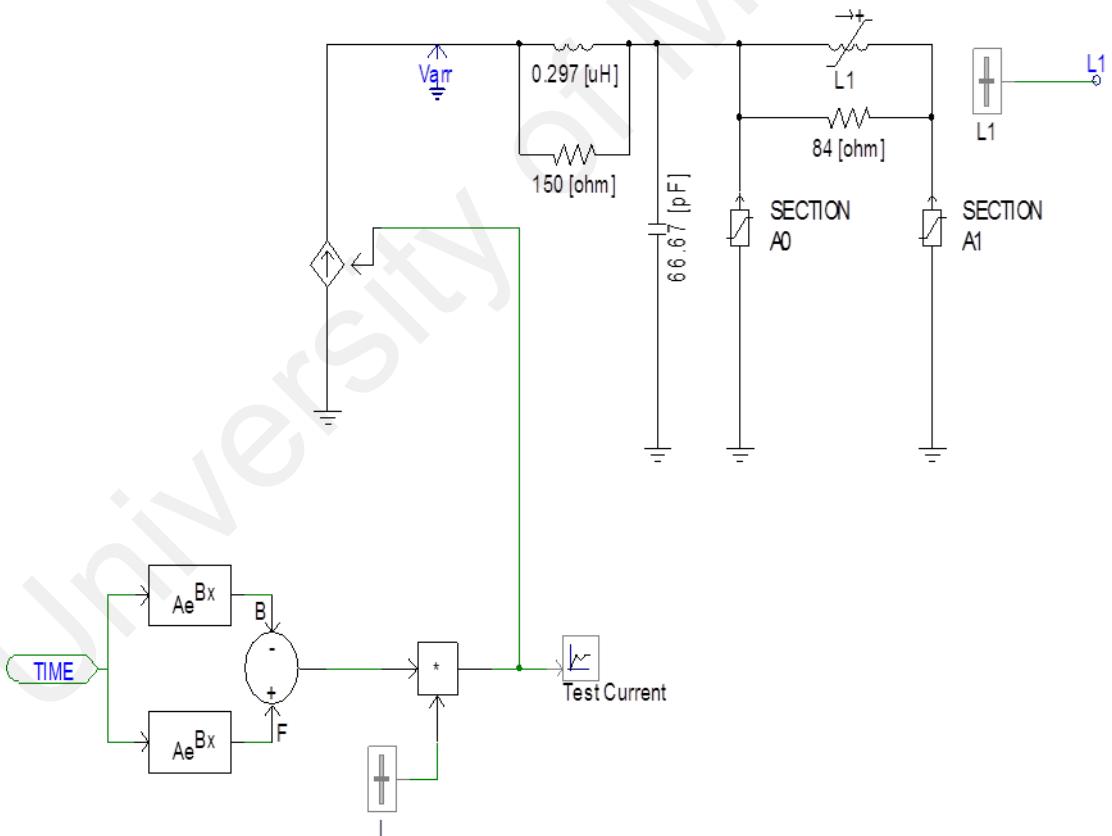


Figure 3.12: Overall surge arrester equivalent circuit in PSCAD

3.3 Chapter Summary

This chapter presents a proposed method based on FEA to determine energy discharge capabilities of surge arresters due to lightning impulse current. Electrical and physical characteristics of a set of transmission line surge arresters with different ratings are given in this chapter. In addition, various main components of the surge arresters that have been developed in the FEA software are described thoroughly. The relevant interface conditions and material domains of the surge arrester's model geometry are also included in this chapter. Further evaluation on the energy discharge capabilities was conducted by applying a single 8/20 μ s impulse current of 10 kA on each of the arresters' high voltage electrode. In order to validate the accuracy of the proposed method, the arrester models were also modeled in PSCAD/EMTDC software and EMTP-RV software. The surge arresters were designed based on the frequency dependent model recommended by the IEEE WG 3.4.11.

CHAPTER 4: MODELING OF 275/132 KV QUADRUPLE CIRCUIT OVERHEAD TRANSMISSION LINE

4.1 Introduction

This chapter presents modeling approaches to determine back flashover tripping patterns of a 275/132 kV quadruple circuit transmission line in Malaysia based on EMTP-RV software. Detailed design parameters of the quadruple circuit which include tower configuration, phase conductor and shield wire, insulator string, and tower footing resistance are discussed thoroughly. Furthermore, actual parameters and equations used to represent lightning stroke current to the shield wire based on the CIGRE current wave shape are also given in this chapter.

4.2 Tower Configuration

The quadruple circuit monopole tower of the transmission line is depicted in Figure 4.1. Each of the towers was modeled as a multi-storey model, which is based on constant-parameter circuit representation. Each section between the tower cross arms was modeled as a lossless line connected in series with a parallel damping resistance and inductance (RL) circuit, as shown in Figure 4.2 (Ishii, et al., 1991). The tower surge impedance of each section, Z_T was deduced by means of Equations (4.1) and (4.2) (Martinez, 2009). Meanwhile, the RL circuit parameters that represent attenuation of the travelling waves were calculated based on Equations (4.3) to (4.6) (Ishii, et al., 1991; Yamada, et al., 1995). For multi-storey model, the representations of the tower crossarms are normally neglected. Travelling wave velocity along the tower was assumed equal to the speed of light. Table 4.1 shows the exact parameter values of the quadruple 275/132kV tower model used in the simulations.

$$Z_r = 60 \left[\ln \left(\frac{h_t}{R} \right) - 1 \right] \quad (4.1)$$

$$R = \frac{(r_1 h_{m_2} + r_2 h_t + r_3 h_{m_1})}{2h_t} \quad (4.2)$$

$$R_i = \frac{-2Z_{t1} \ln \sqrt{r_q}}{h_1 + h_2 + h_3} \quad (4.3)$$

$$R_4 = -2Z_{t2} \ln \sqrt{r_q} \quad (4.4)$$

$$L_i = \alpha_q R_i \frac{2h_t}{V_t} \quad (4.5)$$

$$h_t = h_1 + h_2 + h_3 \quad (4.6)$$

where R is the equivalent tower radius in m, h_t is the tower height in m, r_1 is the radius of the tower top in m, r_2 is the radius of the tower middle part in m, r_3 is the radius of the tower bottom part in m, h_{m1} is the distance between the bending point on tower main post of lower line and ground in m and h_{m2} is the distance between the bending point on tower main post of lower line and tower top point in m. R_i , R_4 and L_i are calculated using Equation (4.3) to Equation (4.5).

Table 4.1: RL circuit parameters of quadruple 275/132kV tower model

Parameter		Value
Tower surge impedance	Z_{t1}	198.839 Ω
	Z_{t2}	198.839 Ω
Surge propagation velocity	V_t	300m/ μ s
Attenuation coefficient	r_q	0.7
Damping coefficient	α_q	1.0
Tower section height	h_1	4.65 m
	h_2	6.70 m
	h_3	6.70 m
	h_4	8.40 m
	h_5	5.0 m
	h_6	5.0 m
	h_7	38.826 m
Damping resistance	R_1	4.38 Ω
	R_2	6.31 Ω
	R_3	6.31 Ω
	R_4	7.91 Ω
	R_5	4.71 Ω
	R_6	4.71 Ω
	R_7	70.92 Ω
Damping inductance	L_1	2.199 μ H
	L_2	3.168 μ H
	L_3	3.168 μ H
	L_4	3.972 μ H
	L_5	2.364 μ H
	L_6	2.364 μ H
	L_7	35.591 μ H

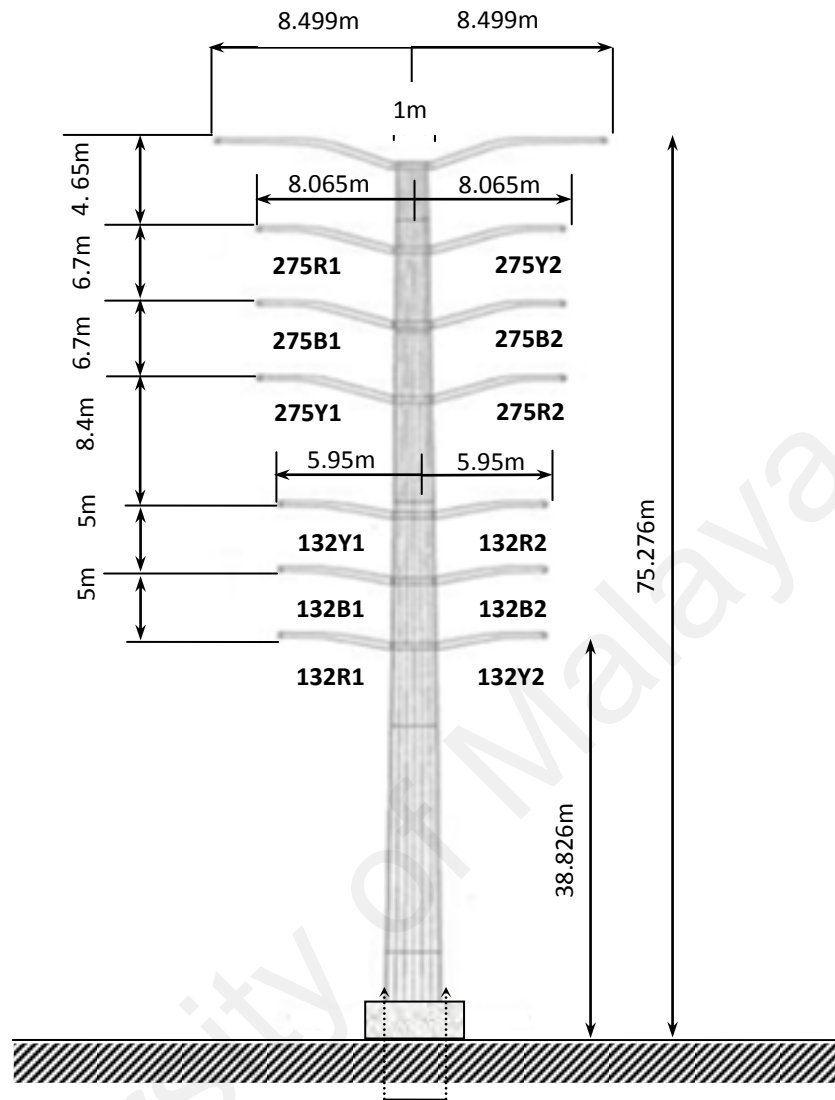


Figure 4.1: Tower representations of 275/132 kV quadruple circuit monopole tower structure

where $i = 1, 2, 3, \dots, n$, Z_{i1} and Z_{i2} are the surge impedance between each cross arm and cross arm to ground, Ω , R_i is the damping resistance, Ω , L_i is the damping inductance, μH , r_q is the attenuation coefficient (in this study, 0.7), α_q is the damping coefficient, taken as 1 in this study, h_t is the total height of the tower, m, h_1 is the vertical distance between the tower top and upper cross arm, m, h_2 is the vertical distance between upper cross arm and middle cross arm, m, h_3 is the vertical distance between middle cross arm

and bottom cross arm, m , h_4 is the vertical distance between bottom cross arm and ground, m and V_t is the surge propagation velocity, 3×10^8 m/s.

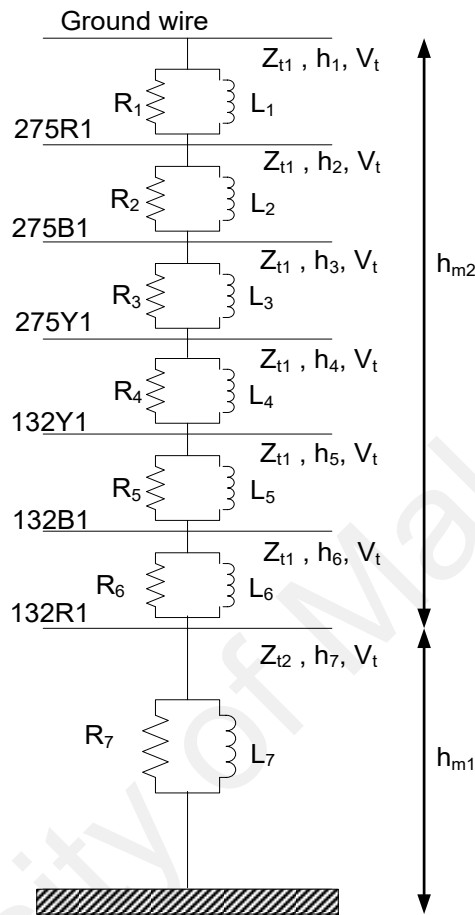


Figure 4.2: Modified M. Ishii's tower model for a quadruple tower modeling

4.3 Phase Conductor and Shield Wire

Figure 4.3 illustrates the quadruple circuit 275/132 kV transmission line configuration analysed in this study. The line consists of 275 kV double circuits and 132 kV double circuits, represented as multi-phases line spans of 200 m each at both sides of the point of impact. A 30 km line was connected to the ends of the sections as line termination to avoid travelling wave reflections. Figure 4.4 shows the overall transmission line model simulated in EMTP-RV. Frequency-dependent model was chosen to model the line sections, in which all line resistance and inductance values

were calculated as functions of frequency (Ametani & Kawamura, 2005; Dommel, 1986). Meanwhile, the phase conductors were configured vertically and two shield wires were installed at the tower top with negative shielding angle. The main characteristics are listed in Table 4.2.

Six spans were simulated in this work because the actual transmission line consists of five monopole towers only. Based on Imece, et al., the number of line spans must be modeled such that the travel time between the struck tower and the farthest tower is more than one-half of the lightning surge front time (Imece, et al., 1996). Since the front time used in the work is $2.0 \mu\text{s}$, the travel time must be greater than $1.0 \mu\text{s}$. The travel time of a span is equal to L/V , where L is span length and V is the speed of light. For three spans of 200 m each, the travel time is about $2.0 \mu\text{s}$. Thus, it is sufficient for the back flashover analysis.

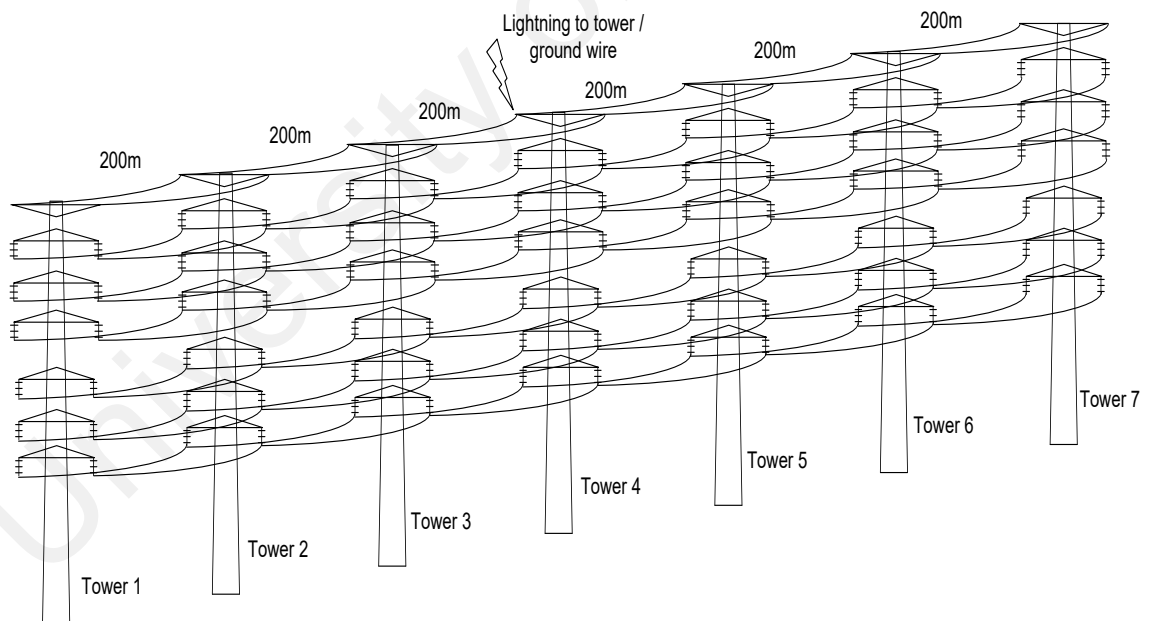


Figure 4.3: The simulated 275/132 kV line configuration

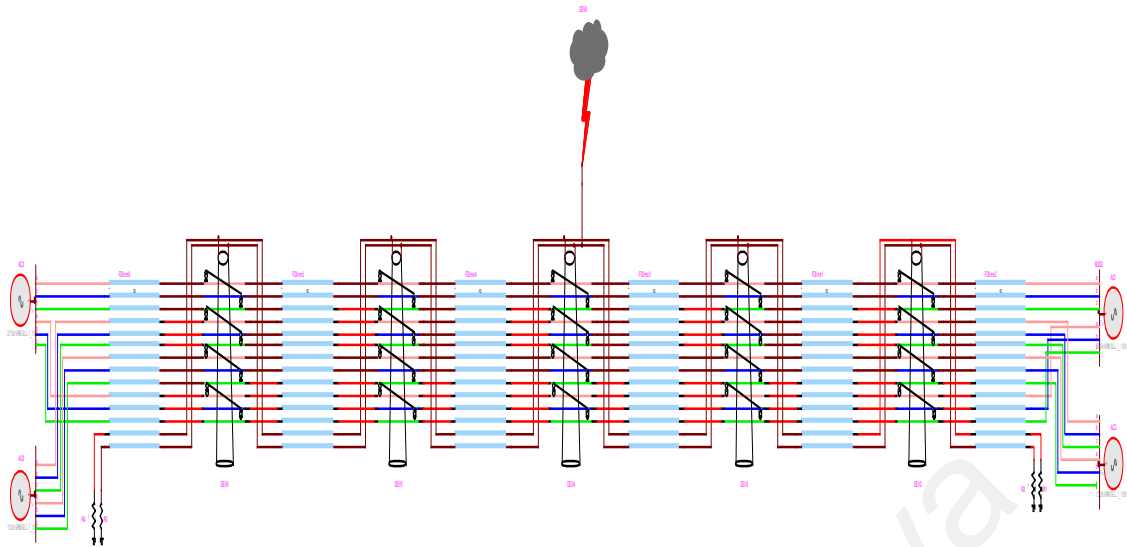


Figure 4.4: 275/132 kV transmission line modeled in EMTP-RV

Table 4.2: Geometrical and electrical data for conductors

Parameter	Type of Conductor		
	ACSR Zebra (275 kV)	ACSR Batang (132 kV)	OPGW (Shield wire)
DC resistance (Ω/km)	0.0674	0.0892	0.537
Outside diameter (cm)	2.862	2.416	1.22
Horizontal distance (m)	8.065	5.95	8.499
Vertical height at tower (m)			
Top cross-arm	70.626	48.826	75.276
Middle cross-arm	63.926	43.826	
Bottom cross-arm	57.226	38.826	

4.4 Power Frequency Voltage

The effect of power frequency voltage when lightning strikes the overhead shield wire was also considered in this work. This is due to the fact that the voltage across line insulation during back flashover is influenced by the surge voltage and the conductor voltage phase angle (Hileman, 1999). Equations (4.7) to (4.9) were used to model the instantaneous power frequency voltages.

$$V_R(t) = V_m \cos(\omega t + \theta_R) \quad (4.7)$$

$$V_B(t) = V_m \cos(\omega t + \theta_B) \quad (4.8)$$

$$V_Y(t) = V_m \cos(\omega t + \theta_Y) \quad (4.9)$$

where $V_R(t)$, $V_B(t)$ and $V_Y(t)$ are the instantaneous power frequency voltages of R,B and Y phase conductors, V; V_m is the RMS line-to-line voltage, V; ω is the angular frequency, rad/s; t is time, s; θ_R is the red phase voltage reference angle; θ_B is the blue phase voltage angle with corresponding phase shift of -120° ; θ_Y is the yellow phase voltage angle with corresponding phase shift of $+120^\circ$. The simulated AC power frequency voltage source connected to the transmission line in EMTP-RV is shown in Figure 4.5.

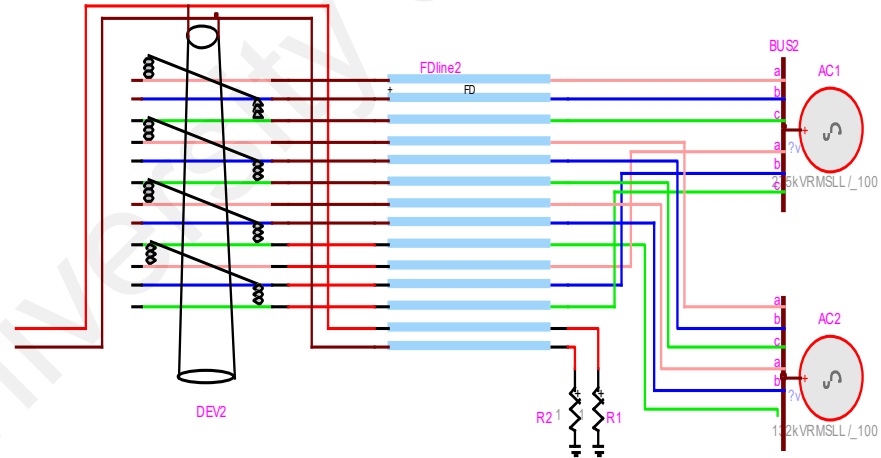


Figure 4.5: AC power frequency voltage source in EMTP-RV

4.5 Line Insulation Flashover

Failure of the 275/132 kV quadruple circuit transmission line was demonstrated by insulator string flashovers associated with lightning strokes terminating on the shield

wire. The main characteristics of both 132 kV and 275 kV insulator strings are given in Table 4.3. The insulator string was modeled as a capacitor connected in parallel with a voltage-controlled switch. In order to predict the insulator strings withstand characteristics due to lightning over voltage, three approaches are normally used; voltage-time curves, integration methods and leader progression models (Datsios, et al., 2014). Each model varies in terms of their capability to deal with non-standard lightning impulse waveform.

Table 4.3: Geometrical and electrical data for insulator strings

Parameter	Type of Insulator	
	275 kV	132 kV
Basic Insulation Level (<i>kV</i>)	650	1050
Length (<i>cm</i>)	1.97	2.36
Material	Composite	Composite
Arcing horn	No	No

In this study, the integration method was applied to determine the dielectric strength of the line insulation. Based on Equation (4.10), flashovers will occur when the integral value becomes equal to or exceeds the critical disruptive effect constant, D (IEEE Std. 1243, 1997; Sadovic, 2009).

$$D = \int_{t_0}^t \left(|V_{gap}(t)| - V_0 \right)^k dt \quad (4.10)$$

where $V_{gap}(t)$ is the voltage across the insulator string, kV; V_0 is the reference voltage, kV; k is the empirical constant; t_0 is time at which $V_{gap}(t)$ is higher than the required minimum voltage, V_0 , μ s; t is elapsed time after lightning strike, μ s. The parameters V_0 , k and D used in the integration method for the 132 kV line are 975.15 kV, 1 and 0.2576

while for the 275 kV lines V_0 , k and D are 1083.24 kV, 1 and 0.3086. These parameters were selected based on voltage-time curve of $V_{gap}(t)$, which is defined as:

$$V_{gap}(t) = \left(400 + \frac{710}{t^{0.75}} \right) d \quad (4.11)$$

where d is the insulator length (CIGRE W.G. 01, 1991). The time to crest, t_{V100} is taken as $2 \mu\text{s}$ while the time to flashover, t_{V50} is taken as $8 \mu\text{s}$. From Equation (4.11) and using t_{V100} and t_{V50} , $V_{100} = 822d$ and $V_{50} = 550d$ are obtained. V_0 is defined as $0.9V_{50}$, hence $V_0 = 495d$. From Equation (4.10), D becomes:

$$D = \frac{1}{2}(V_{100} - V_0)(t_{V100} - t_{V_0}) \quad (4.12)$$

Inserting the values in Equation (4.12), $D = 0.1308d$.

4.6 Tower Footing Resistance

Tower footing resistance was modeled based on the current dependence model, which considers the effect of soil ionization as depicted in Figure 4.6. When high impulse current flows through the footing resistance, breakdown of soils is initiated as the voltage gradient exceeds a critical gradient, E_0 (Hileman, 1999). This phenomenon causes the resistance, R_i , to significantly decrease below the measured low-current values, R_0 . Equations (4.13) and (4.14) describe the tower footing resistance model under high currents (CIGRE W.G. 01, 1991; Gatta et al., 2014)

$$I_g = \frac{\rho E_0}{2\pi R_0^2} \quad (4.13)$$

$$R_i = R_0 / \sqrt{1 + (I_R / I_g)} \quad (4.14)$$

where I_g is the limiting current in soil ionization, kA; I_R is the impulse current through ground, kA; ρ is soil resistivity, Ω/m ; E_0 is critical soil ionization gradient, kV/m; R_0 is

low-current footing resistance, Ω ; R_i is high-current footing resistance, Ω . In this work, the footing resistance of all towers was varied between 10 Ω to 50 Ω because according to utility requirement, the footing resistance for all towers should be limited to 10 Ω and below. However, during dry season the resistance may increase up to 50 Ω .

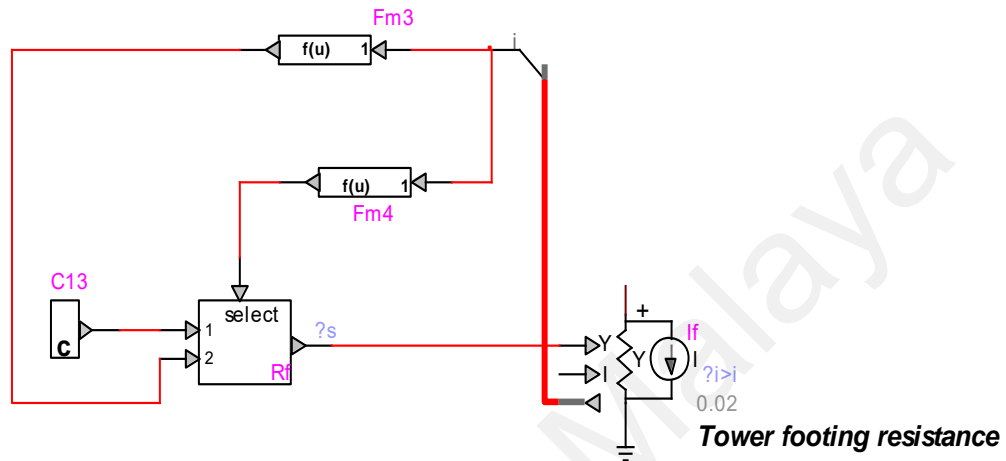


Figure 4.6: Tower footing resistance model in EMTP-RV

4.7 Lightning Surge Current

The lightning wave shape was modeled based on CIGRE model, as shown in Figure 4.7 (CIGRE W.G. 01, 1991). The maximum steepness used in the model was 140 kA/ μ s. A single-stroke lightning current with negative polarity was used for all cases. The front parameters are described by the crest current, I_f , the maximum rate of rise, S_m , time when 90% of crest current, t_n and the equivalent front time duration, t_f . For this study, the time to crest, t_f , and the time to half, t_h , were considered at 2 μ s and 70 μ s respectively.

The recorded average, median and maximum discharge currents of first lightning return stroke in Malaysia from LDS are 37 kA, 32.4 kA and 352 kA respectively (Rawi & Hudil, 2010). However, based on Imece, et al., lightning strokes of high magnitude in

the range of 20 kA up to values exceeding 200 kA may cause back flashover (Imece, et al., 1996; Bakar, et al., 2011). Hence, current magnitudes of less than 200 kA were used in this work for all cases. Figure 4.8 shows the simulated CIGRE current waveform in EMTP-RV.

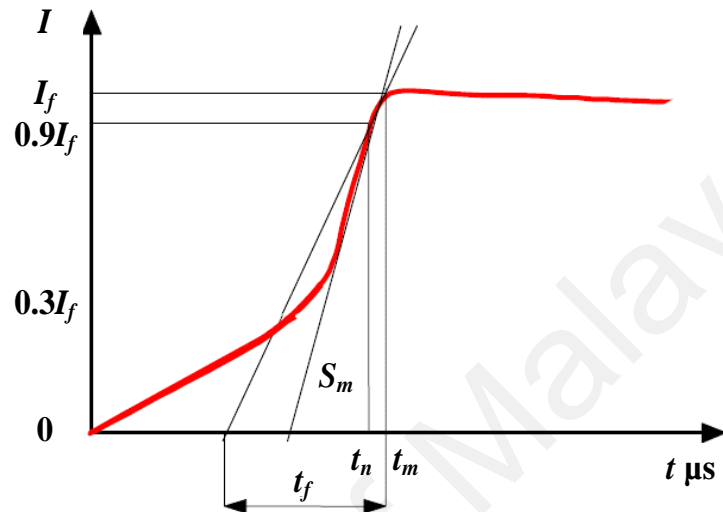


Figure 4.7: CIGRE lightning concave waveform (CIGRE W.G. 01, 1991)

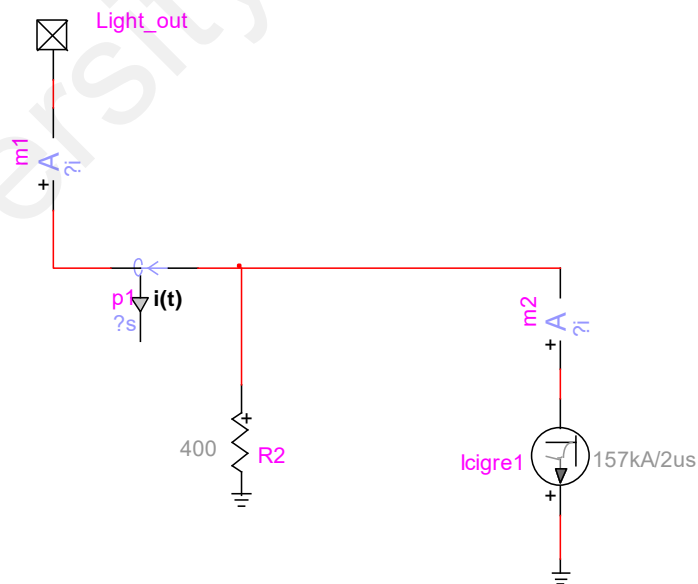


Figure 4.8: Simulated lightning current waveform in EMTP-RV

The waveform is represented by the front current (Equation 4.15) and the tail current (Equation 4.16) as follows:

$$I(t) = At + Bt^n \quad (4.15)$$

$$I(t) = I_1 e^{-(t-t_n)/t_1} - I_2 e^{-(t-t_n)/t_2} \quad (4.16)$$

$$A = \left[(0.9/t_n) \times n - S_m \right] / (n-1) \quad (4.17)$$

$$B = [S_m \times t_n - 0.91] / t_n (n-1) \quad (4.18)$$

where $I(t)$ is the instantaneous lightning current, kA; t is the instantaneous time, μ s; S_m is the maximum current front steepness, kA/ μ s; I_1 and I_2 are the current constants; t_1 and t_2 are the time constants.

4.8 Chapter Summary

This chapter presents a proposed method based on EMTP-RV modeling to investigate lightning performance of a quadruple circuit 275/132 kV transmission line due to back flashover. The characteristics of the transmission line which consists of monopole towers carrying double circuits of 275 kV and 132 kV are given in this chapter. The monopole towers were modeled as multi-storey tower, which is based on constant-parameter circuit representation. The transmission line sections which include the phase conductors and shield wires were designed according to the frequency dependent model. Moreover, the exact parameters of the line insulation flashover derived from the integration method are also included in this chapter. Detailed explanations on the current dependence model are also discussed, as the effect of tower footing resistance is one of the dominant factors in determining flashover performance. Finally, the chapter elaborates on the characteristics of the negative polarity lightning current used in all cases, which was designed based on the CIGRE model.

CHAPTER 5: RESULTS AND DISCUSSION

5.1 Introduction

Voltage-current characteristics of the surge arresters were determined with the use of mathematical models, which were described in the Chapter 3 and Chapter 4. Four types of surge arresters with different ratings were verified by means of finite element analysis (COMSOL Multiphysics software) and electromagnetic transient analysis (PSCAD and EMTP-RV software). In addition, parametric analyses were also conducted to determine the dependencies of different design modifications on the behavior of the arresters during conduction mode. The developed surge arrester models were then used in the next part of the work to determine lightning overvoltage performance of a 275/132 kV overhead transmission lines in the country. Analysis of the surge arrester installation strategy was then carried out by using Electro-Magnetic Transient Program (EMTP-RV) for the purpose of improving the line lightning performance.

5.2 Energy Discharge of Surge Arrester Due to Impulse Current

In order to evaluate the energy absorption capability, a single 8/20 μ s impulse current of peak magnitude 10 kA was applied on the high voltage electrode of the arrester in both model geometries in PSCAD, EMTP-RV and COMSOL software. Applying the previously described current Equation (3.3) for a period of 100 μ s, the discharge current and the residual voltage across the arrester were measured simultaneously. The changes in the electric field distribution were also observed before and after the impulse current injection in the COMSOL Multiphysics software. Absorption of energy in the arrester was then derived by integrating the product of the residual voltage and the discharge current with respect to the duration of the surge as shown by (Savic, 2005):

$$W = \int_{t_0}^t u_A(t) i_A(t) dt \quad (5.1)$$

where W is the energy absorbed by the arrester during the discharge process; Joule, $u_A(t)$ is the instantaneous residual voltage across the arrester; volt, $i_A(t)$ is the instantaneous discharge current across the arrester; amp, t_0 is the time at which the lightning overvoltage appears at the arrester terminal; s, t is the current time instant; s. The assumptions made in the proposed FEA method are as follows:

- i. To reduce the model complexity, removal of small scale parts of the designed surge arrester in the FEA software such as ZnO wall, drilled holes and disc string was done as the parts will not significantly influence the simulation results. Further cleaning on the surge arrester geometry was conducted by removing sharp edges and other small scale features. The final model consists of only four main material domains which are aluminium electrodes, ZnO varistor blocks, silicone rubber weather sheds and fiberglass insulation layer.
- ii. The surge arrester modeled in COMSOL Multiphysics is surrounded by a layer of air with permittivity (ϵ_r) equals to 1, in order to observe the electric potential and electric field distribution along the outer surface of the silicone rubber weather shed.
- iii. Based on the assumption that the surge arrester is symmetrical geometrically, all FEA models were implemented in two-dimensional axial symmetric geometry of 'Electric Current' interface.
- iv. Due to difficulty in getting the actual dimensions from the manufacturer, some of the surge arrester's dimension such as the silicone rubber sheds' profile were assumed and estimated based on previous researches and published standards (Fritz et al., 2011).

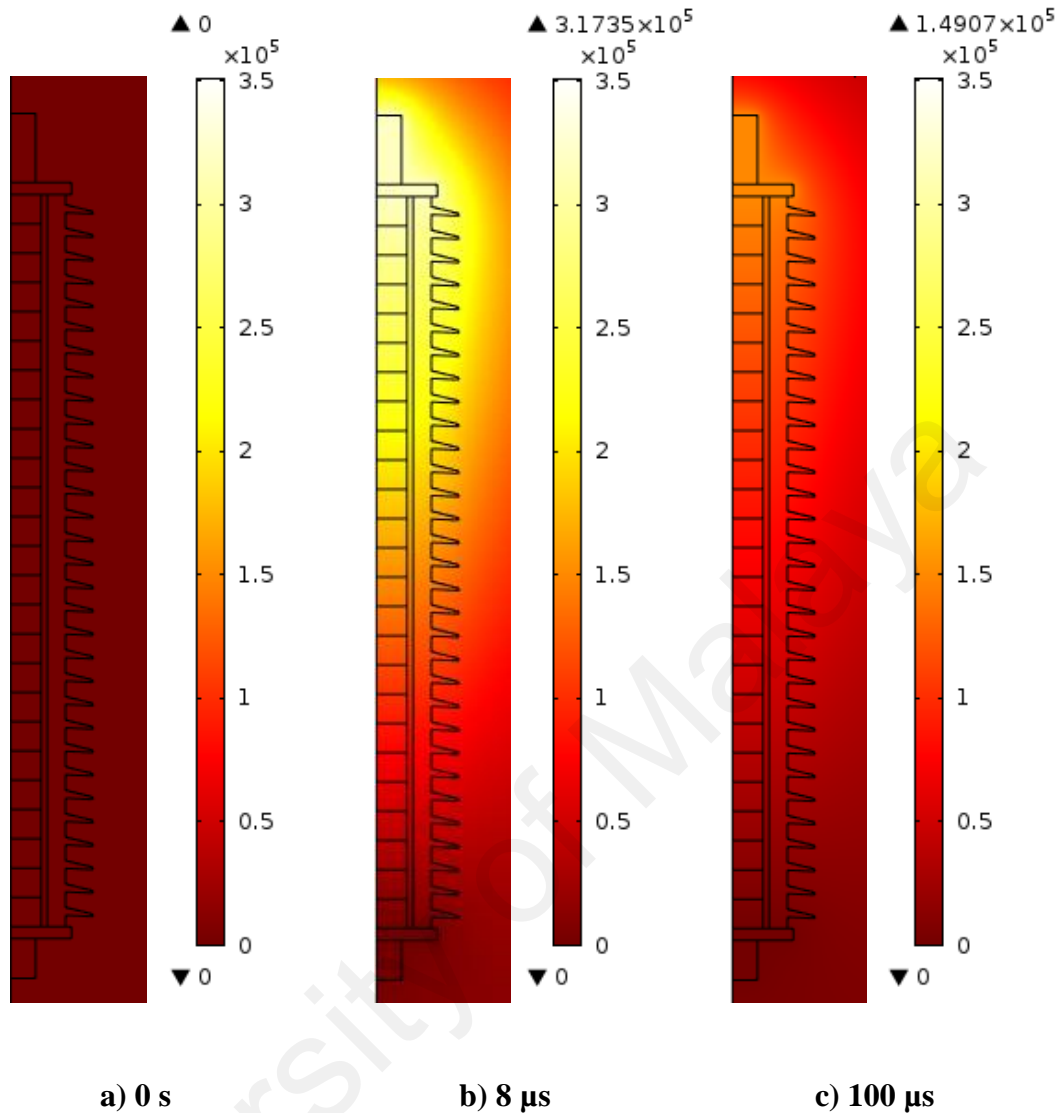


Figure 5.1: Electric potential distribution (V) of surge arrester at different time instants from the FEA model

Figure 5.1(a) shows the voltage distribution from the FEA model at time, $t = 0$ s when the conductivity of the ZnO is zero, based on assumption that no leakage current flows through the arrester during non-conduction mode. During conduction mode, the arrester develops residual voltage which is a function of the magnitude and wave shape of discharge current, arrester design and voltage rating. The relationship between the residual voltage and nominal discharge current is depicted in Figure 5.2 and Figure 5.3. In this case, a maximum voltage drop of 317 kV was observed across the energized and

grounded terminals when impressing a 10 kA lightning current impulse of 8/20 μ s. Throughout the discharging period, the conductivity of the ZnO varistors lies in the high current region which defines the arrester's protective characteristics.

Based on Figure 5.1(b), the electric potential distribution inside the arrester increases until its maximum intensity at time interval of 8 μ s, indicating that nearly all ZnO varistors are turned on in which they behave as perfect conductor to divert the surge overvoltage to the ground. Figure 5.1(c) shows the voltage distribution at 0.1 ms when the surge current impulse is approaching zero. Due to the drop in the current flowing through the ZnO varistors, it can be seen that the electric potential distribution near to the bottom of the surge arrester has decreased, while only some of the top ZnO varistors are still in conduction mode. This implies that the discharge duty was almost completed, and the arrester will return back to its steady state condition as an insulator at normal operating voltage.

In order to assess the feasibility of the developed FEA model, the result obtained was then compared with the PSCAD and EMTP model, as depicted in Figure 5.2 and Figure 5.3. The peak residual voltages of the FEA, EMTP and PSCAD models were recorded at the instantaneous surge duration of 8 μ s with magnitudes of around 317 kV. However, the residual voltage of the FEA model is declining faster than that of the PSCAD and EMTP models as the arrester's discharge current was approaching zero. The primary factor leading to this trend might be due to the different approaches used in the setting of the non-linear characteristics for FEA, EMTP and PSCAD software.

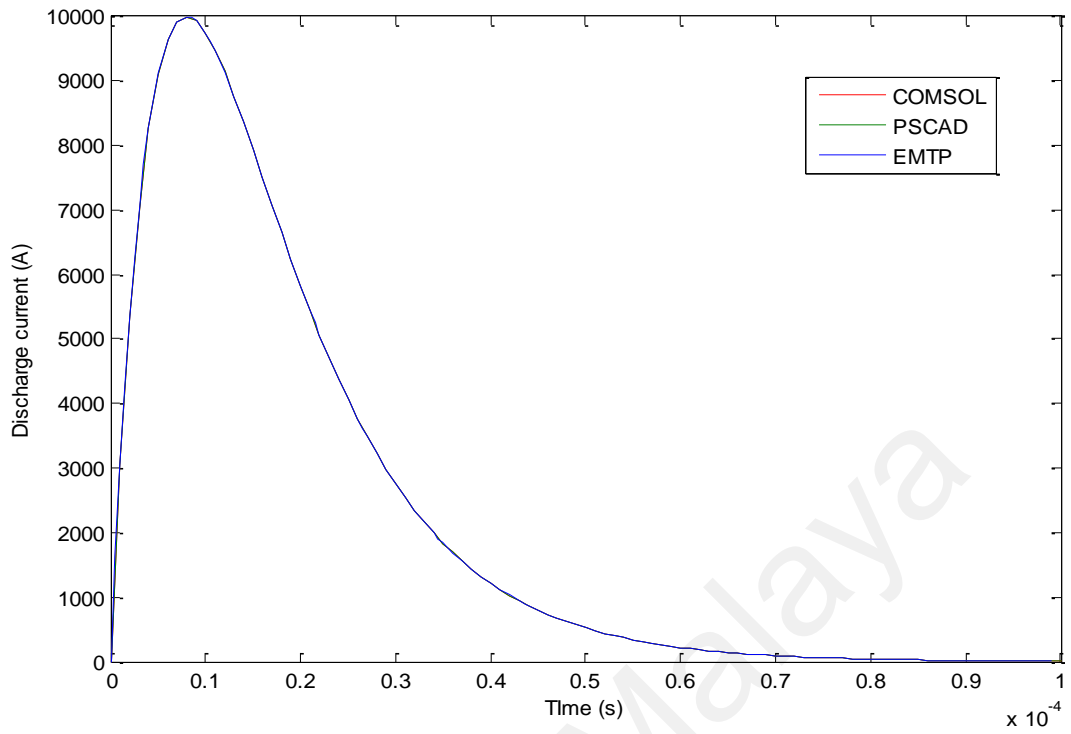


Figure 5.2: Simulated discharge current from FEA, PSCAD and EMTP

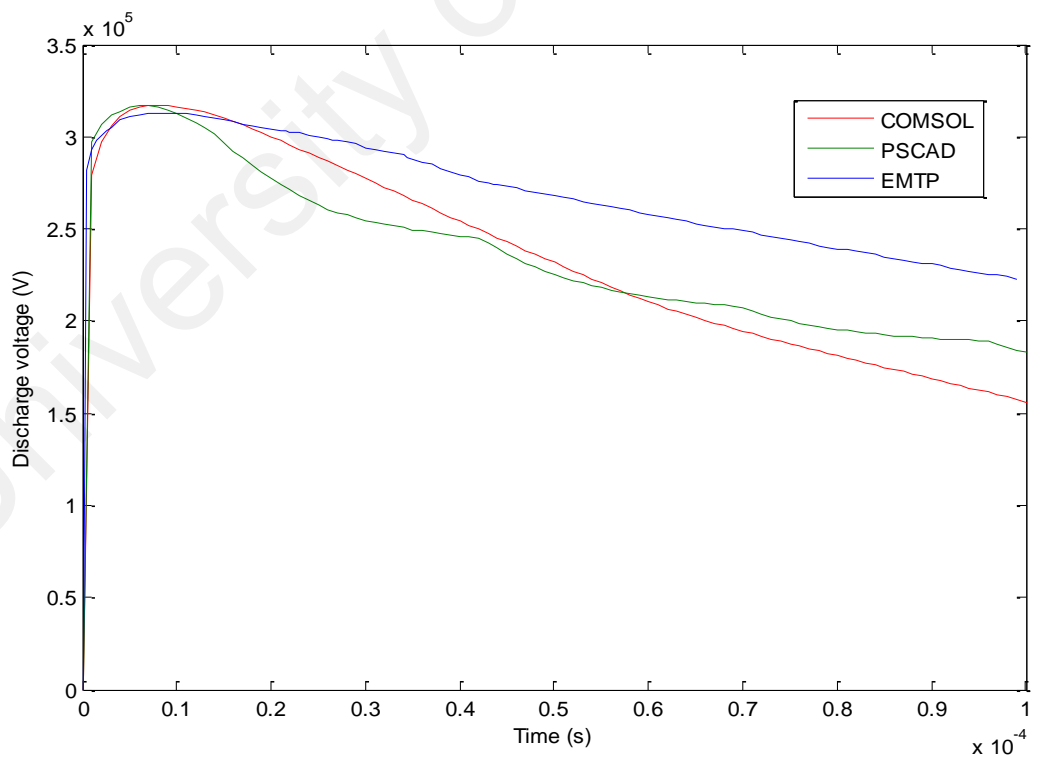


Figure 5.3: Simulated discharge voltage from FEA, PSCAD and EMTP

Further validation on the adequacy of the simulations was made by comparing the residual voltages with the manufacturer's data. The deviation from the actual value for the models is only around 5 kV. In general, all models exhibit similar residual voltage patterns which are in good agreements with the manufacturer's laboratory data. Furthermore, the simulated residual voltage from the FEA model also shows a comparable trend with the residual voltage measured by Schmidt et al. during a discharge test with a 10 kA lightning current pulse (Schmidt, et al., 1989). Moreover, the validity and accuracy of the proposed FEA model were also assessed by comparing the obtained discharge voltage with previous models based on circuit simulation methods (Bayadi, 2008; Li, et al., 2002; Christodoulou, et al., 2010). Good agreement between the results indicates the ability of the proposed FEA model for estimating surge arrester discharge characteristics.

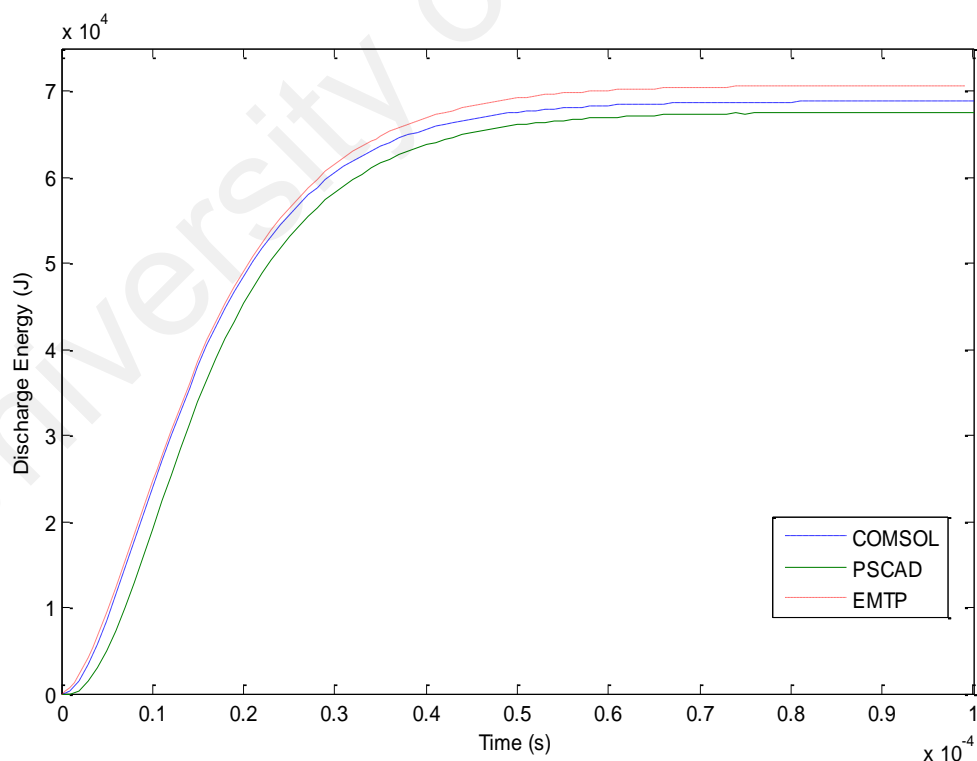


Figure 5.4: Simulated discharge energies from the FEA model, EMTP and PSCAD software

The energy absorbed by the surge arrester during the discharge process was then calculated based on the residual voltage, current and duration of the lightning surge (Equation 5.1). As illustrated in Figure 5.4, the waveforms of the three models exhibit comparable trends in which their upward rises occur nearly at a same rate. A slight difference in the calculated discharge energies might be due to the fact that all models generate different peak residual voltages, which is mainly caused by different non-linear V-I characteristic settings. With a small relative error, it can be concluded that the developed FEA model is adequate in term of estimating the absorbed energy of the surge arrester during single lightning impulse discharge.

The simulation procedures were subsequently repeated for surge arresters of rating 39 kV, 84 kV and 258 kV using nominal discharge current of 5 kA, 10 kA and 20 kA. Figures 5.5 and 5.6 indicate that the simulation results generated by FEA model are consistent with the PSCAD, EMTP and manufacturer's data in term of the peak residual voltage and the discharge energy waveform. Relative errors of the residual voltage were then determined based on Equation (5.2) to evaluate the precision of the simulated voltage-current characteristics. Table 5.1 represents the values of errors which were determined for 8/20 μ s discharge current of 5 kA, 10 kA and 20 kA respectively.

$$\text{Relative error} = \left| \frac{V_{sim} - V_d}{V_d} \right| \times 100 \quad (5.2)$$

where V_{sim} is the simulated value of residual voltage of the surge arrester; kV, V_d is the measured (manufacturer) value of the surge arrester, kV.

Regardless of the surge arrester rating, the good agreement between simulation results and actual measurements has demonstrated that design optimization by FEA model is a valid option for future arrester development. The advantage of using FEA

method to examine the characteristic of surge arrester compared to PSCAD/EMTDC and EMTP-RV is, it can capture the actual physical dimensions and parameters of components in the modeling. We can also determine how it's physical characteristics such as discharge energy and electric field intensity is influenced by the actual design parameters, which is lacking in present analysis. Further improvements on the model can be done by considering omitted features of the surge arrester, which were initially assumed to demonstrate insignificant influences on the simulation results.

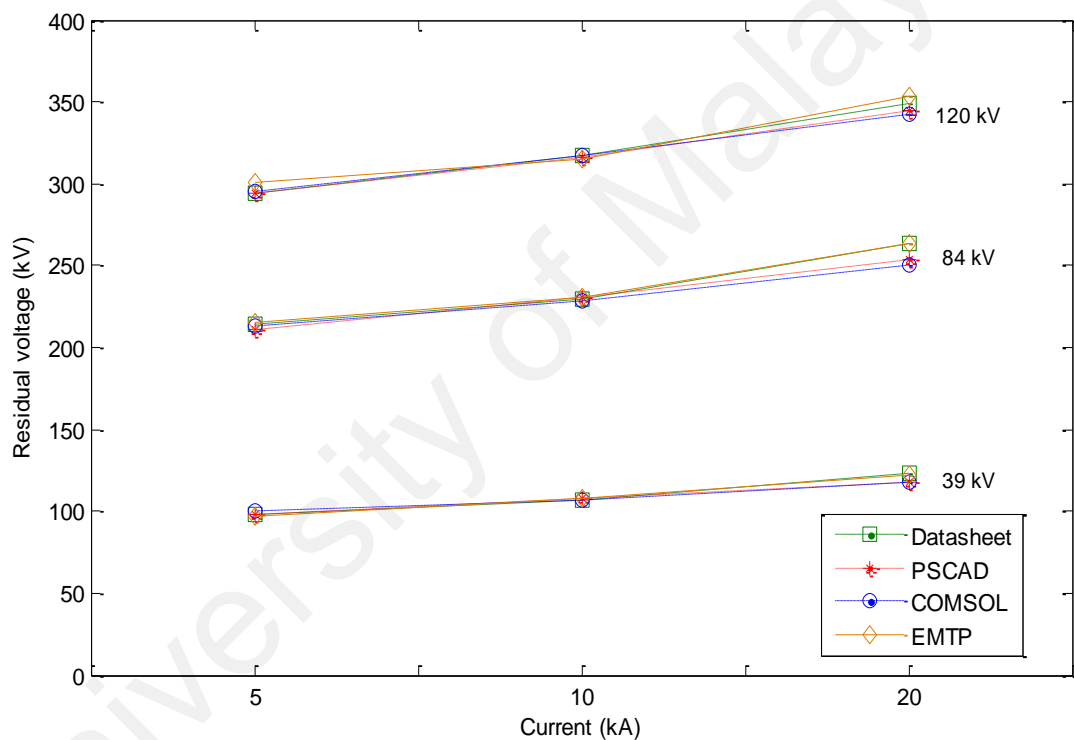


Figure 5.5: Comparison of residual voltages for different arresters' rating

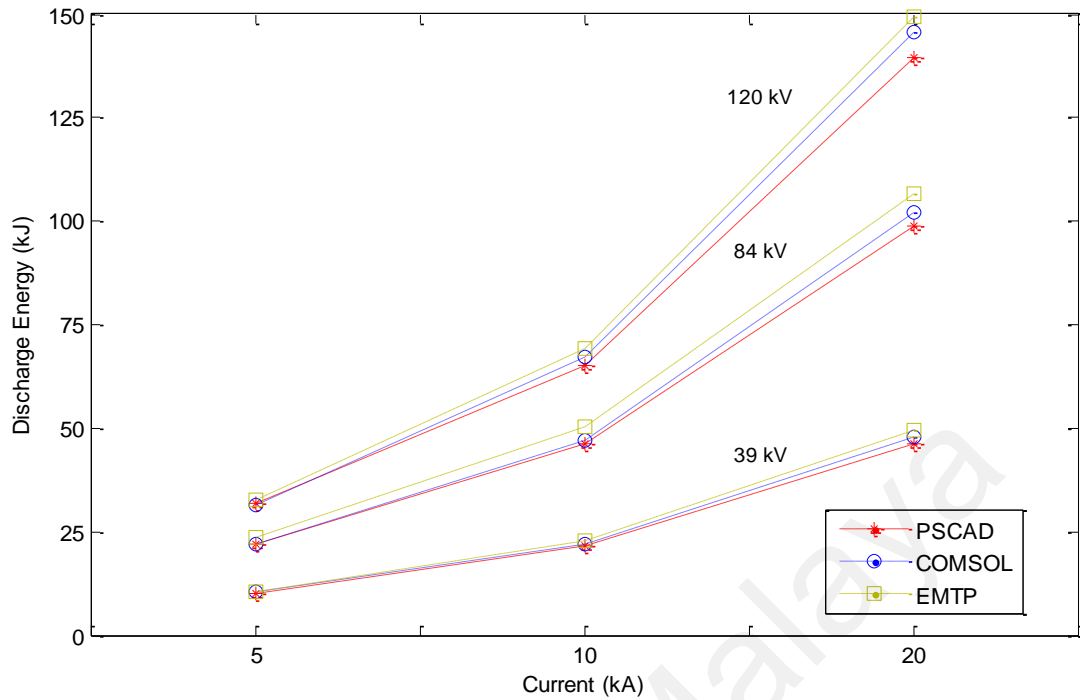


Figure 5.6: Comparison of discharge energies for different arresters' rating

Table 5.1: Relative error of residual voltage for a 8/20 μ s injected impulse current

Rated voltage (kV _{rms})	Percentage of error											
	COMSOL				PSCAD				EMTP			
	V_{5kA}	V_{10kA}	V_{20kA}	Mean	V_{5kA}	V_{10kA}	V_{20kA}	Mean	V_{5kA}	V_{10kA}	V_{20kA}	Mean
39	2.15	0.19	4.63	2.32	0.31	0.93	3.9	1.71	0.21	0.93	0.41	1.55
84	0.24	0.74	4.96	1.98	1.54	0.17	3.78	1.83	0.42	0.39	0.23	0.35
120	0.98	1.6	4.32	2.3	0.1	1.34	2.12	1.19	2.2	0.63	1.14	1.32
258	0.87	0.73	1.93	1.18	1.21	0.49	1.5	1.07	0.9	0.63	1.25	0.93

No experimental study was conducted to validate the simulated results with actual practical data. Previous studies to investigate the dynamic behaviour of surge arresters during impulse current conducted were also based on the comparison of simulation results of peak discharge voltages and the results of 8/20 μ s practical measurement obtained from manufacturer's datasheet (Christodoulou et al., 2010; Nafar et al., 2011).

It is difficult to obtain complete practical measurement data for 8/20 μs current impulse test in order to validate the simulation results, as they are not always available and reported in datasheets. Furthermore, it is also not feasible to carry out a high current impulse test for validation purpose. This is due to the fact that most of the high voltage testing conducted locally only use voltage impulse injection. It is impossible to carry out a test using 10 kA 8/20 μs current impulse since it will be considered as fault current by the national utility, which will then result in power quality disturbance.

5.3 Parametric Analysis Using FEA Model

The feasibility of the developed FEA model has been successfully validated, given the good agreement between the simulated results and the practical data. Further evaluations on the influence of different design modifications relating to the surge arrester's behavior were then conducted using the FEA software. The purpose of the parametric analysis is to evaluate mathematical equations of the electric field intensity and discharge energy as variation of arrester dimension and material properties. This proves that the proposed FEA model is capable in evaluating the arrester's physical behavior during high current discharge, which is impossible to be carried out by using electrical circuit analysis in PSCAD/EMTDC and EMTP-RV software. The parameters tested include the diameter and height of the ZnO blocks and the thickness and dielectric constant of the insulation layer. Note that the analyses were only conducted on the 120 kV rated surge arrester.

5.3.1 Effect of the Diameter of the ZnO Blocks

Further improvement of the energy absorption capability of a surge arrester could be achieved by increasing the volume of the ZnO blocks, which include enlargement of the cross sectional area and the height of the blocks. The benefits of the sensitivity analysis carried out on the ZnO radius and height are to evaluate the mathematical equation of

electric field intensity and discharge energy as a function of ZnO radius and height. This may enhance a better understanding on theoretical aspect of ZnO dimensions. In this study, four different diameters of the ZnO block were tested to investigate their influence on the discharge energy due to lightning impulse. Figure 5.7 indicates that increasing the diameter of the ZnO block results in lower discharge energy. This happens as larger diameter will produce larger cross sectional area, which will then cause reduction in the resistance of the ZnO element. Consequently, more electrons per unit length are available to carry the current which causes the discharging process to be faster. Therefore, less discharge energy will be produced across the arrester due to lower discharge current density of the ZnO element.

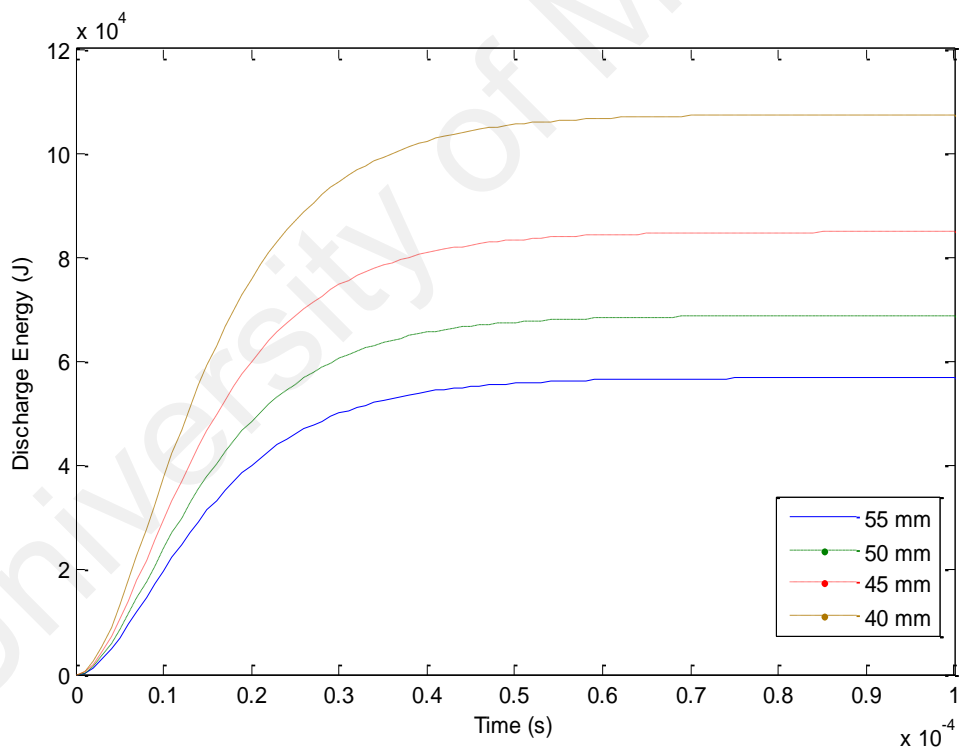


Figure 5.7: Discharge energy as a variation in diameter of ZnO blocks

A mathematical equation which can represent best the discharge energy, E (in Joule) as a function of diameter, d (in mm) of ZnO block is:

$$E = ad^b \quad (5.3)$$

where $a = 1.696 \times 10^8$ and $b = -1.996$.

5.3.2 Effect of the Height of the ZnO Blocks

The effect of the height of the ZnO block on the arrester performance due to lightning impulse was investigated by four different heights of 42.8 mm, 44.8 mm, 46.8 mm, and 48.8 mm respectively. It was found that increasing the height of the ZnO block results in an increase value of the maximum arrester discharge energy, as depicted in Figure 5.8. This is due to the fact that a greater height of the varistor block will produce a higher resistance of the ZnO element. Consequently, fewer electrons per unit length are only available to carry the current which makes the discharging process becomes slower. Therefore, higher discharge energy will be produced across the arrester.

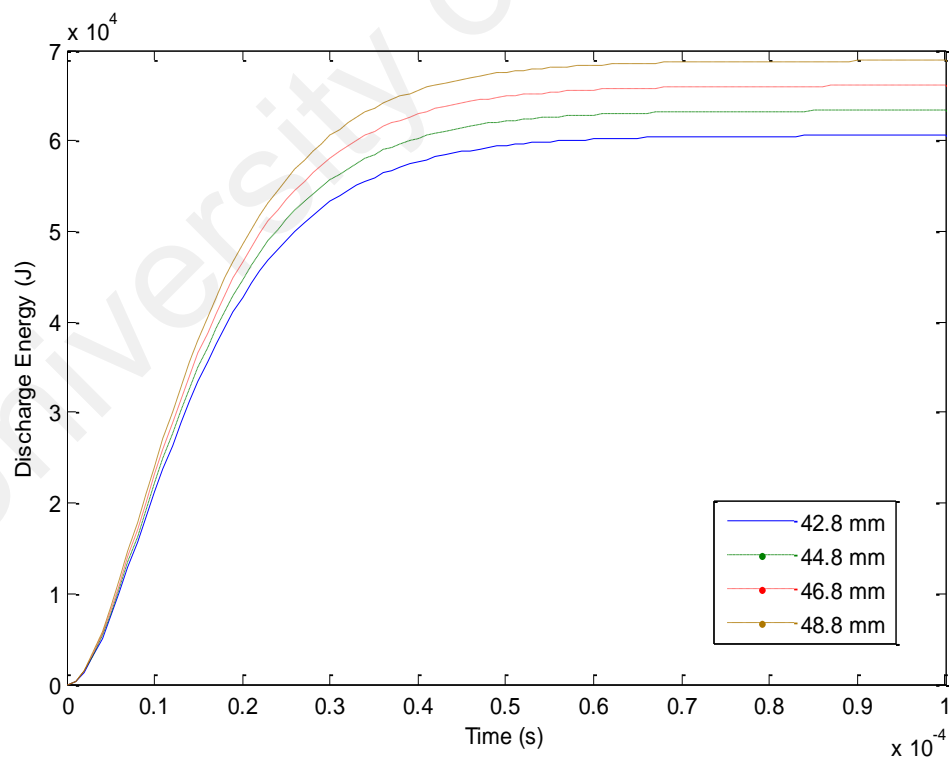


Figure 5.8: Discharge energy as a variation in height of ZnO block

However, it is less effective to increase the height of the ZnO block rather than enlarging the cross sectional area to improve the energy absorption capability of the surge arrester. The greater height of the ZnO block will make it harder to achieve sufficient homogeneity of the material during manufacturing process. Furthermore, the height of the ZnO block cannot be simply increased as the residual voltage of the surge arrester will rise proportionally with the height increment. A mathematical equation which can represent best the discharge energy, E (in Joule) as a function of height, h (in mm) of ZnO block is:

$$E = ah^b \quad (5.4)$$

where $a = 1557$ and $b = 0.9747$.

5.3.3 Effect of the Dielectric Constant of the Insulation Layer

An insulation layer is normally used to cover the lateral surface of ZnO blocks in a surge arrester assembly. The dielectric behavior of the insulation layer plays an important role in determining the ZnO varistor withstand capability towards surface flashover. By reinforcing the insulation strength on the varistor surface, deterioration due to partial discharges or moisture ingress could be prevented. In this study, the effect of the dielectric constant of the fiberglass layer on the maximum discharge energy was examined. It was found that increasing the dielectric constant of the insulation layer results in insignificant change in the energy discharged by the arrester as shown in Figure 5.9.

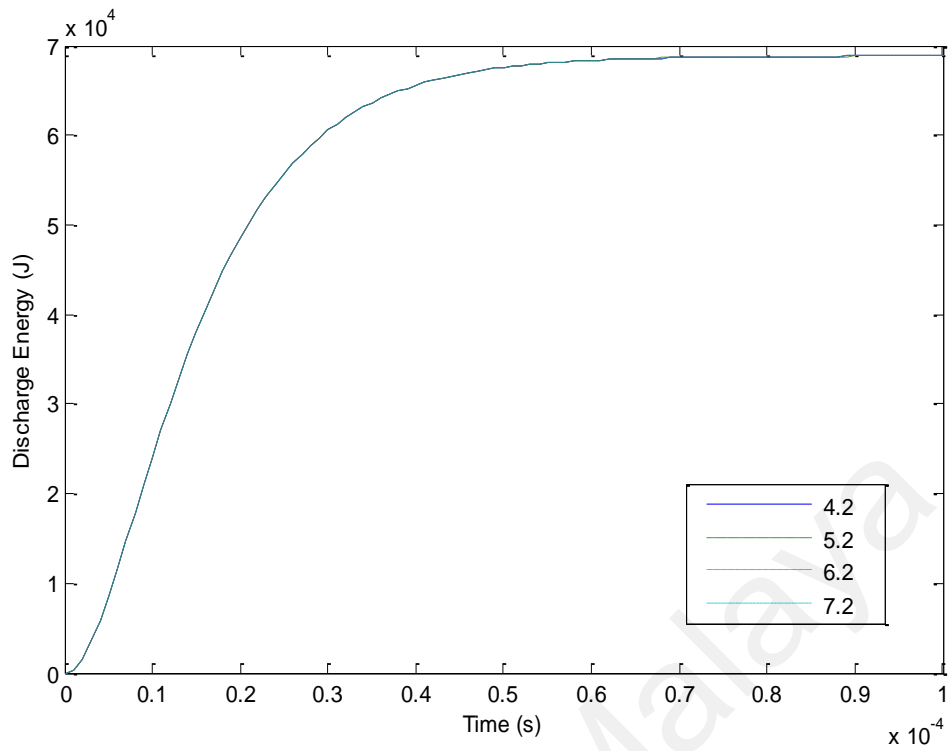


Figure 5.9: Discharge energy as a variation in dielectric constant of insulation layer

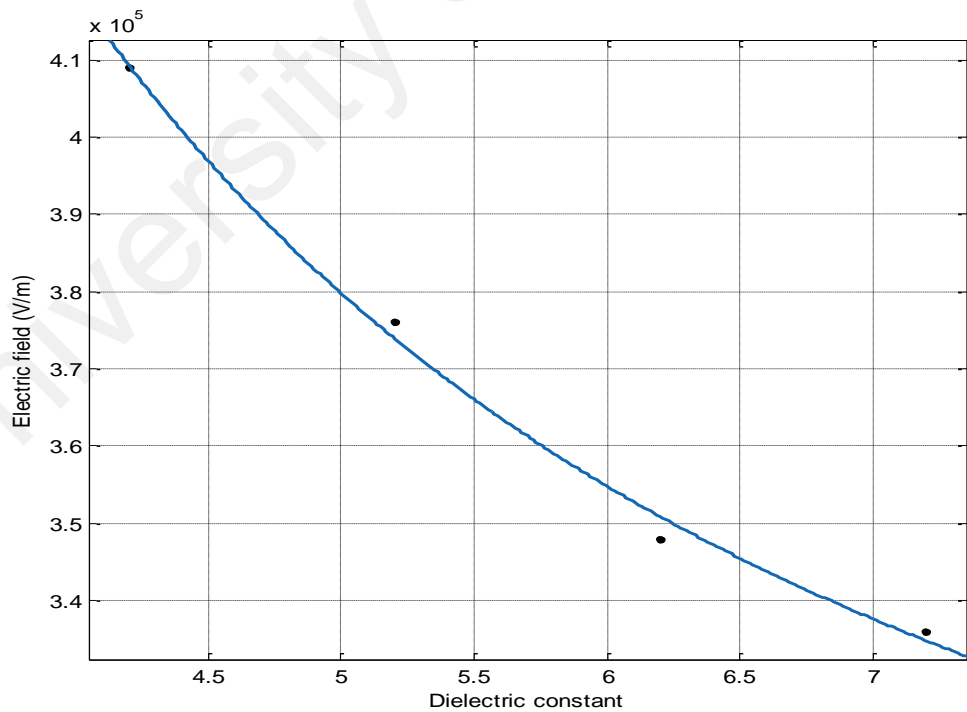


Figure 5.10: Electric field intensity as a variation in dielectric constant of insulation layer

The maximum electric field intensity in the arrester due to variation of the dielectric constant of the insulation layer was also computed, as shown in Figure 5.10. Increasing the dielectric constant decreases the maximum electric field inside the arrester, especially on the lateral surface of the ZnO blocks. Owing to higher permittivity of the insulation layer, the electric field can be aligned easier within the material which will result in lower electric field intensity. This justifies the importance of the insulation layer in preventing the ZnO surface against deterioration.

5.3.4 Effect of the Thickness of the Insulation Layer

One of the most common problems in designing a surge arrester is the effect of non-uniform electric field distribution along the axis of the ZnO blocks (Bartkowiak, et al., 2008). The ZnO blocks placed nearer to the energized electrode are normally stressed by excessive electric field, thus leading to a faster electrical aging of the arrester. A well-known approach to reduce concentration of electric field on the upper ZnO blocks is by proper dimensioning of fiberglass reinforced plastic (FRP) coating.

In this work, the effect of the thickness of the FRP layer on the discharge energy and electric field intensity was investigated. Increasing the thickness of the FRP layer does not affect the energy absorption capability of the arrester as depicted in Figure 5.11. However, a minor reduction on the maximum electric field intensity inside the arrester was observed due to the increased thickness of FRP layer as shown in Figure 5.12. A more uniform electric field distribution was also achieved on the lateral surface of the ZnO block.

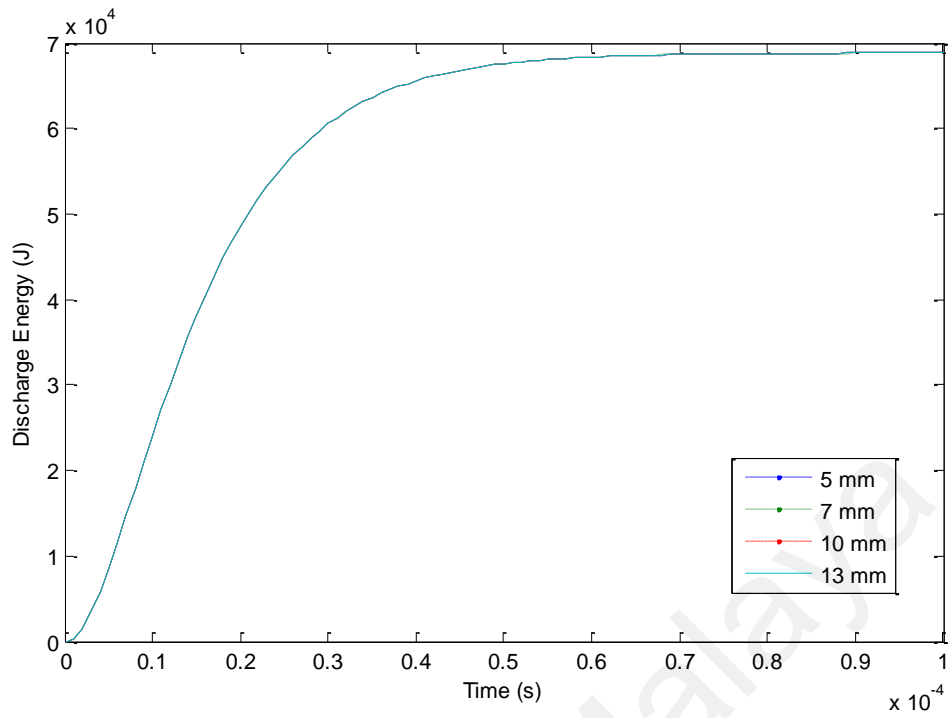


Figure 5.11: Discharge energy as a variation in thickness of insulation layer

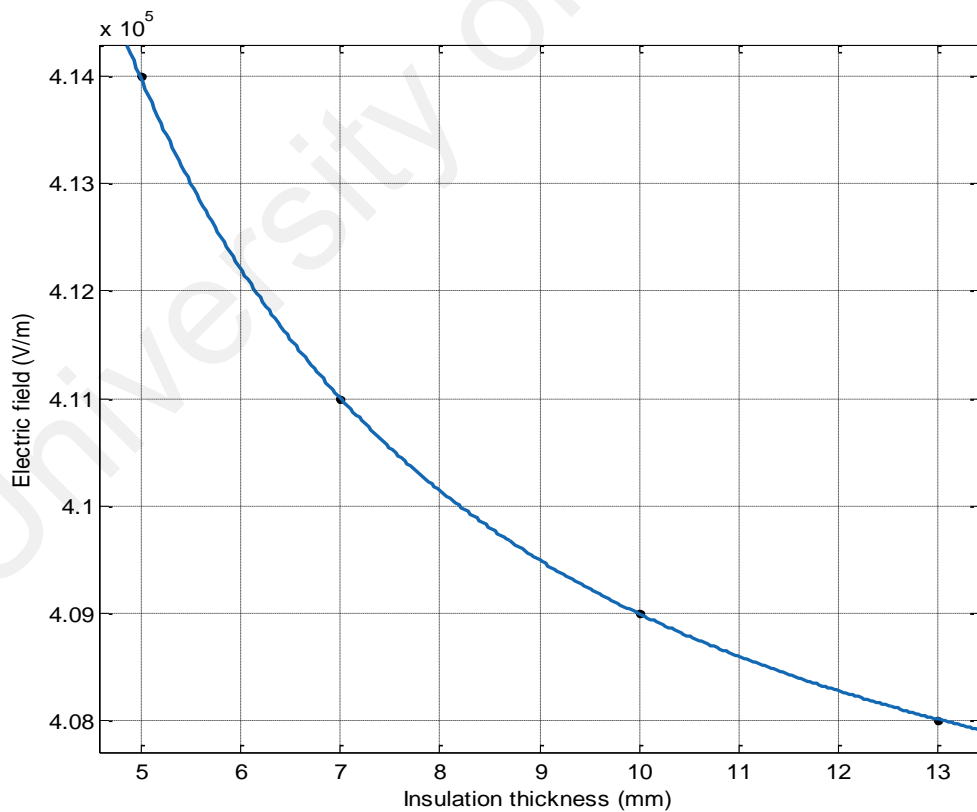


Figure 5.12: Electric field intensity as a variation in thickness of insulation layer

5.3.5 Effect of the Length of the Housing Sheds

The designed surge arrester consists of a single column of ZnO blocks, which was enclosed in silicone rubber weather shed housing. Proper design of the housing is of great importance as the structure mainly protects the active element of the surge arrester (ZnO varistors) from environmental effects while providing an adequate creepage distance. In this study, different lengths of the housing sheds were simulated to determine their effects on the surge arrester's performance due to lightning impulse.

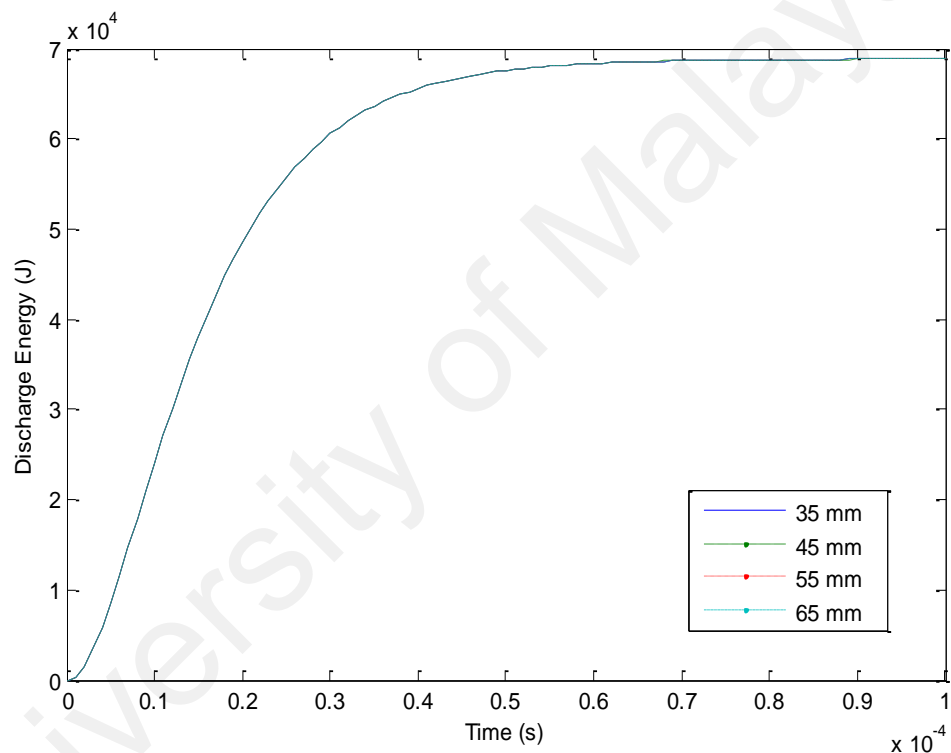


Figure 5.13: Discharge energy as a variation in length of housing sheds

Figure 5.13 shows the maximum discharge energy of the arrester as a function of the housing shed length. Increasing the shed length results in insignificant improvement of the energy absorption capability, in which the recorded value of the energy was around 68 kJ for all simulated cases. However, greater shed length effectively reduces the maximum electric field intensity inside the arrester. Furthermore, the electric field

intensity at certain point within the housing was also decreased, as the tip of the sheds with high electric field intensity was farther from the housing internal structure. Hence, the results indicate that the shed profile design plays an important role on the surge arrester's creepage distance, which determines the insulation withstand level against overvoltage rather than the energy absorption capability.

5.4 Flashover Performance Analysis

The back flashover tripping patterns for the 275/132 kV quadruple circuit transmission line is presented in the following sections. Sensitivity analysis were conducted to determine the influence of several parameters such as lightning current magnitude, tower footing resistance, and power frequency voltage on the line lightning performance. As documented in Table 5.2 to Table 5.7, any phase that experiences flashover during a stroke to the tower top is denoted by 'X'. For each case study, no flashover was recorded on the 275 kV voltage circuits because it has high insulation level. Higher insulation level is the main factor preventing back flashover for the 275 kV transmission line compared to higher coupling with the shield wires. Since 132 kV circuits of the line have lower line insulation critical flashover voltage, majority of back flashover will occur on 132 kV circuits.

5.4.1 Effect of Power Frequency Voltage

The effect of instantaneous power frequency voltages was considered in this work, as lightning strokes can terminate on the line at any time during a power frequency cycle. Table 5.2 shows the results derived when the angle of the instantaneous power frequency voltages were varied by 10° of electrical angle for one cycle (from 0° to 360°). A constant tower footing resistance value of 10 Ω was used for each simulation. The angle of the power frequency voltage for red phase is tabulated in the first column. Meanwhile, the other columns give the critical currents and the phase conductors

tripping. The critical current is defined as the required minimum lightning current magnitude to cause a flashover at one of the phase conductors.

The results show a non-negligible effect of the instantaneous power frequency voltage on the phase conductors tripping due to back flashover phenomena. Referring to Figure 5.14(a) and Figure 5.14(b), the maximum voltage across the line insulation is observed at alternate angles on the red, blue and yellow phases of both circuits. During lightning overvoltage event, the voltage developed across the phase conductor is influenced by both the angle of the instantaneous power frequency voltage, ωt and the incoming surge. Thus, the phase conductor with a higher power frequency voltage at the instant of a lightning stroke termination is more probable to flashover compared to the other phases. In the case of double circuit outages, majority of the flashovers occur at the same phase since both circuits are having synchronised AC voltages.

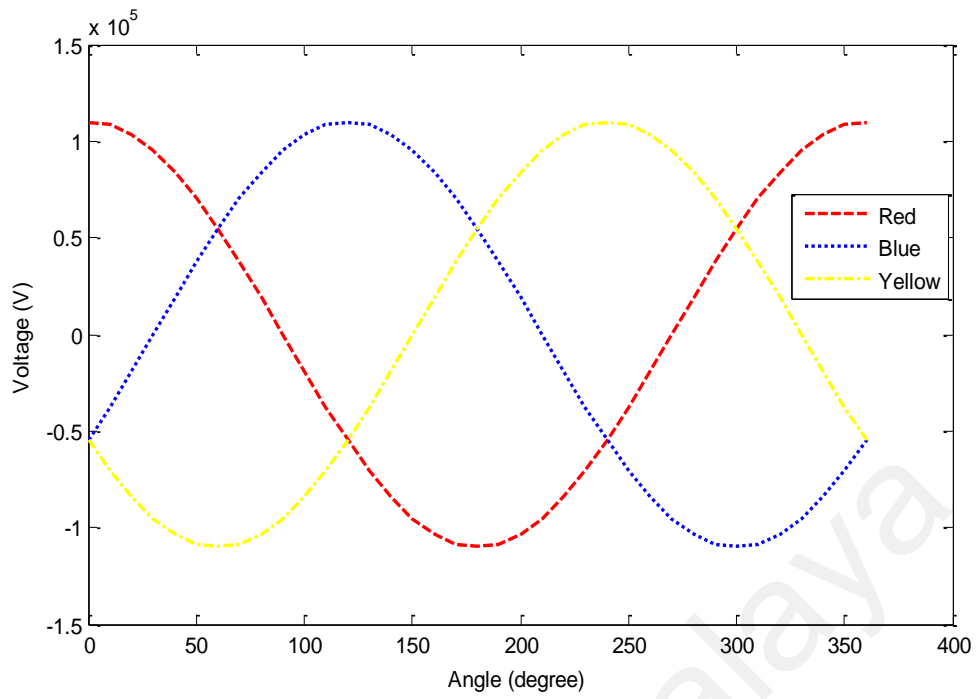
From the simulation results, the red phase of circuits 1 and 2 experiences flashover at the angle between 0° to 40° and 330° to 360° when the low-current resistance was maintained at 10Ω . At these angles, the power frequency voltage of the red phase is the highest amongst the phases, causing it to be more probable to flashover. Flashovers were recorded at alternate phases for the same values of power frequency voltage angle. Referring to Figure 5.14(a), the power frequency voltage of the phases intersects with each other during certain time instants, causing the phases' insulations to have equal voltage magnitudes. For example, the red and blue phases flashover simultaneously when the voltage crossover occurs at the angle of 60° . The same observations were made at 180° for the blue and yellow phases and at 300° for the red and yellow phases.

Table 5.2: Flashover patterns for a variation in power frequency voltage angle ($R_f = 10$)

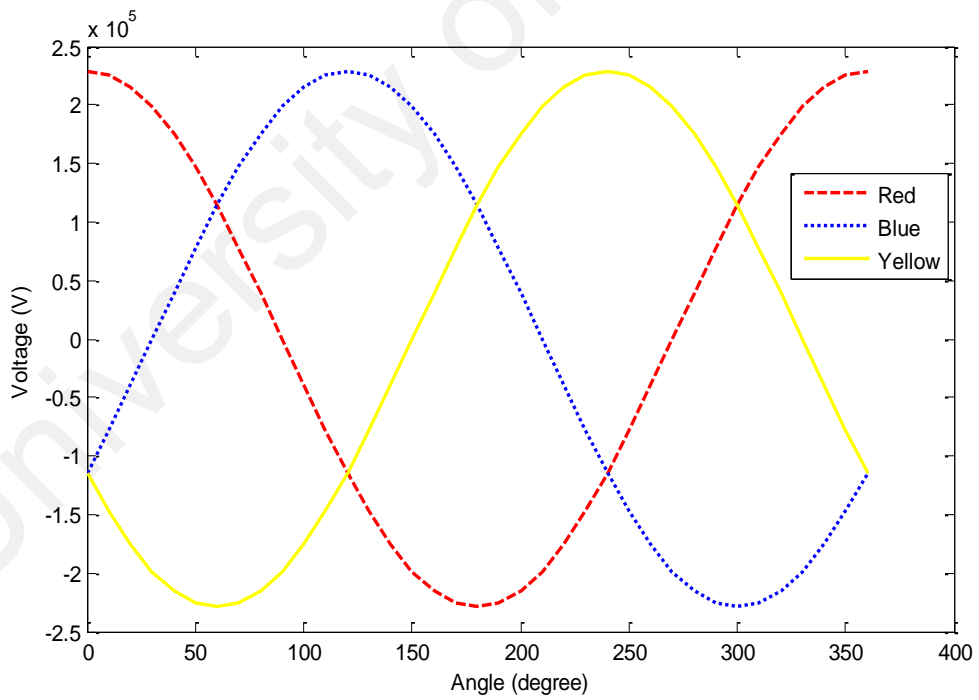
Angle (°)	Phase Conductor												Current (kA)	Phase Flashover	
	132kV line						275kV line								
	R1	R2	B1	B2	Y1	Y2	R1	R2	B1	B2	Y1	Y2			
0	X	X												121	R
10	X	X												122	R
20	X	X												122	R
30	X	X												124	R
40	X	X												125	R
50	X		X	X										126	R&B
60	X		X	X										122	R&B
70			X	X										117	B
80			X	X										115	B
90			X	X										113	B
100			X	X										111	B
110			X	X										110	B
120			X	X										110	B
130			X	X										114	B
140			X	X										114	B
150			X	X										115	B
160			X	X										115	B
170			X	X										117	B
180			X	X		X								122	B&Y
190			X	X		X								126	B&Y
200					X	X								125	Y
210					X	X								124	Y
220					X	X								122	Y
230					X	X								122	Y
240					X	X								121	Y
250					X	X								123	Y
260					X	X								123	Y
270					X	X								125	Y
280	X					X								125	R&Y
290	X					X								121	R&Y
300	X					X								118	R&Y
310	X					X								122	R&Y
320	X					X								125	R&Y
330	X	X												122	R
340	X	X												122	R
350	X	X												122	R
360	X	X												121	R

Furthermore, the simulated results prove that the phase that flashes over has the lowest critical current. Note that the critical current is defined as the required minimum lightning current magnitude to cause a flashover at one of the phase conductors. However, the critical current, which determines the specific conductor flashovers, is not only influenced by the power frequency voltage but also influenced by the coupling coefficient effect. For a certain values of the power frequency angle at 50° , 190° , 280° , 290° , 310° and 320° (tower footing resistance of $10\ \Omega$), the coupling coefficient effect might be more influential on the flashovers pattern, which will be described in the following section.

The flashover patterns are also comparable with the results obtained for a low-current resistance of $50\ \Omega$, as shown in Table 5.3. Further validation has also proven that the overall simulated results were in good agreement with the previously published data (Bakar, et al., 2013).



(a)



(b)

Figure 5.14: Power frequency voltages for (a) lower voltage circuits and (b) higher voltage circuits

Table 5.3: Flashover patterns for a variation in power frequency voltage angle ($R_f = 50$)

Angle (°)	Phase Conductor												Current (kA)	Phase Flashover		
	132kV line						275kV line									
	R1	R2	B1	B2	Y1	Y2	R1	R2	B1	B2	Y1	Y2				
0	X	X													76	R
10	X	X													76	R
20	X	X													76	R
30	X	X													78	R
40	X	X													78	R
50	X	X													79	R
60	X		X	X											77	R&B
70			X	X											76	B
80			X	X											72	B
90			X	X											70	B
100			X	X											70	B
110			X	X											70	B
120			X	X											70	B
130			X	X											70	B
140			X	X											70	B
150			X	X											70	B
160			X	X											72	B
170			X	X											74	B
180			X	X		X									78	B&Y
190					X	X									80	Y
200					X	X									78	Y
210					X	X									78	Y
220					X	X									76	Y
230					X	X									76	Y
240					X	X									76	Y
250					X	X									76	Y
260					X	X									76	Y
270					X	X									78	Y
280					X	X									78	Y
290	X					X									78	R&Y
300	X					X									76	R&Y
310	X					X									78	R&Y
320	X	X													78	R
330	X	X													78	R
340	X	X													78	R
350	X	X													76	R
360	X	X													76	R

5.4.2 Effect of Coupling Coefficient

Coupling coefficient is one of the important parameters in determining flashover tripping pattern. This is due to the fact that the insulation level between overhead ground wires and transmission line is significantly dependent on the coefficient value, which is a function of tower impedance, ground impedance as well as spacing of phase conductors to ground and shield wire. The coupling coefficient is related to phase conductors' configuration at the transmission line for each circuit, where the conductor positioned nearer to the ground plane has a lower coefficient as compared to the upper phases. In the case of a dual-voltage quadruple circuit line with a vertical phase configuration, flashover is more probable to occur at one of the phases having a lower coupling coefficient. Referring to Figure 5.15, the coupling coefficient between the two ground wires and a single phase conductor of the studied system is calculated as follows (Bakar, et al., 2013):

$$C = \frac{\text{average mutual surge impedance}}{\text{equivalent shield wire surge impedance}} \quad (5.5)$$

$$Z_{1R/B/Y} = 60 \log_{10} \frac{D_{1R/B/Y}}{d_{1R/B/Y}} \quad (5.6)$$

$$Z_{2R/B/Y} = 60 \log_{10} \frac{D_{2R/B/Y}}{d_{2R/B/Y}} \quad (5.7)$$

$$C_{R/B/Y} = \frac{(Z_{1R/B/Y} + Z_{2R/B/Y})/2}{Z_n} \quad (5.8)$$

where $Z_{1R/B/Y}$ is mutual impedance between the first ground wire and red, blue and yellow phase conductor respectively, Ω ; $Z_{2R/B/Y}$ is mutual impedance between the second ground wire and red, blue and yellow phase conductor respectively, Ω ; $C_{R/B/Y}$ is coupling

coefficient of red, blue and yellow phase conductor respectively; $D_{1R/B/Y}$ is distance between the phase conductor and the reflected position of the first ground wire; $D_{2R/B/Y}$ is distance between the phase conductor and the reflected position of the second ground wire; $d_{1R/B/Y}$ is distance between the phase conductor and the first ground wire; $d_{2R/B/Y}$ is distance between the phase conductor and the second ground wire; Z_n is equivalent surge impedance of the two ground wires, Ω .

The flashover tripping pattern might be greatly influenced by the coupling coefficient rather than the power frequency voltage, particularly when the voltage waveform of each phases intersect with each other at certain angles. Figure 5.14(a) and Figure 5.14(b) further elucidate the coupling coefficient effect on the flashover pattern. At 50° , both red and blue phases are having almost equally voltage level, which increases the probability of flashover occurrence at these two phases. Although the red phase's voltage is slightly higher at this time instant, the coupling coefficient overcomes the effect of the power frequency voltage where flashover occurs at the red and blue phases of the first circuit and at the blue phase of the second circuit.

Furthermore, flashover was first observed at the red phase of the first circuit as it has lower coupling coefficient compared to the top red phase of the other circuit, as shown in Figure 5.16(a). The blue phase of both circuits also experience simultaneous flashovers at the angle of 50° due to similarity in coupling coefficient with the shield wires. The red phase of the first circuit and the yellow phase of the second circuit flashover concurrently (double circuit flashovers) at 290° as shown in Figure 5.16(b). Both conductors are located at the bottom part of the 132 kV circuits, thus resulting in the lowest coupling coefficient. The findings clearly indicate that the phase conductor positioning on the transmission line also demonstrate a non-negligible effect on the

tripping patterns, even though the majority of flashovers' occurrences are significantly influenced by the power frequency voltages.

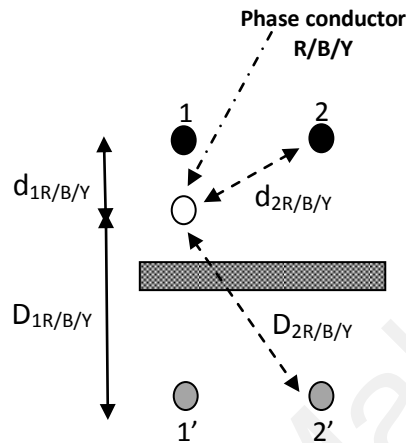
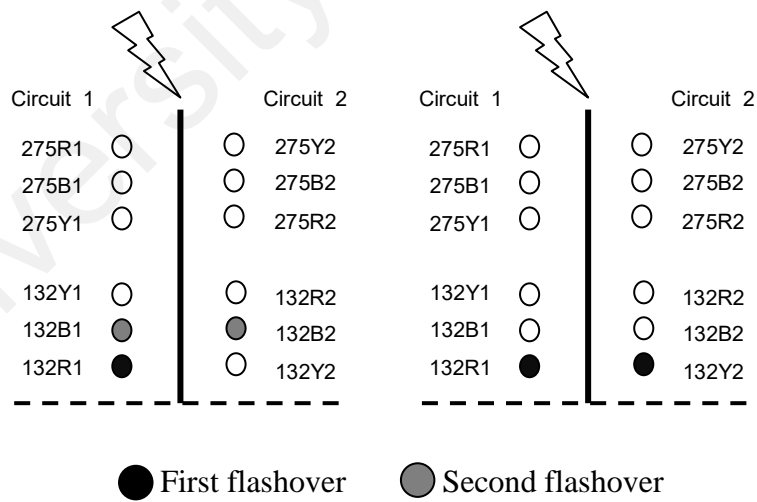


Figure 5.15: Coupling coefficient determination based on phase conductor's position



(a) Reference angle 50° (b): Reference angle 290°

Figure 5.16: Effect of coupling coefficient on the flashover pattern

5.4.3 Effect of Lightning Surge Current Magnitude

The effect of lightning stroke current on the flashover pattern was estimated by simulating peak current magnitude ranging from 85 kA to 200 kA to the tower top. Table 5.4 represents the phases' flashovers when the footing resistance and voltage reference angle were kept constant at 10 Ω and 100° respectively. In case of stroke to the tower top, current magnitudes of 115 kA up to 200 kA have a higher tendency of causing double circuit outages at the middle phase of the 132 kV line. Apart from the effect of symmetrical phase conductor positioning, simultaneous flashovers of both circuits were also influenced by the instantaneous power frequency voltage at the time of the lightning strike, as previously discussed in sections 5.4.1 and 5.4.2.

Table 5.4: Flashover patterns for a variation in lightning stroke current (100°)

Current (kA)	Footing resistance											
	10 Ω						50 Ω					
	R1	R2	B1	B2	Y1	Y2	R1	R2	B1	B2	Y1	Y2
85									X	X		
115			X	X			X		X	X		
120			X	X			X		X	X		
125			X	X			X	X	X	X		
130			X	X			X	X	X	X		
140	X		X	X			X	X	X	X		X
150	X		X	X			X	X	X	X	X	X
160	X	X	X	X		X	X	X	X	X	X	X
170	X	X	X	X		X	X	X	X	X	X	X
180	X	X	X	X		X	X	X	X	X	X	X
190	X	X	X	X	X	X	X	X	X	X	X	X
200	X	X	X	X	X	X	X	X	X	X	X	X

Meanwhile, further increase in the lightning current magnitude causes higher voltage built-up across the insulations, thus, initiating more flashovers at other phases. At 140 kA and 150 kA, a single circuit outage was recorded on the first circuit of the red phase. For a current magnitude between 160 kA and 180 kA, flashovers occur on the red and blue phases of both circuits. Most of the lightning energy was discharged through these two phases; therefore, breakdown occurs only on the lower circuit of the yellow phase (Y2). At a very high lightning current of above 190 kA, all three phases of the stricken tower experience double circuit flashovers.

Table 5.5: Flashover patterns for a variation in lightning stroke current (350°)

Current (kA)	Footing resistance											
	10 Ω						50 Ω					
	R1	R2	B1	B2	Y1	Y2	R1	R2	B1	B2	Y1	Y2
85							X					
115	X						X	X				X
120	X						X	X				X
125	X	X					X	X				X
130	X	X					X	X				X
140	X	X					X	X			X	X
150	X	X				X	X	X	X	X	X	X
160	X	X				X	X	X	X	X	X	X
170	X	X	X	X	X	X	X	X	X	X	X	X
180	X	X	X	X	X	X	X	X	X	X	X	X
190	X	X	X	X	X	X	X	X	X	X	X	X
200	X	X	X	X	X	X	X	X	X	X	X	X

As the footing resistance was increased to 50 Ω , both circuits of the blue phase experience concurrent flashovers at lower current magnitude of 85 kA. Simulating

higher current of 150 kA worsen the line lightning performance where flashovers were observed at all phase conductors. However, the tripping patterns for both footing resistance values are comparable, in which increasing the lightning current magnitude initiates more phases' flashovers. For each simulated case, no flashover was observed at any phase of the 275 kV circuits and the adjacent towers.

Table 5.5 shows the impact of lightning current magnitude on the flashover tripping pattern when the voltage reference angle was simulated at 350° . For footing resistance value of 10Ω , double circuit outages was observed at the red phase of both 132 kV circuits due to lightning current magnitudes of 125 kA up to 200 kA. As the lightning current magnitude was increased between 150 kA and 160 kA, a single circuit outage was recorded on the second circuit of the yellow phase (Y2). The outage occurs dominantly on Y2 rather than Y1 as the lower phase conductor (Y2) is positioned nearer to the ground plane.

Further increase in the lightning current magnitude from 170 kA to 200 kA causes higher overvoltage across the line insulations, thus causing flashovers at all phase conductors of the 132 kV line. As the footing resistance was simulated at 50Ω , both circuits of the red phase start experiencing flashovers at lower current magnitude of 115 kA. By increasing the current magnitude to 150 kA, poor line lightning performance was observed where flashovers occur at all phase conductors of the 132 kV line.

5.4.4 Effect of Tower Footing Resistance

One of the most important parameters to be considered in insulation coordination of overhead transmission line is tower footing resistance design (Wu, et al., 2014; Khodr, 2009; Christodoulou, et al., 2014). During back flashover event, the peak overvoltage occurring at the top of the tower is dependent on the tower footing resistance. Figure 5.17 depicts the overvoltage across the red phase insulation of the first circuit (R1) as a

variation of tower footing resistance of the stricken tower, given a 0° voltage reference angle and lightning current of 200 kA.

A moderate increase of the overvoltage across phase R1 was recorded due to increased footing resistance value. As expected, the lowest magnitude of peak overvoltage occurs when the footing resistance was kept at 10 Ω . This behavior provides justification on the need of maintaining a low resistance value as another conventional method to improve the line lightning performance. To further estimate the worst case lightning performance of the studied line, a footing resistance of 50 Ω was simulated which results in maximum overvoltage developed across the phase's insulation. The effect of tower footing resistance on the flashover characteristics was also investigated based on the magnitude of critical current, I_c . For each simulated value of tower footing resistance, the voltage reference angle was kept constant at 0° while the lightning current magnitude was varied until the red phase conductor of the first circuit flashes over.

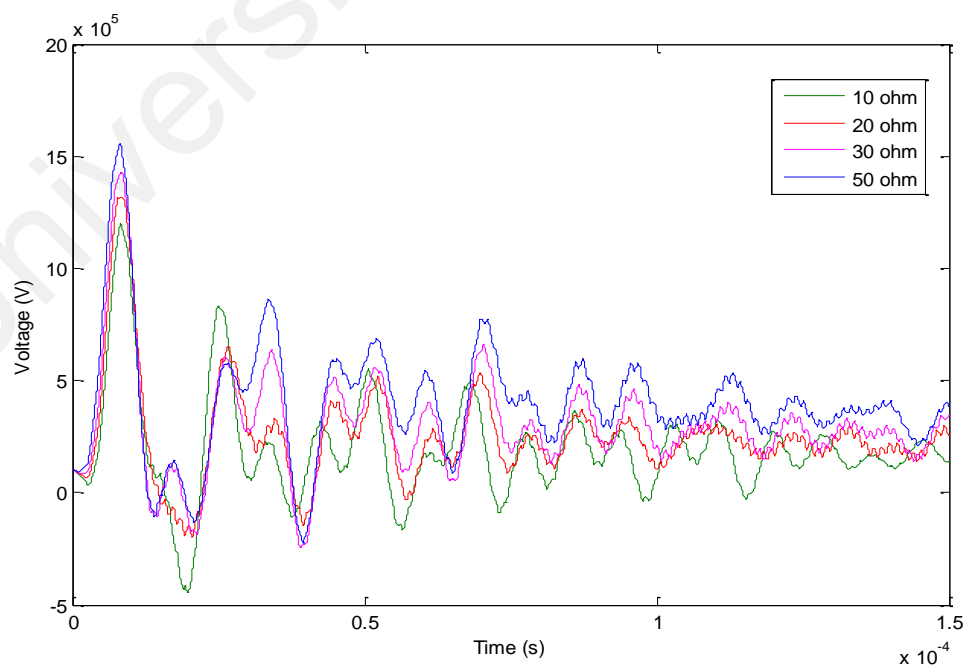


Figure 5.17: Lightning overvoltage at phase R1 for a variation in tower footing resistance

The minimum current initiating the flashover is regarded as the critical current, as shown in Table 5.6. It is clearly seen that increasing the tower footing resistance requires a lower lightning current magnitude to cause a flashover at one of the phases. A higher resistance value produces less negative reflections from the tower base towards the tower top, thus increasing the peak voltage at the tower top. In order to cause flashover, less current magnitude is needed so that a sufficient voltage difference is developed between the phase conductor and the cross arm which exceeds the line CFO voltage. The results suggest the importance of maintaining a low footing resistance value around 10 Ω , as currently practiced by the national utility company.

Table 5.6: Critical lightning current (I_C) for a variation in tower footing resistance

Footing resistance (Ω)	Critical current (kA)
10	121
20	100
30	87
50	76

5.4.5 Effect of Current Wave Front Time

The effect of lightning front time on the back flashover events were derived by keeping constant the tower footing resistance and voltage reference angle at 10 Ω and 0° respectively. Figure 5.18 depicts the dependence of overvoltage across the insulator string of phase R1 when a single-stroke current of 150 kA magnitude with three different front time values of 1.2 μ s, 2.0 μ s and 3.5 μ s was injected to the top of the middle tower.

It can be seen that the resulting overvoltage is inversely proportional with the current wave front time. In spite of the same decay time value, a shorter front time

produces higher magnitude while a longer front time produces lower magnitude for the lightning overvoltage observed across the insulator strings. This implies that the simulated wave front time of lightning strokes has a significant influence on the impulse voltage withstand capability of the line insulation.

The effect of lightning stroke front time can be clarified further by referring to Table 5.7. For a variation of lightning front time magnitudes, the critical current, I_c needed to cause single circuit flashover at the red phase of the lower voltage circuit (132 kV) is tabulated in the second column. The results show a significant dependency of the critical current on the lightning front time. A shorter front time notably decreases the minimum lightning current required to initiate a flashover at the red phase of the first circuit. This happens as less current peak amplitude is required to build up a sufficient impulse voltage across the insulator string which exceeds its impulse voltage withstand capability.

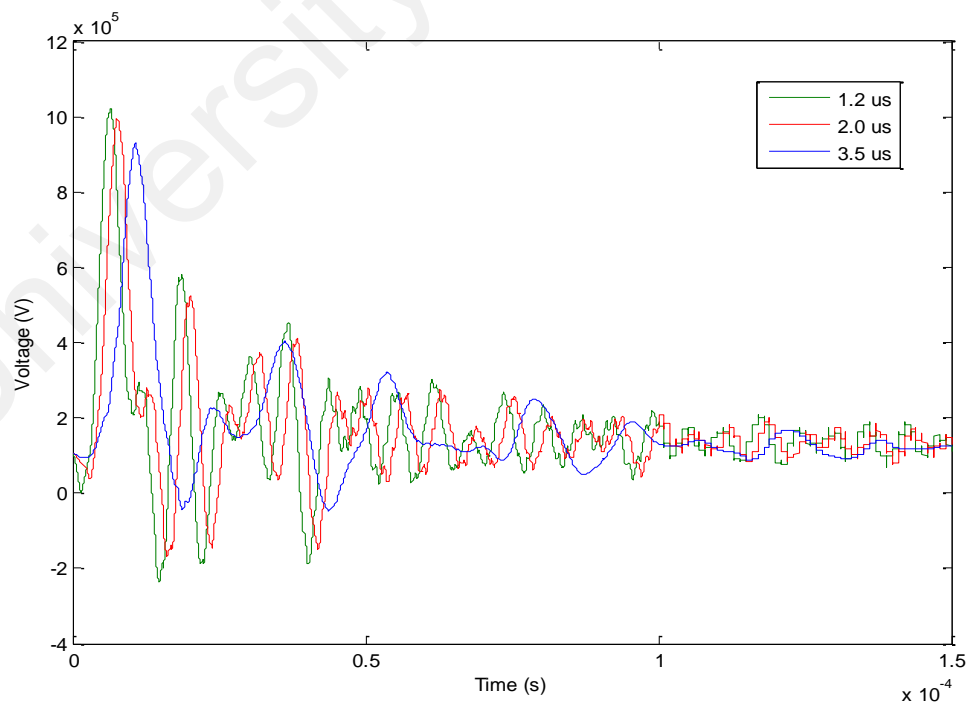


Figure 5.18: Lightning overvoltage at phase R1 for a variation in current front time

Table 5.7: Critical lightning current (I_C) for a variation in current front time (t_f)

Front time (μs)	Critical current (kA)
1.2	106
2.0	111
2.5	116
3.5	128

Table 5.8: Flashover patterns for a variation in current front time (t_f)

a) Front time of 2.0 μs

Current (kA)	Footing resistance											
	132 kV line						275 kV line					
	R1	R2	B1	B2	Y1	Y2	R1	R2	B1	B2	Y1	Y2
115	X											
120	X											
125	X	X										
130	X	X										
140	X	X										
150	X	X				X						
160	X	X	X	X		X						
170	X	X	X	X		X						
180	X	X	X	X	X	X						
190	X	X	X	X	X	X						
200	X	X	X	X	X	X						

b) Front time of 3.0 μ s

Current (kA)	Footing resistance											
	132 kV line						275 kV line					
	R1	R2	B1	B2	Y1	Y2	R1	R2	B1	B2	Y1	Y2
115												
120	X											
125	X											
130	X											
140	X	X										
150	X	X										
160	X	X										
170	X	X				X						
180	X	X	X	X	X	X						
190	X	X	X	X	X	X						
200	X	X	X	X	X	X						

The effect of lightning front time was also verified based on back flashover occurrences at the red phase of the first circuit, as shown in Table 5.8(a) and Table 5.8(b). Different lightning stroke magnitudes ranging from 115 kA to 200 kA were simulated for front time values of 2.0 μ s and 3.0 μ s respectively. The results indicate that a lightning stroke of shorter front time ($t_f = 2.0 \mu$ s) initiates a single circuit flashover at lower current magnitude of 115 kA. As higher current magnitude of above 125 kA was simulated, double circuit outages occur simultaneously at the red phase of both circuits.

Meanwhile, the bottom red phase (R1) experiences flashover when the front time and magnitude of the lightning stroke were simulated at 3.0 μ s and 120 kA respectively. In the case of 3.0 μ s wave front time, double circuit flashovers were observed at higher

lightning current magnitude above 140 kA, as compared to front time of 2.0 μ s. Regardless of the effect of lightning stroke tail time, t_n , the simulation results clearly justify that higher impulse voltage will be produced with decrease in front time, t_f which consequently causes more back flashover occurrences across the phase insulator strings.

5.5 Installation of Surge Arrester

The effect of installing the designed surge arrester on the back flashover tripping pattern for the 275/132 kV quadruple circuit transmission line is discussed in the following sections. Based on the previously obtained tripping pattern, back flashovers did not occur on the 275 kV transmission lines owing to both the higher insulation level of these lines and to their higher coupling with the shield wires. Hence, arresters were only installed on the lower circuit line of 132 kV. Five different surge arrester configurations as shown in Table 5.9 were tested to determine their capabilities in protecting the transmission line from double circuit outages initiated from back flashover event. These configurations were selected for testing based on previously published literatures on arrester installation techniques (Bhattarai et al., 2008; Munukutla et al., 2010).

Furthermore, sensitivity analysis were also conducted with the presence of the installed surge arresters to determine the influence of lightning current magnitude, tower footing resistance and power frequency voltage on the line lightning performance. The most effective configuration was determined based on the minimum number of installed arresters and efficiency in eliminating flashover. As documented in Table 5.10 to Table 5.24, any phase that experiences flashover during a stroke to the tower top is denoted by 'X'. Note that any simulated case without flashover occurrence is denoted as 'NT'. 'ST' denotes a single circuit tripping due to back flashover while a double circuit tripping is denoted by 'DT'.

Table 5.9: Configuration of surge arrester

No.	Surge arrester configuration	Description
1		No surge arrester
2		1-3 arrangement
3		Double bottom arrangement
4		Double top arrangement
5		I-arrangement
6		L-arrangement

○ 275kV circuit without arrester ○ 132kV circuit without arrester
 ● 132kV circuit with arrester

5.5.1 Lightning Current Magnitude

The effect of surge arrester configurations with respect to lightning current magnitude on the line flashover pattern is demonstrated in Table 5.10 to Table 5.14. Table 5.15 summarizes the type of insulator flashovers experienced by the quadruple circuit line for different lightning current magnitudes. The tower footing resistance and voltage reference angle were fixed at $10\ \Omega$ and 0° respectively. In the case of lightning strokes of lower than 122 kA, no double circuit flashover was recorded at any phase of the 132 kV circuits. However, the red phase of both 132 kV circuits without installed surge arresters flashover concurrently when the lightning current was simulated at 122 kA and 150 kA. More double circuit flashovers were recorded at the red and blue phases of the 132 kV circuits when the lightning current magnitude was increased to 170 kA. The worst lightning performance without the presence of surge arrester was recorded at the current magnitude of 200 kA as the red, blue and yellow phases of both 132 kV circuits experience flashover due to lightning strike to the tower top.

To eliminate the double circuit flashovers, configuration 2 to 6 with the application of surge arresters up to 3 units were tested. Configuration 1 which incorporates the use of surge arresters at the yellow and red phases of the first 132 kV circuit was able to prevent double circuit flashover for a current magnitude up to 150 kA. However, the configuration does not improve the line lightning performance where double circuit flashovers were still observed at the unprotected circuits of the blue phase for current magnitudes of 170 kA and 200 kA. It is only capable of reducing the high current effect on the red and yellow phases as only single circuit flashovers were recorded at both phases.

The presence of surge arresters on the top phase of both circuits (Y1 and R2) as per configuration 4 produces comparable results with the first configuration in term of the

flashover type. Although the recorded pattern of the fourth configuration varies from the first configuration in term of the phase flashover sequences, it can be concluded that both configurations offer similar level of line lightning protection. Configuration 3 with the application of surge arresters on the bottom phase of both circuits (R1 and Y2) demonstrates the worst lightning protection, at which double circuit outages tend to occur for lightning current magnitudes of 150 kA and above.

Configuration 5 results in a better line flashover performance compared to configuration 6 even though the same number of surge arresters were installed on all phases regardless of positioning on the circuit. The installed surge arresters of configuration 5 effectively perform the discharge duty without experiencing any double circuit flashover up to 200 kA lightning current magnitude. However, configuration 6 which applies the surge arresters on the bottom phase of both circuits (R1 and Y2) and the red phase of the first circuit (R1) is unable to withstand high magnitude of lightning current. Although the configuration completely protects the line from any outage for current of 122 kA and below, double circuit flashovers were still observed at the blue phase of the 132 kV circuits for current of 170 kA and above.

Table 5.10: Flashover pattern for a 122 kA lightning current

Configuration	Phase Conductor												Flashover
	132kV line						275kV line						
	R1	R2	B1	B2	Y1	Y2	R1	R2	B1	B2	Y1	Y2	
No arrester	X	X											DT
1-3 arrangement		X											ST
Double bottom		X											ST
Double top	X												ST
I-arrangement		X											ST
L-arrangement													NT

Table 5.11: Flashover pattern for a 150 kA lightning current

Configuration	Phase Conductor												Flashover
	132kV line						275kV line						
	R1	R2	B1	B2	Y1	Y2	R1	R2	B1	B2	Y1	Y2	
No arrester	X	X				X							DT
1-3 arrangement		X				X							ST
Double bottom		X	X	X									DT
Double top	X					X							ST
I-arrangement		X				X							ST
L-arrangement		X											ST

Table 5.12: Flashover pattern for a 170 kA lightning current

Configuration	Phase Conductor												Flashover	
	132kV line						275kV line							
	R1	R2	B1	B2	Y1	Y2	R1	R2	B1	B2	Y1	Y2		
No arrester	X	X	X	X		X								DT
1-3 arrangement		X	X	X		X								DT
Double bottom		X	X	X	X									DT
Double top	X		X	X		X								DT
I-arrangement		X		X		X								ST
L-arrangement		X	X	X										DT

Table 5.13: Flashover pattern for a 200 kA lightning current

Configuration	Phase Conductor												Flashover	
	132kV line						275kV line							
	R1	R2	B1	B2	Y1	Y2	R1	R2	B1	B2	Y1	Y2		
No arrester	X	X	X	X	X	X								DT
1-3 arrangement		X	X	X		X								DT
Double bottom		X	X	X	X									DT
Double top	X		X	X		X								DT
I-arrangement		X		X		X								ST
L-arrangement		X	X	X										DT

Table 5.14: Insulator flashovers for different lightning current magnitudes

Configuration	Lightning current (kA)			
	122	150	170	200
No arrester	DT	DT	DT	DT
1-3 arrangement	ST	ST	DT	DT
Double bottom	ST	DT	DT	DT
Double top	ST	ST	DT	DT
I-arrangement	ST	ST	ST	ST
L-arrangement	NT	ST	DT	DT

5.5.2 Tower Footing Resistance

The effect of surge arrester configurations with respect to tower footing resistance on the line flashover performance was demonstrated in Table 5.15 to Table 5.18. Table 5.19 summarizes the type of insulator flashovers experienced by the quadruple circuit line for resistance value of between 10 Ω to 50 Ω . For each configuration, the voltage reference angle and lightning current magnitude were kept constant at 0° and 122 kA respectively.

In case of a lightning strike to the tower top, flashovers were recorded at the red phase of both 132 kV circuits when the footing resistance of all towers was simulated at 10 Ω and 20 Ω . Increasing the footing resistance up to 30 Ω produces a more severe impact on the line flashover performance in which double circuit outages were observed at the red and blue phases of the struck tower. The worst flashover performance was recorded when the resistance value was simulated at 50 Ω , which causes all phases to experience double circuit outages.

Configurations 2 to 6 were tested for a variation in the tower footing resistance value to mitigate the double circuit flashovers. Installation of surge arresters on the bottom phase of both circuits (R1 and Y2) and the red phase of the first circuit (R1) as per configuration 6 improves the flashover performance of the 132 kV line where no circuit tripping was recorded for resistance value of 10 Ω . However, the configuration is insufficient to prevent a double circuit flashover occurrence for a high resistance value of 30 Ω and above.

Configurations 2, 3 and 4 demonstrate the same flashover characteristic for tower footing resistance value up to 50 Ω . The configurations are capable in providing complete protections against double circuit flashover when the resistance was simulated at 10 Ω and 20 Ω . Hence, it can be summarized that these configurations result in similar protection level although the recorded patterns vary in term of the phase flashover sequences.

Simultaneous double circuit line outages due to variation in the tower footing resistance could be significantly eliminated by incorporating configuration 5 in the designed system. The configuration with surge arresters on all phases of one circuit is capable of reducing the overvoltage impact on the line as only single circuit flashovers were recorded for all resistance values of up to 50 Ω .

Table 5.15: Flashover pattern for tower footing resistance of 10 Ω

Configuration	Phase Conductor												Flashover	
	132kV line						275kV line							
	R1	R2	B1	B2	Y1	Y2	R1	R2	B1	B2	Y1	Y2		
No arrester	X	X												DT
1-3 arrangement		X												ST
Double bottom		X												ST
Double top	X													ST
I-arrangement		X												ST
L-arrangement														NT

Table 5.16: Flashover pattern for tower footing resistance of 20 Ω

Configuration	Phase Conductor												Flashover	
	132kV line						275kV line							
	R1	R2	B1	B2	Y1	Y2	R1	R2	B1	B2	Y1	Y2		
No arrester	X	X				X								DT
1-3 arrangement		X				X								ST
Double bottom		X												ST
Double top	X					X								ST
I-arrangement		X				X								ST
L-arrangement		X												ST

Table 5.17: Flashover pattern for tower footing resistance of 30 Ω

Configuration	Phase Conductor												Flashover
	132kV line						275kV line						
	R1	R2	B1	B2	Y1	Y2	R1	R2	B1	B2	Y1	Y2	
No arrester	X	X	X	X		X							DT
1-3 arrangement		X	X	X		X							DT
Double bottom		X	X	X									DT
Double top	X		X	X		X							DT
I-arrangement		X		X		X							ST
L-arrangement		X	X	X									DT

Table 5.18: Flashover pattern for tower footing resistance of 50 Ω

Configuration	Phase Conductor												Flashover
	132kV line						275kV line						
	R1	R2	B1	B2	Y1	Y2	R1	R2	B1	B2	Y1	Y2	
No arrester	X	X	X	X	X	X							DT
1-3 arrangement		X	X	X		X							DT
Double bottom		X	X	X	X								DT
Double top	X		X	X		X							DT
I-arrangement		X				X							ST
L-arrangement		X	X	X									DT

Table 5.19: Insulator flashovers for different tower footing resistances

Configuration	Footing resistance (Ω)			
	10	20	30	50
No arrester	DT	DT	DT	DT
1-3 arrangement	ST	ST	DT	DT
Double bottom	ST	ST	DT	DT
Double top	ST	ST	DT	DT
I-arrangement	ST	ST	ST	ST
L-arrangement	NT	ST	DT	DT

5.5.3 Power Frequency Voltage

The best arrester configuration was also determined based on the flashover performance with respect to the instantaneous power frequency voltage effect, as demonstrated in Table 5.20 to Table 5.21. Table 5.22 summarizes the type of insulator flashovers experienced by the quadruple circuit line for reference angle of 0° , 70° , 180° , and 300° . The ability of each configuration to mitigate insulator flashovers was investigated by simulating constant tower footing resistance and lightning current magnitude of 10° and 122 kA respectively.

Incorporating two surge arresters at the struck tower does not provide a complete protection against double circuit flashover for phase angle step of 70° , as depicted by configurations 2 and 4. These configurations are only capable of reducing the probability of double circuit outages at the red and yellow phases since no surge arresters are installed on any circuit of the blue phase.

Application of two surge arresters on the bottom phases of both 132 kV circuits as per configuration 3 has an advantage over configurations 2 and 4 where the probability

of insulator flashovers was reduced to zero when the reference angle was simulated at 300° . However, the configuration is not effective in restraining double circuit flashover at the angle of 70° and 180° . This happens as the maximum voltage developed across the blue phase insulations due to surge overvoltage is higher than the other phases, thus causing the blue phase to be more probable to flashover occurrence. As configuration 3 does not incorporate any surge arrester at the blue phase of both circuits, double circuit outages could not be prevented.

Configuration 6 notably improves the line lightning performance where no insulator flashover was recorded for each phase step angle of 0° , 180° and 300° . However, the configuration does not successfully restrain the overvoltage from inducing double circuit flashover at the blue phase when the angle was kept constant at 70° .

Installation of surge arresters on all phases of one circuit as depicted by configuration 5 successfully eliminated the simultaneous line outages, where the continuity of service of one circuit was sustained for each simulated value of power frequency voltage angle. The recorded pattern demonstrates the same lightning performance derived from the previous sections, thus proving that this configuration is the most effective solution in eliminating double circuit outages due to back flashover event.

Table 5.20: Flashover pattern for power frequency voltage of 0°

Configuration	Phase Conductor												Flashover	
	132kV line						275kV line							
	R1	R2	B1	B2	Y1	Y2	R1	R2	B1	B2	Y1	Y2		
No arrester	X	X												DT
1-3 arrangement		X												ST
Double bottom		X												ST
Double top	X													ST
I-arrangement		X												ST
L-arrangement														NT

Table 5.21: Flashover pattern for power frequency voltage of 70°

Configuration	Phase Conductor												Flashover	
	132kV line						275kV line							
	R1	R2	B1	B2	Y1	Y2	R1	R2	B1	B2	Y1	Y2		
No arrester			X	X										DT
1-3 arrangement			X	X										DT
Double bottom			X	X										DT
Double top			X	X										DT
I-arrangement				X										ST
L-arrangement			X	X										DT

Table 5.22: Flashover pattern for power frequency voltage of 180°

Configuration	Phase Conductor												Flashover	
	132kV line						275kV line							
	R1	R2	B1	B2	Y1	Y2	R1	R2	B1	B2	Y1	Y2		
No arrester			X	X		X								DT
1-3 arrangement						X								ST
Double bottom			X	X										DT
Double top						X								ST
I-arrangement						X								ST
L-arrangement														NT

Table 5.23: Flashover pattern for power frequency voltage of 300°

Configuration	Phase Conductor												Flashover	
	132kV line						275kV line							
	R1	R2	B1	B2	Y1	Y2	R1	R2	B1	B2	Y1	Y2		
No arrester	X					X								ST
1-3 arrangement						X								ST
Double bottom														NT
Double top	X					X								ST
I-arrangement						X								ST
L-arrangement														NT

Table 5.24: Insulator flashovers for different power frequency voltage angles

Configuration	Power frequency voltage angle			
	0°	70°	180°	300°
No arrester	DT	DT	DT	ST
1-3 arrangement	ST	DT	ST	ST
Double bottom	ST	DT	DT	NT
Double top	ST	DT	ST	ST
I-arrangement	ST	ST	ST	ST
L-arrangement	NT	DT	NT	NT

University of Malaysia

CHAPTER 6: CONCLUSIONS AND RECOMMENDATIONS

6.1 Conclusions

In this work, a surge arrester has been successfully modeled by using finite element analysis, PSCAD/EMTDC and EMTP-RV software. The results demonstrate satisfactory agreement between both computational techniques for the discharge energy subjected to a single impulse current injection. Furthermore, all studied cases were demonstrated to be adequately modeled as the simulated results were comparable with the measured practical data of the residual voltage and energy withstand capability.

On the basis of the reasonable agreement shown by the measured and computed values, further design modifications on the surge arrester's dimension and material properties were conducted to investigate their effect related to the ZnO varistor characteristics. It was found that variation in the height and diameter of the ZnO varistor block results in remarkable effects on the discharge energy capability of the arrester during a single impulse current injection. Meanwhile, varying the thickness and dielectric constant of the insulation layer significantly affects the uniformity of the electric field distribution inside the arrester rather than the discharge energy capability. Therefore, the results obtained from this work may help manufacturers to design surge arresters with better energy absorption capability, which can then improve the performance of surge arresters.

The developed surge arrester models were then used to determine overvoltage protection scheme for a 275/132 kV quadruple circuit transmission line in Malaysia, by means of EMTP-RV software. For each case, the 275 kV voltage circuits with higher insulation CFO voltage are found to be less susceptible to lightning disturbance as flashovers occur dominantly on the lower voltage circuits (132 kV). Although the

higher incidence of back flashover is significantly influenced by the insulation level, the coupling coefficient also plays an important role in determining the flashover pattern. A stronger coupling effect was observed as both 132 kV circuits were positioned on the bottom part of the tower, which consequently causes flashovers to occur prominently on the lower voltage circuits rather than the higher voltage circuits.

The results also indicate that the significant height of the monopole towers does not influence the flashover pattern, in which the recorded tripping characteristics are comparable with previously published data for 132 kV double circuit line study. Improvement of the lightning performance of the 275/132 kV quadruple circuits transmission line could be achieved by solely installing the surge arresters on the lower voltage circuits. The most appropriate arresters' configuration was selected by considering the effects of tower footing resistance, lightning current and power frequency angle on the line lightning performance. In conclusion, configuration 5 with installed surge arresters on each phase of one circuit provides sufficient protection to the line from double circuit flashover occurrence.

6.2 Recommendations

Future works that can be recommended from this research work are:

- i. For the purpose of reducing the modeling complexity, removal of sharp edges and other small scale features of the designed surge arrester in the FEA software can be done as the parts will not significantly influence the simulation results. Further improvements on the model can be done by considering omitted features of the surge arrester such as the zinc oxide wall, disc string and stainless steel rod.
- ii. In this study, the best possible arrangement of line surge arresters was determined based on back flashover phenomena. Based on previous

researches, the back flashover phenomena are of greater concern since a great number of lightning stroke were recorded terminating on the tower top and shield wire rather than the phase conductor. The surge voltage caused by back flashover is also usually more severe than those caused by shielding failure in the case of effectively shielded line. However, the shielding failure occurrences are more severe when lower lightning peak currents of below 31 kA terminate on the phase conductors. The worst case of line flashover due to shielding failure phenomena can be considered in future work to assess the installed arresters' performance towards the overall improvement of the line lightning performance.

- iii. Selection of the surge arrester placement to improve the overall line lightning performance can be conducted by performing sensitivity analysis on the arrester's discharge energy duties due to lightning overvoltage. Evaluation of the discharge energy is important to avoid redundant installation of the surge arresters, which will result in uneconomical line protection design.
- iv. The proposed FEA model can be further extended for other type of surge arrester development tests such as switching surge test and design optimization test.

REFERENCES

- Ab Kadir, M. Z. A., & Cotton, I. (2010). Application of the insulator coordination gap models and effect of line design to backflashover studies. *International Journal of Electrical Power & Energy Systems*, 32(5), 443-449.
- Ametani, A., & Kawamura, T. (2005). A method of a lightning surge analysis recommended in Japan using EMTP. *IEEE Transactions on Power Delivery*, 20(2), 867-875.
- Ancajima, A., Carrus, A., Cinieri, E., & Mazzetti, C. (2010). Behavior of MV insulators under lightning-induced overvoltages: experimental results and reproduction of volt-time characteristics by disruptive effect models. *IEEE Transactions on Power Delivery*, 25(1), 221-230.
- Andoh, H., Nishiwaki, S., Suzuki, H., Boggs, S., & Kuang, J. (2000). Failure mechanisms and recent improvements in ZnO arrester elements. *Electrical Insulation Magazine, IEEE*, 16(1), 25-31.
- Bakar, A. H. A., Rahim, N. A., & Zambri, M. K. M. (2011). Analysis of lightning-caused ferroresonance in Capacitor Voltage Transformer (CVT). *International Journal of Electrical Power & Energy Systems*, 33(9), 1536-1541.
- Bakar, A. H. A., Talib, D. N. A., Mokhlis, H., & Illias, H. A. (2013). Lightning back flashover double circuit tripping pattern of 132kV lines in Malaysia. *International Journal of Electrical Power & Energy Systems*, 45(1), 235-241.
- Bartkowiak, M., Comber, M. G., & Mahan, G. D. (1996). Energy handling capability of ZnO varistors. *Journal of Applied Physics*, 79(11), 8629-8633.
- Bartkowiak, M., Comber, M. G., & Mahan, G. D. (1999). Failure modes and energy absorption capability of ZnO varistors. *IEEE Transactions on Power Delivery*, 14(1), 152-162.
- Bartkowiak, M., Comber & M.G., Mahan, G.D. (2001). Influence of nonuniformity of ZnO varistors on their energy absorption capability. *IEEE Transactions on Power Delivery*, 16(4), 591-598.
- Bayadi, A. (2008). Parameter identification of ZnO surge arrester models based on genetic algorithms. *Electric Power Systems Research*, 78(7), 1204-1209.

- Bhattacharai, R., Rashedin, R., Venkatesan, S., Haddad, A., Griffiths, H., & Harid, N. (2008, September). Lightning performance of 275 kV transmission lines. In *Universities Power Engineering Conference, 2008. UPEC 2008. 43rd International* (pp. 1-5). IEEE.
- Boggs, S., Kuang J., Andoh, I., & Nishiwaki, S. (2000). Increased energy absorption in ZnO arrester elements through control of electrode edge margin. *IEEE Transactions on Power Delivery*, 15(2), 562-568.
- Borghetti, A., Nucci, C. A., & Paolone, M. (2007). An Improved Procedure for the Assessment of Overhead Line Indirect Lightning Performance and Its Comparison with the IEEE Std. 1410 Method. *IEEE Transactions on Power Delivery*, 22(1), 684-692.
- Bruce, C. E. R., & Golde, R. H. (1941). The lightning discharge. *Electrical Engineers-Part II: Power Engineering, Journal of the Institution of*, 88(6), 487-505.
- Caicedo, J. A., Biagi, C., Uman, M. A., Jordan, D. M., & Hare, B. (2016). Return stroke current reflections in rocket-triggered lightning. *Journal of Geophysical Research: Atmospheres*, 121(6), 2973-2993.
- Caulker, D., Ahmad, H., & Abdul-Malek, Z. (2011, September). Lightning Interaction with 132 kV Transmission Line Protected by Surge Arresters. In *Universities' Power Engineering Conference (UPEC), Proceedings of 2011 46th International* (pp. 1-5). VDE.
- Caulker, D., Ahmad, H., Malek, Z. A., & Yusof, S. (2010, December). Shielding failure analysis of 132 kV transmission line shielded by surge arresters associated with multiple strokes lightning. In *Electrical and Computer Engineering (ICECE), 2010 International Conference on* (pp. 298-301). IEEE.
- Chowdhuri, P., Anderson, J. G., Chisholm, W. A., Field, T. E., Ishii, M., Martinez, J. A., & Short, T. A. (2005). Parameters of lightning strokes: a review. *IEEE Transactions on Power Delivery*, 20(1), 346-358.
- Chowdhuri, P., Mishra, A. K., & McConnell, B. W. (1997). Volt-time characteristics of short air gaps under nonstandard lightning voltage waves. *IEEE Transactions on Power Delivery*, 12(1), 470-476.
- Chowdhuri, P., Li, S., & Yan, P. (2001). Review of research on lightning-induced voltages on an overhead line. *IEEE Proceedings- Generation, Transmission and Distribution*, 148(1), 91-95.

- Christodoulou, C. A., Avgerinos, M. V., Ekonomou, L., Gonos, I. F., & Stathopoulos, A. (2009). Measurement of the resistive leakage current in surge arresters under artificial rain test and impulse voltage subjection. *IET Science Measurement & Technology*, 3(3), 256-262.
- Christodoulou, C. A., Ekonomou, L., Fotis, G. P., Karampelas, P., & Stathopoulos, I. A. (2010). Parameters' optimisation for surge arrester circuit models. *IET Science, Measurement & Technology*, 4(2), 86-92.
- Christodoulou, C. A., Ekonomou, L., Mitropoulou, A. D., Vita, V., & Stathopoulos, I. A. (2010). Surge arresters' circuit models review and their application to a Hellenic 150 kV transmission line. *Simulation Modelling Practice and Theory*, 18(6), 836-849.
- Christodoulou, C. A., Vita, V., Ekonomou, L., Chatzarakis, G. E., & Stathopoulos, I. A. (2010). Application of Powell's optimization method to surge arrester circuit models' parameters. *Energy*, 35(8), 3375-3380.
- Christodoulou, C. A., Gonos, I. F., & Stathopoulos, I. A. (2011). Estimation of the parameters of metal oxide gapless surge arrester equivalent circuit models using genetic algorithm. *Electric Power Systems Research*, 81(10), 1881-1886.
- Christodoulou, C. A., Ekonomou, L., Papanikolaou, N., & Gonos, I. F. (2014). Effect of the grounding resistance to the behaviour of high-voltage transmission lines' surge arresters. *IET Science, Measurement & Technology*, 8(6), 470-478.
- Cooray, V. (1993). A model for subsequent return strokes. *Journal of Electrostatics*, 30, 343-354.
- Cooray, V., & Orville, R. (1990). The effects of variation of current amplitude, current rise time, and return stroke velocity along the return stroke channel on the electromagnetic fields generated by return strokes. *Journal of Geophysical Research: Atmospheres (1984-2012)*, 95(D11), 18617-18630.
- Co-ordination-Part, I. (2004). 4: Computational guide of insulation coordination and modelling of electrical networks. *IEC Standard TR*, 60071-4.
- Datsios, Z. G., Mikropoulos, P. N., & Tsovilis, T. E. (2014). Estimation of the minimum shielding failure flashover current for first and subsequent lightning strokes to overhead transmission lines. *Electric Power Systems Research*, 113, 141-150.

- Diendorfer, G., & Uman, M. (1990). An improved return stroke model with specified channel-base current. *Journal of Geophysical Research: Atmospheres (1984–2012)*, 95(D9), 13621-13644.
- Dobrić, G., Stojanović, Z., & Stojković, Z. (2015). The application of genetic algorithm in diagnostics of metal-oxide surge arrester. *Electric Power Systems Research*, 119, 76-82.
- Dommel, H.W., *Electromagnetic Transients Program: Reference Manual: (EMTP theory book)*. Bonneville Power Administration, 1986.
- Ekonomou, L., Christodoulou, C. A., & Mladenov, V. (2014). Estimation of the Electric Field across Medium Voltage Surge Arresters Using Artificial Neural Networks. In *Engineering Applications of Neural Networks* (pp. 227-236). Springer International Publishing.
- Fritz, O., Ljuslinder, M., & Doser, B. (2011). Heat transfer in high-voltage surge arresters. In *Comsol Conference in Stuttgart, Excerpt from the Proceeding of the Comsol*.
- Gatta, F. M., Geri, A., Lauria, S., Maccioni, M., & Santarpia, A. (2014). An ATP-EMTP Monte Carlo procedure for backflashover rate evaluation: A comparison with the CIGRE method. *Electric Power Systems Research*, 113, 134-140.
- Golde, R. H. (Ed.). (1977). *Lightning* (Vol. 1). London: Academic Press.
- Gomes, C., & Cooray, V. (2000). Concepts of lightning return stroke models. *IEEE Transactions on Electromagnetic Compatibility*, 42(1), 82-96.
- Greenwood, A. (1991). *Electrical transients in power systems*. Wiley-Interscience.
- Haddad, A., & Naylor, P. (1998, July). Finite-element computation of capacitance networks in multiple-electrode systems: application to ZnO surge arresters. *IEE Proceedings- Science, Measurement and Technology*, 145(4), 129-135.
- Han, S. J., Zou, J., Gu, S. Q., He, J. L., & Yuan, J. S. (2005). Calculation of the potential distribution of high voltage metal oxide arrester by using an improved semi-analytic finite element method. *IEEE transactions on magnetics*, 41(5), 1392-1395.
- Han, Y., Li, L., Chen, H., & Lu, Y. (2012). Influence of modeling methods on the calculated lightning surge overvoltages at a UHVDC converter station due to backflashover. *IEEE Transactions on Power Delivery*, 27(3), 1090-1095.

- He, J. L., & Hu, J. (2007). Discussions on nonuniformity of energy absorption capabilities of ZnO varistors. *IEEE Transactions on Power Delivery*, 22(3), 1523-1532.
- He, J., Hu, J., Gu, S., Zhang, B., & Zeng, R. (2009). Analysis and Improvement of Potential Distribution of 1000-kV Ultra-High-Voltage Metal Oxide Arrester. *Power Delivery, IEEE Transactions on*, 24(3), 1225-1233.
- He, J., Zeng, R., Chen, S., & Guan, Z. (2003). Potential distribution analysis of suspended-type metal-oxide surge arresters. *IEEE Transactions on Power Delivery*, 18(4), 1214-1220.
- Heidler, F., Cvetic, J. M., & Stanic, B. V. (1999). Calculation of lightning current parameters. *IEEE Transactions on Power Delivery*, 14(2), 399-404.
- Heidler, F., Traveling current source model for LEMP calculation (1985). In Proc. 6th International Symposium on EMC, Zurich, Switzerland, 29F2, 157-162.
- Hileman, A. R. (1999). *Insulation coordination for power systems*. CRC Press.
- Hinrichsen, V. (2001). Metal-oxide surge arrester. Siemens AG.
- IEEE Working Group. (1997). IEEE guide for improving the lightning performance of transmission lines.
- Imece, A. F., Durbak, D. W., & Elahi, H. (1996). Modeling guidelines for fast front transients, *IEEE Transactions on Power Delivery*, 11(1), 493-506.
- International Conference on Large High Voltage Electric Systems. Study Committee 33 (Overvoltages and Insulation Co-ordination). Working Group 01 (Lightning). (1991). *Guide to procedures for estimating the lightning performance of transmission lines*. CIGRE.
- International Electrotechnical Commission.(1996). IEC 60071-2. *Insulation Co-ordination Part, 2*.
- Ishii, M., Kawamura, T., Kouno, T., Ohsaki, E., Shiokawa, K., Murotani, K., & Higuchi, T. (1991). Multistory transmission tower model for lightning surge analysis. *IEEE Transactions on Power Delivery*, 6(3), 1327-1335.

- Jones, R., Clifton, P., Grotz, G., Lat, M., Lembo, F., Melvold, D., et al. (1992). Modeling of metal-oxide surge arresters. *IEEE Transactions on Power Delivery*, 7(1), 302-309.
- Kasemir, H. W. (1960). A contribution to the electrostatic theory of a lightning discharge. *Journal of Geophysical Research*, 65(7), 1873-1878.
- Khodr, H. M. (2009). Optimal Methodology for the Grounding Systems Design in Transmission Line Using Mixed-integer Linear Programming. *Electric Power Components and Systems*, 38(2), 115-136.
- Lee B.H., & Kang S.M. (2006). Properties of ZnO varistor blocks under multiple lightning impulse voltages. *Current Applied Physics*, 6, 844-851.
- Lee, S. B., Lee, S. J., & Lee, B. H. (2010). Analysis of thermal and electrical properties of ZnO arrester block. *Current Applied Physics*, 10(1), 176-180.
- Levinson, L. M., & Philipp, H. R. (1977). ZnO varistors for transient protection. *IEEE Transactions on Parts, Hybrids, and Packaging*, 13(4), 338-343.
- Li, H. J., Birlasekaran, S., & Choi, S. S. (2002). A parameter identification technique for metal-oxide surge arrester models. *IEEE Transactions on Power Delivery*, 17(3), 736-741.
- Lucas, J. R. (2001). High voltage engineering. *Colombo, Open University of Sri. Lanka*, 64-89.
- Martinez-Velasco, J. A. (Ed.). (2009). *Power system transients: parameter determination*. CRC press.
- Munukutla, K., Vittal, V., Heydt, G. T., Chipman, D., & Keel, B. (2010) A practical evaluation of surge arrester placement for transmission line lightning protection. *IEEE Transactions on Power Delivery*, 25(3), 1742-1748.
- Nafar, M., Gharehpetian, G. B., & Niknam, T. (2011). A new parameter estimation algorithm for metal oxide surge arrester. *Electric Power Components and Systems*, 39(7), 696-712.
- Nafar, M., Gharehpetian, G. B., & Niknam, T. (2011). Improvement of estimation of surge arrester parameters by using modified particle swarm optimization. *Energy*, 36(8), 4848-4854.

- Nucci, C. A., Mazzetti, C., Rachidi, F., & Ianoz, M. (1988). On lightning return stroke models for LEMP calculations. In *19th International Conference on lightning protection* (No. LRE-CONF-2008-104).
- Nucci, C. A., Rachidi, F., Ianoz, M. V., & Mazzetti, C. (1993). Lightning-induced voltages on overhead lines. *IEEE Transactions on Electromagnetic Compatibility*, 35(1), 75-86.
- Ogawa, T., & Brook, M. (1964). The mechanism of the intracloud lightning discharge. *Journal of Geophysical Research*, 69(24), 5141-5150.
- Okabe, S., Tsuboi, T., & Takami, J. (2011). Analysis of aspects of lightning strokes to large-sized transmission lines. *IEEE Transactions on Dielectrics and Electrical Insulation*, 18(1), 182-191.
- Petit, A., Do, X. D., & St-Jean, G. (1991). An experimental method to determine the electro-thermal model parameters of metal oxide surge arresters. *IEEE Transactions on Power Delivery*, 6(2), 715-721.
- Rakov, V. A., & Dulzon, A. A. (1991, March). A modified transmission line model for lightning return stroke field calculations. In *Proc. 9th Int. Symp. Electromagn. Compat* (pp. 229-235).
- Rawi, I., & Hudil, N. S. (2010, May). TNB experience on the application of transmission line arresters 132 kV Teluk Ewa-Teluk Apau. In *CIGRE C4 Colloquium on Lightning and Power System* (pp. 16-19).
- Ringler, K.G., Kirkby, P., Erven, C. C., Lat, M.V., & Malkiewicz, T.A. (1997) The energy absorption capability and time-to-failure of varistors used in station-class metal-oxide surge arresters. *IEEE Transactions on Power Delivery*, 12(1), 203-212.
- Romero, F., Piantini, A., & Cooray, V. (2014). On the influence of stroke current propagation velocity on lightning horizontal electric fields. *IEEE Transactions on Electromagnetic Compatibility*, 56(4), 940-948.
- Sadovic, T., & Sadovic, S. (2009, April). EMTP–RV modelling for the transmission line lightning performance computation. In *User Group Meeting* (Vol. 20).
- Samitz, U., Siguerdidjane, H., Boudaoud, F., Bastard, P., Dupraz, J., Collet, M., et al. (2002). On controlled switching of high voltage unloaded transmission lines. *e&i Elektrotechnik und Informationstechnik*, 119(12), 415-421.

- Sarajcev, P. (2015). Monte Carlo method for estimating backflashover rates on high voltage transmission lines. *Electric Power Systems Research*, 119, 247-257.
- Sardi, J. (2009). *Simulation and Analysis of Lightning Backflashover for the 132 Kv Kuala Krai–Gua Musang Transmission Line Using PSCAD* (Doctoral dissertation, Universiti Putra Malaysia).
- Sargent, R. A., Darveniza, M., & Dunlop, G. L. (1991, July). Effects of multiple current pulses on the microstructure and electrical properties of zinc oxide varistors. In *Properties and Applications of Dielectric Materials, 1991., Proceedings of the 3rd International Conference on* (pp. 509-512). IEEE.
- Savic, M. S. (2005). Estimation of the surge arrester outage rate caused by lightning overvoltages. *IEEE Transactions on Power Delivery*, 20(1), 116-122.
- Seyyedbarzegar, S. M., & Mirzaie, M. (2015). Heat transfer analysis of metal oxide surge arrester under power frequency applied voltage. *Energy*, 93, 141-153.
- Schmidt, W., Meppelink, J., Richter, B., Feser, K., Kehl, L., & Qui, D. (1989). Behaviour of MO-surge-arrester blocks to fast transients. *IEEE Transactions on Power Delivery*, 4(1), 292-300.
- Standard, I. E. C. (2006). 60071-1: Insulation Co-ordination Part 1. *Definitions, Principles and Rules*.
- Stockum F. R. (1994). Simulation of the nonlinear thermal behavior of metal oxide surge arresters using a hybrid finite difference and empirical model. *IEEE Transactions on Power Delivery*, 9(1), 306-313.
- Thottappillil, R., McLain, D. K., Uman, M. A., & Diendorfer, G. (1991). Extension of the Diendorfer-Uman lightning return stroke model to the case of a variable upward return stroke speed and a variable downward discharge current speed. *Journal of Geophysical Research: Atmospheres (1984–2012)*, 96(D9), 17143-17150.
- Tuczek, M.N., & Hinrichsen, V. (2014). Recent experimental findings on the single and multi-impulse energy handling capability of metal–oxide varistors for use in high-voltage surge arresters. *IEEE Transactions on Power Delivery*, 29(5), 2197-2205.
- Uman, M. A., & McLain, D. K. (1969). Magnetic field of lightning return stroke. *Journal of Geophysical Research*, 74(28), 6899-6910.

- Vipin, P. M., Nagabhushana, G. R., & Jayaram, B. N. (1991). *Investigations on electro-thermal ageing of metal oxide surge arrester elements: a realistic laboratory simulation*. In Proceedings of the 3rd International Conference on Properties and Applications of Dielectric Materials.
- Vojta, A., & Clarke, D. R. (1997). Microstructural origin of current localization and “puncture” failure in varistor ceramics. *Journal of Applied Physics*, 81(2), 985-993.
- Wagner, C., & Hileman, A. (1960). A New Approach to the Calculation of the Lightning Performance of Transmission Lines III-A Simplified Method: Stroke to Tower. *Power Apparatus and Systems, Part III. Transactions of the American Institute of Electrical Engineers*, 79(3), 589-603.
- Wahab, Y. A., Abidin, Z. Z., & Sadovic, S. (2003, June). Line surge arrester application on the quadruple circuit transmission line. In *Power Tech Conference Proceedings, 2003 IEEE Bologna* (Vol. 3, pp. 7-pp).IEEE.
- Wu, J., Zhang, B., He, J., & Zeng, R. (2014). Optimal design of tower footing device with combined vertical and horizontal grounding electrodes under lightning. *Electric Power Systems Research*, 113, 188-195.
- Yamada, T., Mochizuki, A., Sawada, J., Zaima, E., Kawamura, T., Ametani, A., Ishii, M., & Kato, S. (1995). Experimental evaluation of a UHV tower model for lightning surge analysis. *IEEE Transactions on Power Delivery*, 10(1), 393-402.
- Zhong, Z., Boggs, S. A., Imai, T., & Nishiwaki, S. (2010). Computation of Arrester Thermal Stability. *Power Delivery, IEEE Transactions on*, 25(3), 1526-1529.

LIST OF PUBLICATIONS AND PAPERS PRESENTED

- 1) Illias, H. A., Halim, S. A., Abu Bakar, A. H., & Mokhlis, H. Determination of surge arrester discharge energy using finite element analysis method. *IET Science, Measurement & Technology*, 9(6), 693-701.
- 2) Halim, S. A., Abu Bakar, A. H., Illias, H. A., Hassan, N. H. N., Mokhlis, H., & Terzija, V. Lightning Backflashover Tripping Patterns on a 275/132 kV Quadruple Circuit Transmission Line in Malaysia. *IET Science, Measurement & Technology*, 10(4), 344-354.

University of Malaya